uOttawa

L'Université canadienne
Canada's university

FACULTÉ DES ÉTUDES SUPÉRIEURES ET POSTOCTORALES

uOttawa

L'Université canadienne
Canada's university

FACULTY OF GRADUATE AND POSDOCTORAL STUDIES

Jérémie Lefebvre
AUTEUR DE LA THÈSE / AUTHOR OF THESIS

Ph.D. (Physics)
GRADE / DEGREE

Department of Physics
FACULTÉ, ÉCOLE, DÉPARTEMENT / FACULTY, SCHOOL, DEPARTMENT

Dynamic of a Sensory Network of ON and OFF Cells with Global Delayed Feedback
TITRE DE LA THÈSE / TITLE OF THESIS

André Longtin
DIRECTEUR (DIRECTRICE) DE LA THÈSE / THESIS SUPERVISOR

Victor LeBlanc
CO-DIRECTEUR (CO-DIRECTRICE) DE LA THÈSE / THESIS CO-SUPERVISOR

Alain Bellrive

Lora Ramunno

Ivan L'Heureux

Ralf Wessel
Washington University

Gary W. Slater
Le Doyen de la Faculté des études supérieures et postdoctorales / Dean of the Faculty of Graduate and Postdoctoral Studies

Dynamics of a sensory network of ON and OFF cells with global delayed feedback

BY
Jérémie Lefebvre

A thesis presented to the University of Ottawa
in fulfillment of the requirements for the degree of
Doctor of Philosophy in Physics

uOttawa

L'Université canadienne
Canada's university

Your file Votre référence
ISBN: 978-0-494-74242-6
Our file Notre référence
ISBN: 978-0-494-74242-6

Contents

List of Figures

Abstract

We study the sensory processing features of a network built of ON and OFF cells with global delayed feedback. We investigate the response of neural populations to spatio-temporal forcing, mimicking that found in most sensory systems. The network architecture is inspired from the physiology of the electrosensory lateral line lobe (ELL) of the weakly electric fish, where we describe the collective behavior of populations in the pyramidal cell layer. ON pyramidal cells receive sensory inputs directly, while OFF cells receive a mirror image of the stimuli via an interneuron, inverting their response. The two opposed responses propagate upstream where they recruit the inhibitory feedback pathways. To enhance the distinction between the sub-populations, different baseline firing rates are implemented (to which we refer as asymmetry). As a novel approach to this problem, we model the neural circuit using a system of neural field equations, where the connectivity is determined solely by all-to-all and non-topographic inhibitory recurrent connections. Motivated by numerical and experimental results on the electrosensory system, we determine the conditions for which global rhythmic activity states appear in response to spatially organized stimuli. Novel responses to localized pulses are shown in the steady state regime, where the feedback connections interfere with local ON and OFF activities. These effects are systematically compared to the dynamics of a noisy Integrate-And-Fire network sharing the same architecture and parameters with the neural field formulation. Lastly, we investigate the impact of intrinsic cellular adaptation on oscillatory dynamics. Together these results establish the theoretical basis for input driven transitions to rhythmic states in delayed feedback networks with realistic neural populations.

Résumé

Dans cette thèse, nous étudions les propriétés d'intégration d'un réseau de cellules ON et OFF avec rétroaction globale à délai. Nous portons notre attention sur la réponse de populations neurales vis-à-vis un forçage spatio-temporel, reproduisant les entrées observées dans la plupart des systèmes sensoriels.
L'architecture de notre réseau est basée sur les données physiologiques concernant le lobe latéral électrosensoriel (ELL) chez le poisson électrique, dans lequel nous décrivons le comportement collectif des populations à travers la couche pyramidale. Les cellules pyramidales de type ON reçoivent les signaux sensoriels directement, alors que les cellules OFF perçoivent une image miroir issue d'un interneurone, qui inverse la polarité du signal. Ces deux réponses opposées se propagent verticalement et activent alors la boucle de rétroaction inhibitrice. Afin d'amplifier la différence qui existe entre les sous-populations présentes, des niveaux d'activité de base sont implémentées (que l'on associent au degré d'asymmétrie). En tant que nouvelle approche au traitement de ce problème particulier, nous modélisons le circuit neural à l'aide d'un système d'équations de type champ neural, où la connectivité entre les différentes parties du réseaux est traitée uniquement par une connexion inhibitrice non topographique et globale. En se basant sur des études numériques et expérimentales sur le système électrosensoriel, nous déterminons ici les modalités selon lesquelles des solutions oscillatoires globales apparaissent en réponse à des stimuli spatialement organisés. De nouveaux comportements vis-à-vis des pulses localisés sont mis à jour dans le régime des points fixes, dans lequel la rétroaction interagit avec les activité locales des cellules ON et OFF. Ces résultats sont systématiquement comparés du point de vue quantitatif avec un réseau équivalent composés de cellules de type Integrate-And-Fire avec bruit. Il est alors possible d'observer la correspondance entre la description obtenue avec les champs neuraux, et celle obtenues avec les modèles plus traditionnels. Finalement, nous étudions l'effet de l'adaptation cellulaire intrinsèque sur la dynamique oscillatoire du système. Ces résultats établissent les fondements théoriques décrivant les transitions vers le comportement oscillatoire causés par des entrées sensorielles dans les systèmes neuronaux récurrents composés de populations cellulaires réalistes.

Acknowledgment

I would like to thank André and Victor for their support during the last five years. I am very grateful for their trust, by giving me so much freedom in conducting research. I believe this independence truly stimulated my interest in my work and gave me the confidence I needed to pursue my work up to this point. I would also like to emphasize how understanding they were with respect to my family duties.

I would like to thank my friend and temporary supervisor Axel, who generously spent his time guiding me on many fruitful occasions, and for giving me so many opportunities to promote myself.

I would like to thank my family and friends, for their ever-lasting support and trust.

I also thank FQRNT for financial support, without which many good things in my life would perhaps have not occurred the way they did.

Lastly, I would like to give credit to a very special Friend, who supported me throughout this adventure. Merci.

Introduction

Neuroscience addresses the questions of physiology and function of neural systems. While the research on the physiological mechanisms underlying cognition has been the main motivation of neuroscientists and psychologists, some properties shared by the neural tissue with many physical systems have attracted the interest of physicists as well. The brain exhibits cases of spontaneous organization, non-linearity, non-locality and delayed interactions, resulting in various effects, like the propagation of activity waves, stochastic and chaotic dynamics, which have also been reported in many physical systems.

Mathematical models have proven to be fruitful tools in analyzing idealized representations of single and/or groups of neural cells, where experiments might be easily reproduced and theoretical predictions tested. Indeed, various parameters dictate the dynamics of single neurons and neural systems alike, defining the role they play in information processing. Such parameters obey a set of constraints, and through modelling, one seeks a mathematical representation of these constraints. Via the use of formal and often idealized representations of neural systems, it becomes possible to predict what the state of the system will be in the close future, according to its current and past state. This approach has been used since the beginning of the last century in a attemp to grasp the troubling complexity of real neural systems. Chapter 1 discusses several pioneer models of neural cells in detail.

One of the major challenges in modern neuroscience is to understand the ways sensory systems, like vision and audition for instance, process the immense amount of sensory information they receive from the primary receptors. The efficiency of sensory system to encode and extract meaningful information out of sensory signals is of foremost importance to understand behavioural responses of various organisms. While sensory pathways might project up to cortical areas, a significant portion of information encoding is performed by the early stages of sensory systems. There, non-linear and delayed components already start to

extract temporal and spatial components of stimuli and project to higher brain centers for further processing. The physical nature of the stimuli which initiated such processing mechanisms further supports the relevance of a physical approach to these problems.

The realization of sensory processing tasks is a direct consequence of the architecture of the microcircuitry. The topographic or spatial organization of both stimuli and connections plays a crucial role in the integration of sensory information. Various studies have tried to elucidate the dynamical impact of various network architectures on the stability of neural firing patterns [1, 2, 3] and/or on the phase of connected oscillators [4, 5]. These results have mainly been formulated in the context of cortical interactions, where they have been linked to experimental recordings like EEG (electroencephalography) and MEG(magnetoencephalography). In particular, feedback and recurrent connections are one of the fundamental ingredients of neural systems, being influential in control and motor tasks [6], implementation of memory [7, 8] and receptive field geometry [9]. See also [10] for an extensive review on feedback.

Many early physiological studies depict the circuitry of sensory systems as a collection of static components. However, real sensory systems are highly fluctuating environments, where the states of individual cells are highly influenced with the various time-varying signals they receive from their surroundings. As such, neurons are subject to a plethora of noisy and chaotic fluctuations, which shape the response pattern of the cells. It has been shown that noise is a fundamental component of neural systems, being necessary for the stability of organized network states [11]. Further, noisy fluctuations are responsible for spatially organized activity [12, 13], firing correlations [14] and resonance [15]. For in-depth reviews of noise in neural systems, see [16, 17, 18]. As a result, the information processing capabilities of the most basic neural nets requires a deeper understanding of the response mechanisms involved in the integration of fluctuating signals. Spiking dynamics might be used to track fluctuating signals

[19], but the role of non-linear connectivities combined with recurrent effects is still not clearly understood. From the point of view of physical modelling, it is believed that the response properties of sensory networks are related to the non-linear dynamical changes (either quantitative or qualitative) initiated by external driving forces. Analytic treatment of models of sensory systems might expose these dynamical changes and help elucidate the role of non-linear and delayed components in sensory processing tasks.

Electroreception in the electric fish has received significant attention from neurophysiologists in great part because of its relative simplicity compared to mammals. On the other hand it exhibits highly evolved behaviors such as navigation, foraging and communication with other fishes. Electroreception is used by the gymnotiforms fish, where the neural circuitry involved is well known. Well established experimental recording techniques combined with relative availability of such fishes further make electroreception a system of choice in the analysis of sensory responses. Primary sensors on the skin known as electroreceptors respond to electrical fluctuations on the fish skin and then project to a unique structure called the Electrosensory Lateral Line Lobe (ELL). The ELL is the first and unique relay in sensory processing and has been shown to be responsible for stimuli feature extraction. Many studies (see [20, 21, 22, 23, 24] and references therein) have exposed the detailed physiology of the ELL (mostly in Eigenmannia viriscens and Apteronotus leptorhynchus species). The ELL shares many features with other processing structures found in the visual system.

The ELL circuitry is characterized by the presence of several feedback loops, which exhibit quite distinct topographies. From the receptor units found on the fish skin up to the pyramidal cells layer, the sensory inputs are conveyed in a feed forward and parallel fashion. The pyramidal cells send synaptic contacts with the Nucleus Praementialis Dorsalis (Pd) and the Eminentia Granularis Pars Posterior (EGp), two cell clusters which feedback to the sensory layer with

both excitatory and inhibitory connections. Thus, the spiking behavior of the pyramidal cells is influenced by the signals they project up to these nodes, after some time lag associated with the non-instantaneous propagation of action potentials and the processing time of the cells present in the recurrent pathway. The circuitry of the ELL has inspired various computational and numerical studies (for instance [25, 26, 27, 28, 29]), which successfully exposed the relationship between neural dynamics and sensory stimulus, in order to correlate the sensory information with behavioral responses and/or specific pyramidal cell activity patterns. This kind of circuitry is also present in the so-called nucleus isthmi found in the visual system of many animals [30, 31].

In 2003, Doiron et al. [32] demonstrated that electrosensory stimuli showing sufficient spatial correlation triggered synchronous oscillatory activity states in a network with global delayed feedback, where the firing rate oscillations were situated in the gamma range (20-50Hz). This computational study used a network of noisy leaky Integrate-And-Fire cells, connected via a delayed recurrent loop. This model reproduced the behaviour of the pyramidal cells under spatio-temporal stimulation. For increased spatial correlation or "binding" of the stochastic stimulus, global oscillatory states become stable, where "global" means that are cells are involved. This very important result sheds light on a fundamental feature of electrosensory input processing made by the ELL, namely to differentiate between prey-type and communication-type signals. Local stimuli initiated by small objects in the pyramidal cells receptive field elicit localized responses in the sensory layer. Thus, only a small portion of the pyramidal cells are responding to relatively weaker spatial correlations of the input. In contrast, large or global stimuli, overlapping multiple pyramidal cell receptive fields, trigger a massive and coherent response across the pyramidal cells layer. This strong response has been shown to recruit inhibitory feedback connections, resulting in synchronous neural firing. The resulting strong spectral power in the gamma range caused by increased input spatial correlation was further analyzed via calculations based on linear response theory, and supported by

experimental recordings on the weakly electric fish where the spatial correlation of the stimulus could be adjusted gradually [33] . Additional details about this result may be found in these references [34, 33].

Several concerns are raised by this result. First, one might ask what is the dynamical mechanism responsible for the cyclic response of the cells? While the setup of the study points toward an Andronov-Hopf bifurcation, cyclic solutions are usually triggered by the variations of the feedback delay, not by external non-homogeneities. Further, the Integrate-And-Fire network considered is non-continuous and essentially stochastic, meaning that it is very hard to determine analytically what the threshold for this transition is. The network considered in [32] consists of a sensory layer interacting with a single delayed recurrent connection. This feedback pathway corresponds to the so-called direct feedback pathway [22], where the pyramidal cells feedback travels via the Pd. These connections are mainly inhibitory, and are spatially diffuse. In contrast, another component of this same recurrent connection local to the ELL and thus involves a much smaller delay, and is of mixed polarity, but has received much less consideration in the literature. Further, an indirect pathway from the EGp back to the pyramidal cell layer also influences the sensory responses of those cells. This indirect pathway has been almost completely neglected from the modelling perspective. As feedback has been shown to significantly alter the response properties of systems, it is natural to ask: what are the effects of these additional feedback loops on the genesis of rhythmic states found in [32]?

Pyramidal cells receive the electrosensory inputs from p-units afferents. In contrast to [32] where the cellular responses are purely excitatory, the sensory pathway in the ELL is divided into ON and OFF pathways. The pyramidal cells are also referred as E and I cells in the electrosensory literature. As illustrated in Fig. 2.1, ON pyramidal cells are innerved directly by the afferents and OFF cells receive the inputs via a granular interneuron, which mediates the signals sent from the p-units to the pyramidal cells. The interneuron inverts the polarity of

the signal it receives from the receptors, which is essentially excitatory. Thus, stimuli initiate two parallel and opposed neural responses: excitatory (ON) and inhibitory (OFF). Such di-synaptic circuitry is ubiquitous in most sensory systems, like vision, audition and pain processing. Both ON and OFF cells then act seemingly similarly with respect to feedback: they both excite the feedback population Pd in the same way. It is not clear then how feedback connections behave when these two responses are combined. Further, the spontaneous firing rates of ON and OFF cells can show significant differences [35]. From this perspective, are oscillatory states as likely to appear? Are the results presented in [32] robust when a second neural population of similar size (i.e. cell number) is added?

Another issue raised by [32] is the properties of the noisy signal used to model electrosenrory inputs. Many computational and information theoretic studies on electroreception model sensory signals using zero mean random processes. Even though these types of signals have been shown to accurately represent certain real sensory stimuli, this particular choice of forcing is not ideal to elucidate the effects of feedback on the behaviour of the neural population. How ELL-inspired circuits might integrate deterministic signals has received very little attention, especially in the context of parallel ON and OFF pathways.

Pyramidal cells are also subject to cellular adaptation. Cellular post-synaptic responses to steady stimuli exhibit typical decreases in amplitude, over a specific period of time. This decrease in amplitude has various causes, from transient ionic currents to synaptic depression. This form of stimulus habituation or fatigue alters the response behaviour of the cells and shapes the frequency tuning properties to fluctuating currents. It has indeed been shown that cellular adaptation interacts with synchronous states and influences the response to stimulation [36, 37, 38, 39]. This particular form of adaptation has not been included as a state variable in [32], but is likely to influence the rhythmic patterns of the system.

In this thesis, we address each of these questions using a neural field model. Most analytical and computational studies on the ELL have dominantly been performed using noisy Integrate-And-Fire networks. In contrast, neural fields constitute a class of continuous models (in both time and space), which greatly facilitates the steady state and bifurcation analyses from the population perspective. Designed for modeling relatively slower dynamics on patches of cells rather than the firing activity of individual cells, neural fields have been used to explore sleep [40], the spatial organization of working memory [41, 42] and even the cause of some visual hallucinations [43]. There they have proven to be tools of choice in the study of neural populations. For a more extensive review of neural fields, see Section 1.3.3. Neural fields use deterministic dynamics to represent noisy networks, where the slower time scale and coarser spatial graining average-out random fluctuations. Further, the model predictions have been shown to be in good agreement with extra-cellular recordings known as local field potentials which register the firing activity of populations of cells [44].

The analysis of our model is segmented in a series of published or submitted articles, where specific issues are studied in detail. Prior to those articles, Chapter 1 introduces the necessary background material, related to neuronal physiology and modelling, especially in the context of sensory systems and ON and OFF cells. An exhaustive description of the ELL is also provided, as well as an overview of generic neural field models. Our model is derived in Chapter 2, where we construct an idealized network inspired by the circuitry involved in electroreception. In Chapter 3, we demonstrate how global rhythmic states are triggered by deterministic spatio-temporal inputs. We study the impact of multiple feedback loops of different polarities (either excitatory or inhibitory) on the genesis of cyclic solutions. On the basis of these results, Chapter 4 constitutes a complete bifurcation analysis of our model, where we study the role of asymmetrical firing rates and feedback delay on the sensory response of the system to static and time-periodic stimuli. There, we expose novel effects

caused by recruitment of recurrent connections by the ON and OFF populations, and we systemically compare the predictions of the neural field model with an equivalent network of noisy Integrate-And-Fire cells. In Chapter 5, we perform a comparative study between the response properties of networks built of ON and OFF cells, and those built solely of excitatory cells. We expose the possible functional advantages of di-synaptic circuitry on the integration of both static and time-periodic pulses. In Section 5.7, we present novel results concerning stochastic forcing in an Integrate-And-Fire network of ON and OFF neurons. Chapter 6 discusses the role of cellular adaptation on the stability of global oscillations and on the oscillatory response threshold. We also show how adaptative forces enhance the response amplitude of the sub-units to a time-varying stimulus. The thesis then ends with a discussion and some concluding remarks in Chapter 7.

Non-homogeneous problems (like the ones considering external stimulation) are evoking a vivid interest across the dynamical systems literature. As most physical (and biological) systems are highly fluctuating environments, the need for theoretical tools to approach non-linear driven systems, often times involving delays, has become of prime importance. From a general standpoint, Dynamical Systems Theory does not yet provide the analytical tools required to deal with the stability of generic driven systems. As such, must of the current advances are made using specific examples of differential equations which admit an explicit solution, or by using computational techniques to solve the aforementioned systems numerically. This is especially true when one considers non-linear delay differential equations (DDE). Although they are extensively used in mathematical biology, laser theory and control, a standard technique to approach non-homogeneous problems is still missing. As a parallel project to this thesis, we have developed a center-manifold approach to investigate the unfolding of solutions in parameter space near a bifurcation for a generic scalar non-linear and non-autonomous delay differential equation. A short description of the work is presented in Appendix A.

Statement of Originality

This thesis is an article-based work. As opposed to a monograph, it presents papers that are either published or submitted. The status of each paper or manuscript is clearly indicated in the following list, as well as the respective contributions of the co-authors. The work in all the papers was guided by my co-supervisors.

- Chapter 3.

  This chapter is a copy of the article:

  J. Lefebvre, A. Longtin, and V. G. Leblanc. Oscillatory response in a sensory network of ON and OFF cells with instantaneous and delayed recurrent connections. *Philosophical Transactions of the Royal Society A: Mathematical, Physical and Engineering Sciences*, **368**:455-467, 2010.

  This article analyzes in detail how global oscillations appear in a network of ON and OFF cells with all-to-all delayed feedback with external stimuli. In particular, we studied the impact of additional non-delayed or instantaneous feedback loops on input-induced Andronov-Hopf instabilities. I performed all the numerical simulations and theoretical analysis. I am the main author of the text and figures, while corrections and comments were added by A. Longtin and V.G. LeBlanc.

- Chapter 4. This chapter is a copy of the article:

  J. Lefebvre, A. Longtin, and V.G. LeBlanc. Dynamics of driven recurrent networks of ON and OFF cells. *Phys. Rev. E*, 80:041912, 2009.

  In this article, we performed a complete bifurcation analysis of our model, and exposed multiple types of responses caused by spatio-temporal inputs. We systematically compared the results predicted by our neural field model with numerical simulations of an equivalent noisy Integrate-And-Fire network. I did all the analysis and numerical simulations, along with all the figures contained in the article. The text was written con-

jointly with A. Longtin, and corrections were added by V.G. LeBlanc.

- Chapter 5. This chapter is a copy of the manuscript:
  J. Lefebvre, A. Longtin, and V.G. LeBlanc. Comparison of responses of recurrent nets of ON and ON/OFF cells to deterministic stimuli, *Journal of Biological Physics*, 2010, in press

  This article analyzes in detail the input response distinctivenesses between networks built solely of ON cells and those with both ON and OFF cells, with respect to spatio-temporal sensory forcing. I performed all the numerical simulations and theoretical analysis. I am the main author of the text and figures, while corrections and comments were added by A. Longtin and V.G. LeBlanc.

- Chapter 6 This chapter is a copy of the submitted manuscript:
  J. Lefebvre, A. Longtin, and V.G. LeBlanc. Neural adaptation facilitates oscillatory responses to static inputs in a recurrent network of ON and OFF cells, Submitted to the Journal of Computational Neuroscience on July 16, 2010

  In this short paper, we study the effect of cellular adaptation on the genesis of input-induced Andronov-Hopf instabilities. I am the main author of the text and figures, while corrections and comments were added by A. Longtin and V.G. LeBlanc.

- Appendix A. This Appendix constitutes an overview of the preprint:
  J. Lefebvre, A. Hutt, A. Longtin, and V.G. LeBlanc. Non-autonomous center manifold reduction in a model of delayed feedback, under review for Physica D, 2009

  This article puts forward a novel way of computing center manifolds for non-autonomous scalar differential equations with time delay. This project was realized during an internship held at LORIA, Nancy, France. The ar-

ticle was co-written with A. Longtin and A. Hutt. I wrote the theory and analytics, and performed all the numerical simulations. A. Hutt wrote the section on the boundary value problem, and performed the calculations related with the Greens function approach. A. Longtin wrote the introduction. V.G.LeBlanc detailed the center manifold theorem section and the applicability of our approach. All the co-authors corrected and commented the manuscript until it reached its present form.

Chapter 1

Background

In this thesis, we investigate non-linear sensory processing features in a neural field model with delayed recurrent connections. Neural field models form a class of high level representations of neural networks. There exists two natural ways to introduce such models. The first approach presents neural fields as ideal mathematical models of spatially structured activity patterns in large-scale networks like the cortex. The network equations are formulated as abstract representations of neural activity, and it becomes harder to connect with the specific example at hand. The other approach builds the neural field formalisms on the basis of cellular behavior and network dynamics. I chose the latter because of its greater connection with physiology. Thus, in order to understand the language and shape of the model we investigated, we must go through a review of the building blocks of neural dynamics and modelling. In this Background section we will outline the most salient elements in mathematical neuroscience by reviewing some fundamental properties of cellular and network models . This will be done from the standpoint of modeling and computation.

The review given here is by no means exhaustive. In Section 1.1,1.2 and 1.3, we will review the foundational elements of computational neuroscience. We will follow the lines of [45, 46, 47, 48]. In Section 1.3.3 we will introduce and derive a neural field model of a large scale neural network. Specialized references will

be given there. Further, in Section 1.4, we will present an overview of the visual and electrosensory systems. This will expose the circuitry and features on which our model is based. Explicit references will follow the text.

1.1 The Neuron

Neural interactions are mediated by cells, called *neurons*, which transmit and relay *action potentials*, which are electrical pulses in the form of propagating chemical gradients of electrically charged molecules. The neurons themselves evolve in an environment built of glial cells, which provide both structural support and energetic resources. Neurons come in various shapes and sizes, but can nevertheless be physiologically divided into three primary segments: the *dendrites*, the *soma* and the *axon*, whose structures varies immensely in size and extent. Aside from their morphological specificities, these segments possess very distinct roles in the reception, emission and relay of action potentials towards other cells.

Neurons are highly specialized, and thus possess various functional roles, ap-

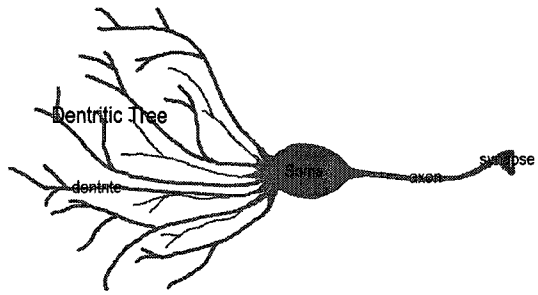

Figure 1.1: **Neuron.** Simplified schematic of a pyramidal cell

pearing in circuits ranging from the retina up the cortical regions . Irrespective of their shape, size or location, the relay of electrical signals occurs via a sequential polarization and depolarization of the membrane, performed by a sudden discharge of electrically charged particles in and out of the confinement of the soma. At rest, these charged particles are segregated in and out

of the membrane coherently with their species, resulting in different chemical concentrations across the cell membrane, which in turn result in an equilibrium voltage of about -80mV. The reception of electrical perturbations, or inputs, alters the electro-chemical balance across the somatic membrane. If the resulting transmembrane voltage increases up to a threshold value of around -50mV, the involved cations and anions (K+, Na2+, Ca2+, Cl-, etc) travel in and out of the membrane using specific conduits called *channels*. The ion channels are protein pumps which are activated by high polarization levels, and possess very specific timing and transport properties. Thus if the potential across the membrane exceeds some ion species-specific level, the associated channels open up, allowing some ions to leave and other to enter the soma. Because the ion channels do not operate all simultaneously, the somatic voltage follows a sharp stereotyped jump, and then comes back to its original level. This depolarization-hyperpolarization sequence forms an action potential. The resulting electrical pulse travels down the axon in a regenerative fashion all the way to the synapse, where it is relayed to the post-synaptic cell, as a new input.

Each of the steps in a neuron discharge is a complex electro-chemical process that involves many physiological details, especially in regard to the role played by the different components or branches of the cell in the relay and discharge processes. The reception of pre-synaptic action potentials and their propagation across the selected dendrite involves important resistive and capacitive influences, further aggravated by the spatial structure and ramification of the dendritic tree. Axonal conduction and the role played by myelin, for instance, in the regeneration and transport of electrical pulses further complicates the issues of decay and timing of signal transport through the cell. Nevertheless, all these details involved in the emission of an action potential, although relevant and impacting on the behavior of the cell, do not alter qualitatively its basic function: the genesis and transfer of electrical signals. Detailed discussion of the electrical and molecular dynamics involved in the discharge of action potentials can be found in [49, 48, 46].

1.2 Models of the neuron

The purpose of mathematical and computational neuroscience is to design sets of mathematical models and numerical algorithms to explain and potentially predict neural processes. The ways cells and networks transmit and process information are investigated by looking at the properties and outcomes of these models, by means of theoretical analysis and numerical simulations. Of foremost interest is the ability to predict the response of neural systems, given some pre-synaptic input. In this section, we outline the main discoveries and advances in neuroscience modeling. For an complete review of computational models classification and evolution through the last decades, see [50] .

1.2.1 Integrate-And-Fire model

Attempts to replicate single cell spiking behaviour can be dated as early as 1907 with Lapicque and his Integrate-and-Fire model, still widely used today ([51] and references therein). Lapicque description of the neuron is empirical, in the sense that even though one could record the spiking activity of cells, the exact mechanisms underlying the emission of the action potential were not known. In the Integrate-and-Fire model (IF), the neuron is mapped to a simplified electrical accumulator, which is said to emit an action potential or "fire" whenever some artificial voltage threshold is met. The voltage increases according to incoming pre-synaptic input current. The Integrate-and-Fire model is the first example of single-compartment models, which reduces the behavior of the neuron to its somatic dynamics and where dendritic and synaptic effects are neglected. The advantage of this type of model lies in the fact that an Integrate-And-Fire description allows a good estimate of the cell spiking behavior with respect to incoming inputs, without a precise mapping of the internal processes. Such a mapping is highly non-linear, and can become quite computationally consum-

ing to reproduce. As a result, the Integrate-And-Fire model is an oversimplified and artificial representation of the neuron, providing an easy manipulation of a large number of cells. This makes the Integrate-And-Fire model ideal tool for the study of networks. The IF model has proven its relevance and has been repeatedly adjusted and modified since its first incarnation, to incorporate more advanced physiological processes like spike adaptation or spiking latency and to map more elaborate circuits. In its most common form, the Integrate-And-Fire model contains a negative term to account for the various current leaks; it is thus often referred as LIF, for "leaky Integrate-And-Fire".

The Integrate-And-Fire is the first example of a conductance-based model. It

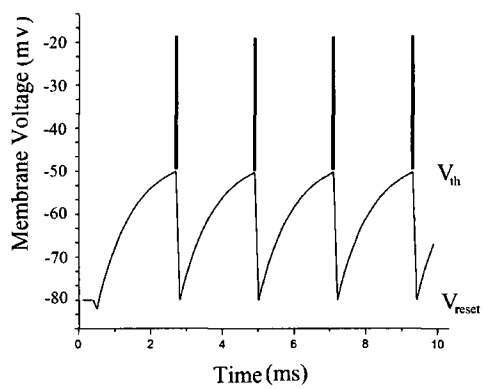

Figure 1.2: **Spiking dynamics reproduced by an Integrate-And-Fire model.** Here, a constant bias input of $I = 50mA/cm^2$ drives the cellular membrane, making it emit a series of action potentials as per Eq. 1.1. Parameters where chosen such that $V_{reset} = -80mV$ and $V_{th} = -45mV$ for $g_{leak} = 1mS/cm^2$. The time scale was adjusted.

indeed describes the time evolution of the voltage across the membrane of the cell, taken at the soma, as a function of the total input current $I(t)$ it might receive from its surroundings, considering the pre-synaptic and dendritic processes as *passive*. The voltage variable $V(t)$ in this case obeys

$$C\dot{V}(t) = C\frac{dV(t)}{dt} = -g_{leak}V(t) + I(t), \tag{1.1}$$

where C is the capacitance of the membrane and g_{leak} is the conductance gain of the leaking potential. Fig. 1.2 illustrates the time evolution of $V(t)$ in Eq. 1.1. Given that the total current to the soma constitutes an excitatory input (i.e. $I(t) > 0$), the membrane potential will increase until it reaches an articifial threshold value from below. This threshold is typically labelled V_{th}. Whenever $V = V_{th}$, a spike is said to be emitted, and the value of the voltage is reset to some sub-threshold value, labelled V_{reset}. In contrast, if the input is inhibitory (i.e. $I(t) < 0$), the voltage decreases, reducing the probability of meeting the voltage threshold. The resulting ability of the model to mimic the evolution of the membrane voltage is restrained to sub-threshold dynamics. Variants of the LIF incorporate adaptation currents, noisy inputs, other more specific ionic currents, synaptic currents due to feedforward and feedback connections, to replicate the neural behavior with increased accuracy, but without sacrificing the computational advantage this class of models provides compared to the more physiological representations available.

1.2.2 Hodgkin-Huxley model

The mechanisms underlying action potential discharge were first implemented successfully in a conductance based model in 1952 [52]. Experiments performed on the giant squid axon allowed Andrew Hulxey and Alan Hodgkin to describe the emission of an action potential as being similar to the charge and discharge of a capacitor, where the involved ionic currents are activated by voltage-gated nonlinear conductance channels. The emission of an action potential is the consequence of the interplay of multiple voltage-gated ionic currents having distinct timings, activating and de-activating according to the current membrane potential and rest voltage, resulting in a quite realistic description of somatic dynamics. As stated before, the transit of the most common ions involved in spike discharge across the membrane, namely sodium Na+, calcium Ca 2+, potassium K+ and chloride Cl- , temporarily perturb the electrical equilibrium

that is maintained across the somatic membrane; the incoming electrical pulse will not affect each of those channels simultaneously nor with the same strength. The resulting deviation of the membrane potential from its resting states was shown to have both the shape and properties of an action potential. This result led to the award of the Nobel Prize in Physiology and Medicine to Alan Hodgkin and Andrew Huxley in 1963.

The concentration of ions inside and outside the soma is responsible for their respective equilibrium potentials, called the *Nernst potentials*, towards which the individual voltages try to relax. For some ionic species m, it is defined by

$$E_m = \frac{RT}{zF} ln \frac{C_{m.outside}}{C_{m.inside}},$$

where R is the ideal gas constant, z the valence of the concerned ion, T the temperature, and C_m are the concentrations inside and outside the soma. F is the Faraday contant. A neuron at rest is in electrical equilibrium whenever the ions generate a voltage that corresponds to a weighted function of their respective Nernst potentials. Upon electrical perturbations, however, the transmembrane transit of electrically charged particles create currents flowing in and out the membrane. These species-dependent currents have amplitudes that depend on the instantaneous value of the potential V and the Nernst potentials, resulting in a non-linear conductance function $g_m(V)$ of the ionic species. Ionic currents I_m for a species m are given by

$$I_m = g_m(V)(V - E_m),$$

where E_m is the associated Nernst potential. According to Kirchhoff law, the sum of the ionic currents across a patch of the soma must be 0, so that the flow of charged particles in and out the membrane equilibrates. Thus, one may write

$$0 = \sum_m I_m + C\dot{V} - I,$$

where $C\dot{V}$ is the capacitive current of the membrane, and I constitutes the pre-synaptic input current to the cell. The resulting form has the structure of a conductance-based evolution equation governing the somatic potential $V(t)$,

$$C\dot{V} = -\sum_m g_m(V)(V - E_m) + I.$$

If we then restrict the dynamics to K, Ca, Na and Cl ions, we obtain a dynamical model of the cells voltage respectively to these ionic species

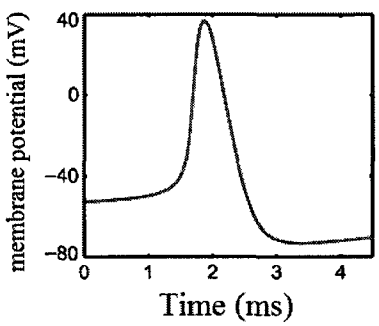

Figure 1.3: **Time evolution of the voltage variable in the Hudgkin-Huxley model.** The state variable $V(t)$ reproduces accurately the shape and timing of a real action potential. An input current depolarizes the cell's membrane, and triggers an action potential. The voltage build-up to the firing threshold (around -45mV), although less apparent than in the Integrate-and-Fire case, still takes place. The membrane voltage evolution is governed by Eq. 1.2, while the values of the parameters for this case may be found in [46].

$$C\dot{V} = -g_K(V - E_K) - g_{Ca}(V - E_{Ca}) - g_{Na}(V - E_{Na}) - g_{Cl}(V - E_{Cl}) + I, \quad (1.2)$$

where the exact structure of the conductance functions $g_m(V)$ have been voluntarily omitted, but may be found elsewhere [46, 49, 48]; note that the specific conductance values and Nernst potentials vary across different types of neurons. Each of those conductances is in fact governed by one or more rate equation describing the states of opening and closing of the associated channel; these "gating" dynamics thus increase the dimensionality of the model. As in the case of the Integrate-And-Fire model, the Hodgkin-Huxley model has seen many vari-

ants emerging since its introduction, to incorporate additional conductances in the form of supplementary ionic species, adaptative terms, and more elaborate conductance functions. In Fig. 1.3, we plot the membrane potential $V(t)$ as a function of time when an action potential is emitted.

1.2.3 Other conductance-based models

The Integrate-And-Fire and Hodgkin-Huxley models represent only two of the best known conductance-based models describing the electric temporal activity of a cell, on which a plethora of alternate models have evolved to fit certain physiological contexts. The Integrate-And-Fire and Hodgkin-Huxley models stand quite far away from each other in terms of physiological precision. Since then, progress has been achieved using simpler versions of the Hodgkin-Huxley model, where some physiological aspects are set aside in order to get greater mathematical insight on the underlying mechanisms at work in the spiking process. This trade off between physiological precision and mathematical simplicity has proven to be quite successful in describing neuronal excitability and spike generation. The Fitzhugh-Nagumo model (1961) corresponds to a two-dimensional equivalent of the Hodgkin-Huxley model, where conductance dynamics has been replaced by an artificial recovery variable, and where the intrinsic non-linearities have been given a cubic polynomial form. The resulting two-dimensional dynamical system allows a full representation of the solutions in phase space, where potential instabilities caused by an external current may be both analytically and geometrically determined. The Fitzhugh-Nagumo model has been used to explain excitation block and anode break excitation.

In contrast to the simplification approach commonly used in conductance based models, more elaborated models have been developed to investigate the spiking behavior of neural cells in greater details. The software NEURON[53] allows a compartmental description of the neurons as a vast construct of sub-units which obey sets of dynamical laws. One can then build a three-dimensional model of

the cell, where the axon, membrane and dendrite are built out of individual compartments, which interact with each other. The resulting computational construct allows the monitoring of hundreds of physiological and chemical variables which evolve in real time, and obeying the constraints of the cell design.

1.2.4 Rate models

From the point of view of mathematical neuroscience, single-compartment models describe and hopefully predict the time evolution of a neuron. In most cases, the solution of these systems is a time series of the voltage as a function of time i.e. $V(t)$ which takes the form of successive jumps, called *spikes*. These sudden perturbations of the voltage occur at very precise times, corresponding to moments when the neuron emits action potentials. The action potentials convey a lot of information, encoded through their shape, but these depend on many variables that are not readily measurable. For instance, the level of activation of sodium-gated channels at some time t might not be recordable at all. Further, many dynamical variables may be subject to random fluctuations. Therefore, it might prove useful to extract computationally meaningful information from a neuron's behavior by means of some data sampling. The most common and simple way of doing this is to record solely the timing of the spikes emitted. The resulting representation of $V(t)$ is the firing history of the neuron and is called a *spike train*. A spike train $s(t)$ is a series of Dirac delta function located at the moments t_i when the cell fired:

$$s(t) = \sum_i \delta(t - t_i).$$

The spiking behavior of the neuron is fully determined by the quantity $s(t)$. This digital way of describing the behavior of a neuron is ideal for statistical and probabilistic descriptions of neurons. A main challenge in the analysis of spike trains is to get rid of their variability. Indeed, neural systems are intrinsically noisy. This implies that even in cases where identical stimuli are presented to

cells, they do not necessarily produce identical outputs. In order to predict the behavior of neural systems, one requires a higher reliability in the responses.

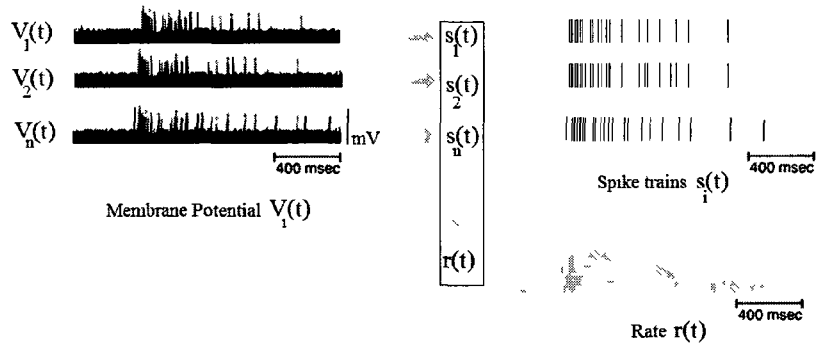

Figure 1.4: **Rate description of neural membrane voltages.** The membrane voltages $V_i(t)$ are first expressed in terms of spike trains $s_i(t)$, where the action potentials take the form of singular stereotyped events. Averaging as in Eq. (1.3) yields a rate description of individual cells or network.

Action potentials correspond to excursions of the somatic voltage that last for 1-5ms, while axonal and synaptic processes have much slower dynamics i.e. in the range between 10 ms and several seconds. On short time scales, the voltage of individual cells is subject to various sources of inputs and noise, which, as mentioned, influence the response of the cells. The two main sources of neural noise are random openings and/or closing of ion channels and synaptic inputs from by distal cells [48]. These fluctuations result in a great variability of the response pattern on several successive trials with the same stimulus. These variations might however be filtered and averaged out by slow synaptic components. Furthermore, if one considers a network of sufficient size, the average fluctuations of responses decreases towards zero, as long as the inputs given to the cells are not or only weakly correlated. Indeed, common neural inputs introduce correlations in the firing patterns of stimulated cells, which may cause or amplify differences between the responses. However, if the firing variability is sufficiently reduced, a smooth firing rate description may provide an accurate description of spiking activity. The panel of dynamical effects exposed by a

firing rate model exhibits a close proximity with that of spiking models [54]. It has been shown than the rate, on the top of specific spike timing, is also used for coding purposes [45, 55, 56]. Even though the exact mapping between spiking and rate models has not yet been exposed, several studies have shown that unless the inputs received by the cells are highly correlated, the two description share very common behavior [57, 56, 58, 59, 60].

As Fig. 1.4 illustrates, rtate models replace the spike train function $s(t)$ by a rate function $r(t)$, defined by

$$r(t) = \frac{1}{T}\int_{t}^{t+T} s(\tau)d\tau, \tag{1.3}$$

where T is a usually short averaging period. This quantity may be further averaged over several different cell responses i.e. over many $s_i(t)$ to obtain the rate description over a small population of cells. The most direct way of achieving a firing rate description of a cell's spiking activity is to use the output voltage profile $V(t)$ of a conductance-based model as in Eq. 1.1 or Eq. 1.2, for instance, and use the resulting spike train as an input for Eq. 1.3. In the context of steady-state systems, the firing rate obeys $r = f(I)$, where f is a bounded activation function, which oftentimes has the form of a sigmoidal function. Increasing pre-synaptic input current I will generate sustained spiking activity, until saturation is met, partly due to the recovery period of the neuron after a spike - also known as the refractory period. However, for time-dependent dynamics $I(t)$, the rate $r(t)$ is typically modelled as a linear process around the steady state relationship $r(t) = f(I(t))$, namely

$$\frac{dr(t)}{dt} = -r(t) + f(I(t)), \tag{1.4}$$

where I corresponds to the sum of inputs to the cell. It is also common to express post-synaptic voltages in conductance-based models by functions of the pre-synaptic rates. This assumption is motivated especially in the context of networks, where the neurons integrate a vast number of pre-synaptic inputs.

Combined with the filtering performed by the slow conductances and synaptic processes, a smooth pre-synaptic input function may represents well the signal integrated by the cell if the time scale is chosen properly. Indeed, the ability of Eq. 1.4 to accurately describe the evolution of the firing rate depends on the averaging period T on which the rate is computed, and further specifies the range on which the approximation $r(t) = f(I(t))$ holds. Further details may be found here [45].

1.3 Networks

Neurons form ensembles, and rarely take part in any process without the active contribution of many other neurons, which also participate in a information processing tasks .These networks are found throughout the brain, and are involved in all tasks performed by sensory, motor and cognitive systems. The neuron models seen in the previous section represent the neuron behavior as a complex process in which ions and protein pumps interact to generate action potentials. In the context of networks however, it is the wiring scheme between the neurons that determines the function of a network and dictates the appropriate weight given to individual activity patterns.

At the end of the axon lies the synapse, which constitutes a biochemical junction between two neurons. As the action potential propagates along the axon and reaches the pre-synaptic bouton, the potential fluctuation activates calcium channels. Calcium-sensitive vesicles are then activated and merge with the membrane, releasing neurotransmitter across the synaptic cleft. These neurotransmitters diffuse up to the post-synaptic receptors, located at the ends of the post-synaptic dentrites. The main transmitters found in the brain are glutamate and γ-aminobutyric acid(GABA). The transmission of glutamate activates excitatory receptors. These glutamate sensitive receptors (mostly AMPA and NMDA) increase the probability that the post-synaptic cell will emit an action potential given a pre-synaptic signal. GABA-sensitive receptors generally do

the opposite, that is to decrease the probability of post-synaptic firing. These connections are thus labelled inhibitory. Once the synaptic transmission has occured, the dendrites undergo post-synaptic spike reconstruction and relay the action potential up to the soma of the target cell.

This process, called the chemical synapse, is one of the few ways neurons connect to each other. Electrical synapses or "gap" junctions, which are physiological connections between cells at various points on the cellular body, play the same functional role: electrico-chemical signals travel from one cell to another. Synaptic connections create correlations between the states of the networks elements. In order to determine the state of a given neuron, one has to know the state of all cells with which there exists a connection. These cells may also share synaptic contact with others, thus exponentially increasing the amount of information required to determine the state of the members of the network. Synaptic connections vary greatly in strength and range, and are often *plastic* i.e. their properties evolve with time. As the neurons are very specific, so are the networks in which they evolve. The biological circuits are the result of active evolutionary pressure, which has shaped the physiology of the neural systems and optimized them to perform a specific task. From the functional standpoint, the scheme of connections, or *connectivity*, dictates the architecture of a network, on which subsequent dynamics will depend. Pre-synaptic inputs stimulating some cells in the system may influence the response of the full network.

As in the case of single neurons, the study of neural networks is subject to many different approaches, some of which take into account some details provided by physiology, and some do not. This has led the fields dealing with neural networks to undertake quite separate paths. The single cell models seen in the previous section describe the evolution of the somatic membrane potential as a function of incoming input currents, ion-channel activation and leaking currents. Network models incorporate signals coming from neighbouring units,

and model the transition from pre-synaptic inputs to post-synaptic responses. The amplitude of the pre-synaptic signals will depend on the architecture or connectivity profile considered.

1.3.1 Neural Nets

In contrast with the physiologically inspired and fine grained descriptions of the neuron like the Hodgkin-Huxley model, some models use abstract representations of the neurons, where the focus is on the computational and logical operations performed in ensembles. These functional models address high order cognitive issues like learning, memory, and pattern formation using networks built of simple interacting units.

Such functional representations of the neuron can be traced back to the McCulloch-Pitts model [61], describing the action potential transmission as a simple logical operation. The "neurode" (simplified version of the neuron) becomes little less than an binary operator that switches between "on" and "off" or "0" and "1" states. As all internal dynamics and extra-cellular influences are being neglected, the cell is implemented as a binary operator: if the input I is *larger* than a given threshold h, the state u of the cell is set to *active* ($u = 1$), and set to *silent* ($u = 0$) otherwise. Mathematically,

$$u = H(I - h), \tag{1.5}$$

where H is the Heaviside step function centered at 0. When a network of such cells is considered, the input I becomes the sum of the pre-synaptic inputs. The interaction between elements of such a network is commonly implemented via a *connexion matrix* W, for which the elements w_{ij} represent the weight of the synaptic coupling between the neurodes i and j. The pre-synaptic input I_i received at the i-th neurode is a weighted sum of the activities or states of all the units in the network, namely

$$I_i = \sum_j w_{ij} u_j . \tag{1.6}$$

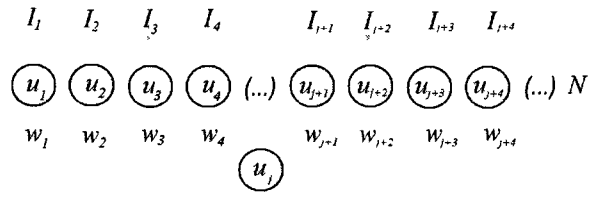

Figure 1.5: **McCulloch-Pitts network schematic.**

where the individual states are u_j. Combining Eq.1.5 and 1.6, we obtain an example of a one-dimensional neural net

$$u_i' = H(\sum_j w_{ij} u_j - h). \tag{1.7}$$

Equation (1.7) is called the McCulloch-Pitts network, and is illustrated in Fig. 1.5. Similar neural nets, like the *perceptron* [62], have been used since their introduction to model the most basic forms of learning. The perceptron is the simplest form of such networks, where the dynamics is constrained to a pre-determined output pattern. In this case, the strength of the connections between the members of the network changes according to some predefined rule (see [63]). Advances in neural nets theory, as in the case of the Hopfield model of associative memory [64] for instance, have made significant impacts on the artificial intelligence, statistical mechanics and computer science communities. For a good review of the early developments in neural nets and applications, see [65].

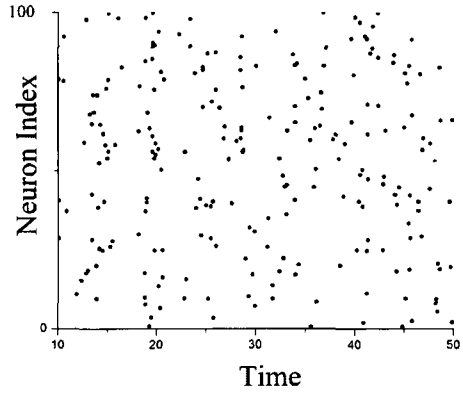

Figure 1.6: **Raster plot of an Integrate-and-Fire network of $N = 100$ cells.** In this example, the neurons are driven by some external noise and a minimal bias current.

1.3.2 Conductance-based networks

The ongoing development of computers gave access to important computational capabilities. In this context, the use of oversimplified cellular models, like the McCulloch-Pitts unit, becomes less relevant. Networks built of Integrate-And-Fire, Hodgkin-Huxley or even more elaborate neuron models is now common across the literature. In these computational networks, the equation for the time-evolution of the voltage contains inputs associated with pre-synaptic inputs. In the case of Integrate-And-Fire neurons, Eq. 1.1 may then be re-written as

$$C\frac{dV_j(t)}{dt} = \sum_i^N w_{ij} I_i(t), \tag{1.8}$$

where $I_i(t)$ is the pre-synaptic input at the j-th from the i-th neuron, where $i \neq j$ in a network of N cells. In this example, the synaptic weights are also labelled w_{ij}. Numerical simulations facilitate the analysis of large scale networks i.e. for large N, where it is possible to investigate the effects of various connectivity profiles and architectures on the input response of the cells. A specific network behavior is plotted in Fig. 1.6. In such a figure called a rasterplot, only the moments when a neuron fires are plotted. We thus see the individual spike

trains.

1.3.3 Neural Fields

The number of cells in real neural tissue is of the order of 10^3 to 10^5 individuals per millimetre cube (for estimates in the human visual cortex, see [66, 48]). At this scale, obtaining a blueprint of the three dimensional circuitry involved in action potential transmission is a task still far beyond the capabilities of experimentalists. Furthermore, real cells are systems subject to multiple noise sources, which may be hard or even impossible to monitor or to identify. While conductance-based networks may be used in conjunction with numerical experiments to test relatively large noisy networks ($n > 100$), these still do not approach the complexity of real neural systems, and do not give sufficient insight into the dynamical mechanisms responsible for the formation of activity patterns and into the information processing properties of biological tissue in general. These facts suggest to use another approach.

Neural fields are models that describe neural systems using coarse space and time graining. They are designed to consider a neural system as a spatio-temporal manifold on which a state variable, the mean firing rate or the mean membrane potential, evolve. Instead of looking at a network as interconnected nodes which possess individual yet correlated dynamics, a neural field lumps the neural activities into a single neural mass [67, 68]. This continuum approach of neural systems was proposed mainly by Wilson and Cowan[69, 70] who first designed a model where the state variable is the proportion of active cells. Later, Amari extended this approach to pattern formation problems [71].

The purpose of this different description scale is two-fold: 1. From the population perspective, the neural tissue is vast and each spatial location contains a large number of neural cells. It has been shown that the dendritic tree of neurons in most neural systems constitutes the more volumetric component [72]. Thus, on average, the spatial properties of the neural tissue are largely domi-

nated by axo-dendritic interactions. Local sub-networks are connected to each other via a complex circuitry of synapses, dendrites and axons, which form a spatially homogeneous domain. With this formulation, the neural tissue forms an excitable medium, through which the activity propagates. 2. On much slower time scales, the neural temporal dynamics are vastly dominated by the synaptic processes. Random fluctuations typically operate on the shorter time scale of the soma, and are averaged out from the state variable, which takes the form of mean firing rates. The resulting formalism should then be deterministic (for the study of stochastic neural fields, see [12, 73]). Neural fields have been used to reproduce collective activity patterns monitored via field potentials [44]. Spatially structured solutions of neural field equations have also been applied to understand cortical phenomena observed through EEG imaging, like visual hallucination, rhythms and short term memory [74, 68, 75].

Neural field equations

We will now derive a typical neural field equation from the spike and rate descriptions outlined in Section 1.3. By doing this, we will follow the lines of some reviews available [76, 68, 72, 60, 74, 77, 44, 78, 75]. A neural field describes a scalar function $u(\xi, t)$ corresponding to the spatio-temporal state of the mean somatic membrane potential, or activity, taken amongst a sub-network of cells, located at position ξ and at time t. The post-synaptic potential $u(\xi, t)$ is determined by a temporal convolution of the total pre-synaptic potential function $U(\xi, t)$ over a synaptic response function $\eta(t)$. The convolution operator is denoted by $*$, and is defined for two time-dependent functions $a(t)$ and $b(t)$ by $a * b = \int_{-\infty}^{t} a(t-s)b(s)ds$. The function η is also called a synaptic filter, and is a solution of models describing the neurotransmitter vesicles opening probabilities [45]. It models the post-synaptic response to a stereotyped delta function-shaped action potential. A sudden neurotransmitter release facilitates the signal transmission until enzyme degradation causes an exponential decrease in synaptic conductance. In Fig. 1.7, two common synaptic response functions

are plotted, namely the exponential and alpha functions.

In an infinite domain, the post-synaptic potential $u(x,t)$ at $\xi = x$ may be

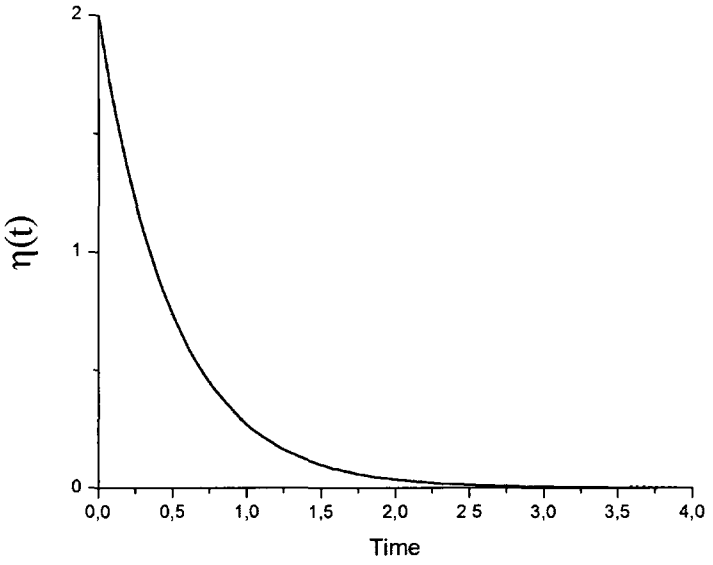

Figure 1.7: **Synaptic response functions.** The response functions model the post-synaptic response to a delta-function action potential, The membrane decay follows a rapid increase in post-synaptic potential (PSP) with time constant a. The bold line plots the exponential function: $\eta(t) = ae^{-at}$. The dashed line plots the alpha function: $\eta(t) = a^2te^{-at}$. Both functions are equal to 0 whenever $t < 0$ The synaptic time scale was chosen to be $a = 2$ in both cases

expressed as a function of the total pre-synaptic activity $U(x,t)$ accumulated since $t = -\infty$,

$$u(x,t) = (\eta * U)(x,t) = \int_{-\infty}^{t} \eta(t-s)U(x,s)ds. \tag{1.9}$$

The post-synaptic field u depends on the local and non-local interactions between spatially distant sources of potentials, and is entirely determined by the

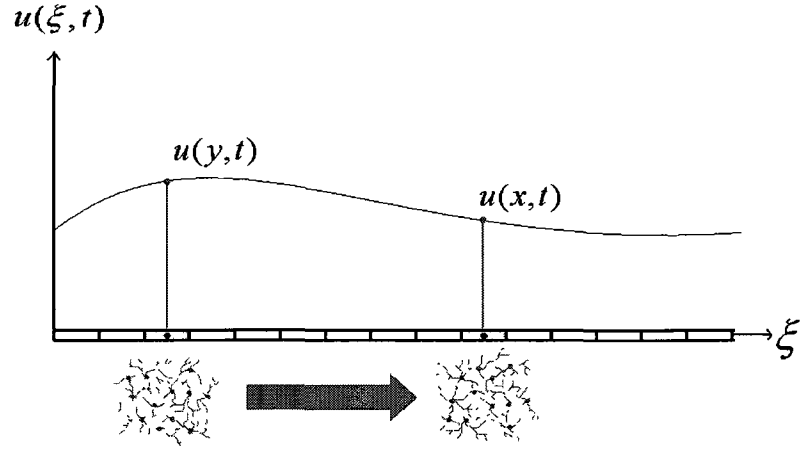

Figure 1.8: **The mean somatic membrane potential as a continuous variable.** The mean somatic membrane potential $u(\xi, t)$ is derived from the synaptic interaction between all possible neural sites. The field at $\xi = x$ is determined by integrating all the contributions from all ξ.

sum of the synaptic interaction interactions that the units share with their surroundings. These define the transition between axonal pre-synaptic activities $u(y, t)$, initiated at some position $\xi = y$, and post-synaptic potentials $u(x, t)$ at $\xi = x$ (see Fig. 1.8). Consequently, the total pre-synaptic potential $U(x, t)$ corresponds to the sum of all action potentials received at location x from across the domain,

$$U(x,t) = \int_{-\infty}^{\infty} w(x,y) \sum_{i} \delta(t - t_i(y)) dy, \tag{1.10}$$

where $w(x, y)$ is the connectivity function, also called kernel or anatomy of the network. It defines the polarity (excitatory or inhibitory) and weight given to a specific synaptic connection as a function of the location where the spikes were initiated (y) and where they were integrated (x). The connectivity represents how the network integrates signals. In homogeneous systems, connectivity typically takes the form of an exponential,

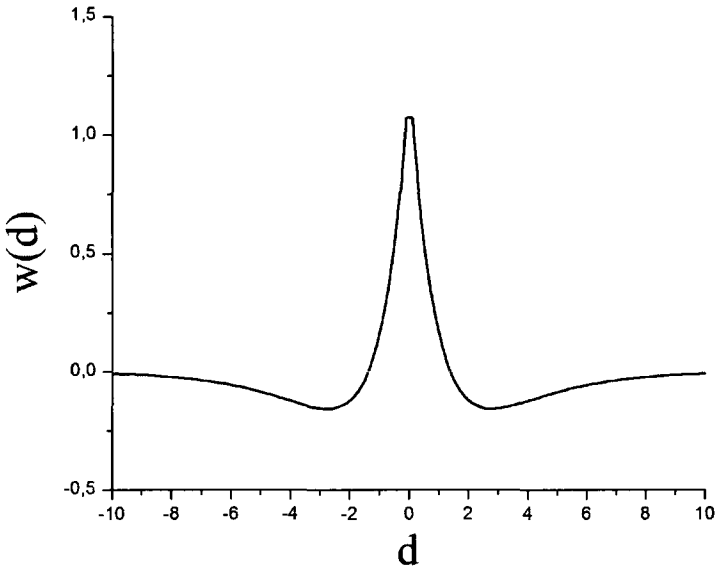

Figure 1.9: **Mexican-Hat connectivity kernel.** Center-surround connectivity profile produced by the difference between exponentially shaped kernels as in Eq. (1.11) for $g(x,y) = -|x-y| \equiv -d$. An excitatory kernel is subtracted by an inhibitory kernel, so that signals synaptically transferred very close to the center of the receptive field ($d = 0$) are amplified, while more distant ones are inhibited. This shape refers to local excitation-lateral inhibition connectivities, used in many neural field studies. Here, the excitatory kernel has a range of $\sigma = 1$ while the inhibitory kernel has a range of $\sigma = 2$. The amplitude for both kernels is the same i.e. $A = 5$.

$$w(x,y) = \frac{A}{2\sigma} e^{g(x,y)/\sigma}, \tag{1.11}$$

where A and σ are the amplitude and range of the connections, respectively. $g(x,y)$ is some function of the spatial variables x and y. A common choice for w is a difference of exponentials which results in the so called "Mexican-Hat" connectivity, as depicted in Fig. 1.9. It represents the network connections with local excitation but distal inhibition, a profile close to the "center-surround" spatial organisation of receptive fields in the visual system. In this case, the function g expresses the distance between neural sites as the variable defining the shape of the kernel i.e. $g(x,y) = -|x-y|$. Such kernels lead to homoge-

neous systems, which are also translationally invariant. Real neural systems are however not homogeneous, and thus studies have begun on general or statistical distributions of kernels [1], while oftentimes domain inhomogeneities are modeled with the use of some additive and space-dependent term [79, 80].

It may be shown [54] that if the action potential duration is very small compared to the synaptic time scale, the spike train may be well characterized by a smooth firing rate function of the mean somatic membrane potential across the sub-units i.e.

$$\sum_i \delta(t - t_i(x)) \approx f(u(x)). \tag{1.12}$$

The function f, called firing rate function, is determined from single cell dynamics and captures the frequency tuning properties of spiking models [81]. While it is known that the function f is shaped by the temporal fluctuations of the input currents, it is here considered to be constant. A common choice is a sigmoidal shaped function, as depicted in Fig. 1.10. The choice of this particular function is motivated by the frequency tuning properties of neural cells. The mapping that exists between firing rate and input amplitude (commonly called *f-I* curve) takes the form of a sigmoidally shaped function, where the firing rate varies between zero and some maximal value. Other non-linear functions do map this relationship as well, but make the analytics more involved. The firing rate response function is parameterized by the threshold h around which the firing rate increases significantly, and the gain β, defining the slope at the inflexion point. Combining Eq. (1.12) and (1.10), we obtain a self-consistent equation of the activity across the domain

$$u(x,t) = \int_{-\infty}^{t} \eta(t-s) \int_{-\infty}^{\infty} w(x,y) f(u(y,s)) dy ds. \tag{1.13}$$

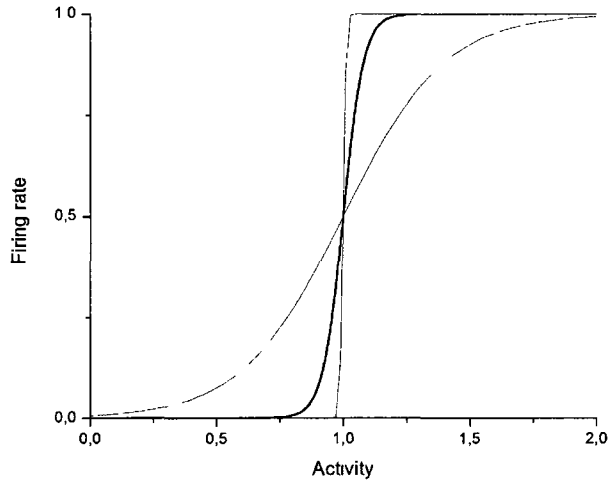

Figure 1.10: **Firing rate functions reproducing the frequency tuning curves of spiking neurons for various gains.** The curves represent the sigmoidal function $f(u) = (1 + exp(-\beta(u-h)))^{-1}$. The bold curve is such that $\beta = 25$. If the gain is decreased to $\beta = 5$, a considerably smoother version of the curve is obtained. A curve for $\beta = 150$ is also shown, where the firing rate function may be approximated by a Heaviside step function i.e. $f(u) \approx H(u-h)$ with $H(u) = 0$ whenever $u < h$ and $H(u) = 1$ otherwise. The threshold chosen here is $h = 1$.

The above equation is a neural field model for a single neural population and expressed in integral form. From the stability analysis point of view, it may be convenient to express Eq. (1.13) as a integro-differential equation. Differentiating with respect to time gives

$$\frac{\partial u(x,t)}{\partial t} = \frac{\partial}{\partial t}\int_{-\infty}^{t} \eta(t-s)\int_{-\infty}^{\infty} w(x,y)f(u(y,s))dyds. \qquad (1.14)$$

Applying Liebnitz rule yields

$$\frac{\partial u(x,t)}{\partial t} = \int_{-\infty}^{\infty} w(x,y)[\eta(0)f(u(y,t)) + \int_{-\infty}^{t} \frac{d}{dt}\eta(t-s)f(u(y,s))ds]dy. \quad (1.15)$$

For an exponential synaptic response function i.e. $\eta(t) = ae^{-at}$ for $t > 0$, we obtain

$$\frac{\partial u(x,t)}{\partial t} = \int_{-\infty}^{\infty} w(x,y)[af(u(y,t)) - a\int_{-\infty}^{t} \eta(t-s)f(u(y,s))ds]dy, \quad (1.16)$$

which may be simplified with Eq. (1.13) into

$$\begin{aligned} \frac{\partial u(x,t)}{\partial t} &= a\int_{-\infty}^{\infty} w(x,y)f(u(y,t))dy - a\int_{-\infty}^{\infty}\int_{-\infty}^{t} w(x,y)\eta(t-s)f(u(y,s))dsdy \\ &= a\int_{-\infty}^{\infty} w(x,y)f(u(y,t))dy - au(x,t), \end{aligned} \quad (1.17)$$

such that we obtain Eq. (1.13) in a differential form

$$\frac{1}{a}\frac{\partial u(x,t)}{\partial t} = -u(x,t) + \int_{-\infty}^{\infty} w(x,y)f(u(y,t))dy. \quad (1.18)$$

Various forms of Eq. (1.18) have been studied, leading to a wide variety of dynamical effects. The structure of the spatial kernels give rise to stable localized solutions, like fronts and bumps [44, 1, 82, 74, 83]. Introduction of time delays due to finite signal propagation speeds results into waves and breathers [80, 84, 85], while kernel inhomogeneities perturb the stability of activity patterns [86]. As a natural extension of this model, two populations networks have also been investigated [69, 87, 85, 88]. The main advantage neural fields have is that the existence and stability of solutions may be proven analytically, which is not possible in most noisy conductance-based models. In particular, the stability of spatially structured solution can be performed via the use of Evans functions in the limit when the firing rate function is a Heaviside step function [89, 90].

1.4 Sensory Systems

Sensory systems are the primary relays of information processing pathways from the outer world up to the brain. They typically form the transition between cellular receptors and higher brain centers involved in perceptive tasks. These specialized "support" systems provide organisms with the necessary information about their environment to perform various behavioral tasks. Through the various senses, like vision, audition and touch, sensory information is processed and integrated by various parts of the brain. This information is first initiated by sensory stimuli, to which a sensory system, via specialized receptors, is attuned. The various stimulus modalities evoke neural responses of cells with respect to their receptive field geometry. A receptive field of a cell is defined by the array of receptors to which it responds. How receptive fields are organized, along with where they project, determines the basic network architecture on which more elaborate forms of circuitry may occur.

Sensory systems form a class of relatively simple neural systems. As a first relay to the high level brain centers, the architecture and physiology of sensory systems is typically well known. Cellular recordings may be correlated with external signals controlled by the experimenter. This is not the case in cortical systems for instance, where a given cell might be receiving inputs from various sources, not necessarily linked solely to the outer world. Further, the relative similarity of these systems across various organisms suggests that much of the sensory processing tasks are performed at these early stages, and that the high degree of specialization sensory systems demonstrate is an attribute of those circuits. As such, sensory systems are a subject of choice to study general neural systems. Thus, sensory neuroscience addresses the questions: how is sensory information integrated by neural systems? How are the information processing capabilities of sensory system linked to circuit shape and features?

In the following sections, we will review the main properties and architecture of the visual and electrosensory systems, to set the stage for the derivation of our

general model. The review of the visual system refers to the detailed discussions found in chapter 14 of [49] and [91]. The review of the electrosensory system follows [20], [22] and the excellent online introduction and literature review [92].

1.4.1 Vision

The visual system deals with the processing of optical information perceived by an organism about its surroundings. While the spatial and temporal content of a stimulus is responsible for determining shape and movement, the frequency and intensity of the light perceived confers additional information regarding color and brightness. This combined information is vital to a visually dependent organism to behave in its environment and make decisions. The extraction of these features from a visual scene is performed by highly specialized neural circuits that extend from the bottom of the retina up to the visual cortex starting with the optic nerve. From there, the visual system must build and identify representations of objects and determine their location.

A schematic representation of the retinal pathway is shown in Fig. 1.11. The first stage of visual perception occurs in the response of several types of photoreceptors, which are attuned to specific attributes of the visual signal, like the frequency or amplitude for instance. In humans, the photoreceptors populate the inner surface of the eye, and are distributed according to their sensitivity. After activation by a visual stimulus, the photoreceptors project through several layers of cells, concentrically superposed on one another. These cells, like the horizontal, amacrine and bipolar cells, all possess very specific connection polarity and receptive field structures. The activity is transmitted to successive layers post-synaptically with either an inhibitory or an excitatory effect. Indeed, synaptic connections within the retinal circuit are either excitatory, which induce a hyperpolarizing post-synaptic response (ON type cells) or inhibitory, with a depolarizing post-synaptic response (OFF type cells). The ON and OFF response pathways form almost parallel vertical circuits. These are initiated by the synaptic response of bipolar and horizontal cells to photoreceptor hyperpolarization. The presence of these two asymmetrical neural response types,

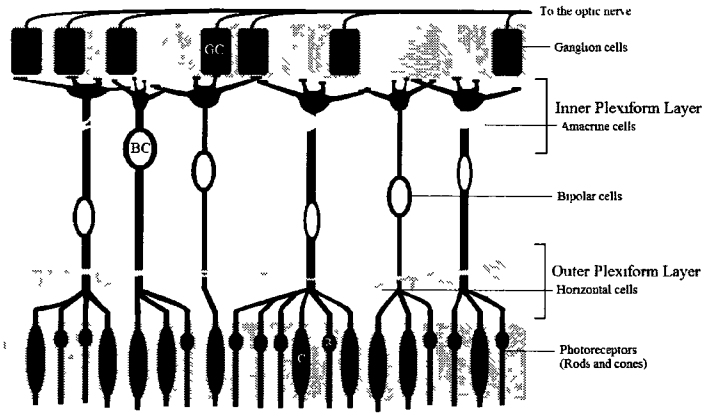

Figure 1.11: **Schematic of the multi-layered structure of the retina.** The visual information encoded travels upwards. Surprisingly, the photodetectors (rods (R) and cones(C)) are located at the very bottom of the retina. The outer plexiform layer is populated by the horizontal cells(HC), which synapse to distant bipolar cells(BC), resulting in large receptive fields of the ganglion cells(GC). Amacrine cells(AC) perform a similar task in the inner plexiform layer, and further enhance the contrast of the responses. The responding ganglion cells project to higher processing centers of the visual system via the optic nerve .

conveyed by independent pathways, is responsible for the parallel processing performed in most sensory systems, as in the retina. These separate circuits operate and integrate receptor responses and generate dual signals, which both contain meaningful information about a visual scene Sensory signals are processed by the successive layers and reach the ganglion cells, which digitize an analog signal pattern (light intensity map in two dimensions) up to the visual cortex.

Feedback also plays an important role in input encoding. This is especially apparent in the outer plexiform layer, where horizontal cells receive information from photoreceptors (either cones or rods) and transmit to bipolar cells. Horizontal cells are characterized by large surface gap junctions between neighbouring and distant dendrites of other horizontal cells These allow a lateral

flow of molecules (dopamine retinoic acid and nitric oxide) and ions (hydrogen) present in the intra- and extra-cellular medium, thus contributing to the propagation of the response of horizontal cells. The resulting conductivity allows the electrical activity to flow through a lateral pathway, and hence contributes to a very large horizontal cell receptive field (>1mm). Although horizontal cells are post-synaptic to cones, hemi-gap junctions are believed to transmit information back to the photoreceptor, which feedbacks to the horizontal cell.

Inter-laminar feedback shapes receptive fields. The combined action of both the response of the other laterally distributed ON or OFF horizontal cells and the cone photoreceptor feedback gives birth to the center-surround spatial organization of the receptive field of ganglion cells. As a stimulus is moved from center to the boundaries of a ON-type ganglion cell receptive field, the response shifts from excitatory to inhibitory. This ON-OFF spatial antagonism is also called Mexican-hat connectivity. The exact opposite occurs for OFF-type ganglion cells. This is because glutamatergic synapses tend to be less distal than GABAergic ones (this point is still debated, see [3] and references therein).We also observe feedback loops within the inner plexiform layer, where amacrine cells, whose functional role is similar to horizontal cells but less understood, make lateral electrical synaptic connections with the rod vertical pathway, while still participating vertically in the rod pathway through chemical synapses with rod ganglion cells. The presence of these lateral connections introduces correlations between the signals conveyed by the ON and OFF pathways. The density of rod and/or cone photoreceptors as well as the extent of the lateral projections vary within the retina, so that the receptive field size is minimal near the center of the retina (called *fovea*), resulting in a high resolution.

Other sources of feedback in the visual system exist. In the outmost layer of the retina, ganglion cells synapse to various parts of the brain through the optic nerve. These sites are involved in perceptive tasks, like the saccade movement of the eye, the pupil reflex, and many others. Through the visual pathway, one

also finds a projection from lateral geniculate nucleus (LGN) in the thalamus to the primary visual cortex (V1). Feedback from V1 back to LGN has been involved in the modeling of high level encoding tasks, generating network oscillations and synchrony.

The research on the visual system is a very broad topic. In the context of neural computation, models have tried to reproduce the response of the retina via representations of the multiple lateral and inter-laminar interactions. Motion, shape and color coding also represent important challenges. From the network perspective, one of the major goal is to put forward novel effects due to the topography of the ganglion cell receptive fields, and how the geometry of the connections is mapped to higher brain centers by the long-range connections. Further, the effects of various feedback loops, especially from LGN to V1 in the visual cortex, on the activity profiles of the neural populations are still subject of active research. These information theoretic predictions are tested not only with spike trains, but also various forms of data imaging, like EEG. For excellent reviews of the early modeling trends in the visual system and their mathematical foundations, see [93, 67]. The thalamo-cortical system has inspired numerous neural and mean field approaches to identify the mechanisms by which activity patterns appear on the surface of the cortex.

This excursion into the visual system has a specific purpose, namely to highlight salient circuit features shared by the visual and electrosensory systems: large scale networks, spatially organized receptive fields, local (inter laminar) versus global (LGN-V1) recurrent connections and the simultaneous encoding performed by parallel ON and OFF-type pathways. These circuit traits also participate in the processing of sensory signals in the electrosensory system, which is the main focus of this thesis.

1.4.2 Electroreception

The visual sytem shares many properties with other senses. The electrosensory system is present in a subgroup of the teleost fishes called the gymnotiforms. These fishes are capable of producing a self-generated electric field around their body, which they use to scan their environment and communicate. Across the various sub-species of fish using electro-reception, *Eigenmannia virescens* and *Apteronotus leptorhynchus* have well known neurophysiology, gathered through many anatomical, behavioral and physiological studies (see [22, 24, 20, 92] and references therein). The *electrosensory lateral line lobe* (ELL) constitutes the first relay in the sensory pathway of the weakly electric fish. All electrosensory information concerning the environment the fish obtains via the receptors found on the skin converge to this specific neural structure, located at the back of the brain. The ELL shares many similarities with the main processing units of the visual and auditory systems. The relative physiological simplicity and small size of the ELL makes it a candidate of choice in the analysis of more complex sensory encoding devices in general. The weakly electric fish produces a wave-type electric field via the electrical organ discharge (EOD), where the electrical influx is caused by the sudden discharge of modified motor neurons. The alignment and discharge timing of these motor neurons is responsible for the temporal structure of the emitted signal, which in the case of *Apteronotus leptorhynchus* is close to a sine wave oscillating with a frequency of 600-1300Hz [24, 20].

The communication and location tasks are initiated by the response of ampullary and tuberous electroreceptors located over the skin of the fish. Nearby objects or perturbations of the EOD will affect the conductivity of the water and alter the response of the receptors. Two types of afferents encode for frequency (T-units) and amplitude (P-units) of the electroreceptor responses. The ELL, located at the back of the brain, is divided into four segments: the medial segment (MS), the centro-medial segment (CMS), the centro-lateral segment (CLS) and finally the lateral segment(LS). Receptor afferents project to each of

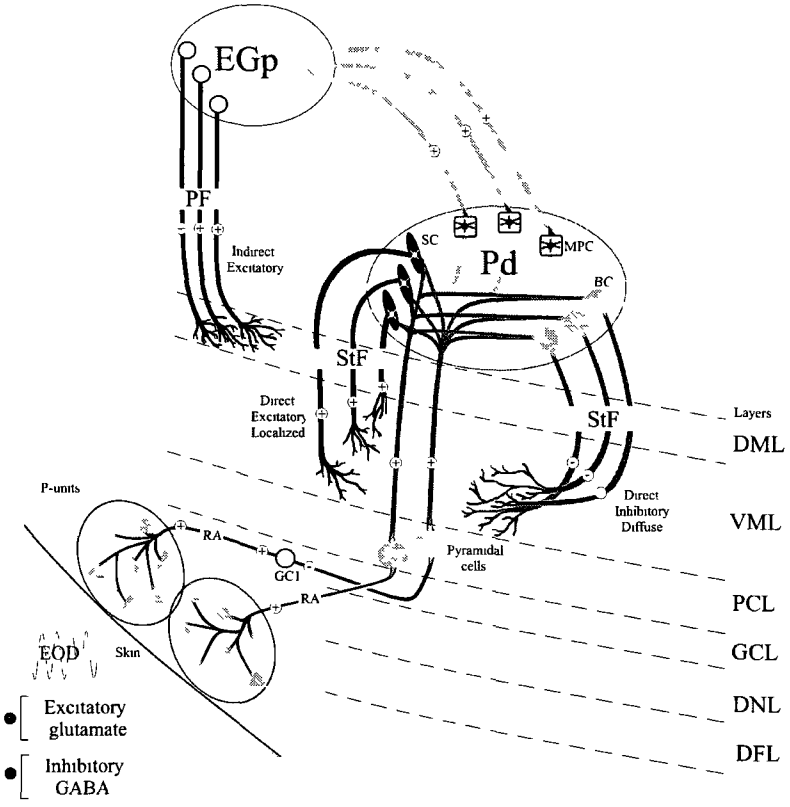

Figure 1.12· **Coarse circuitry of the electrosensory lateral line lobe (ELL).** Each synaptic connection is labelled by either a plus (+) or minus (-) sign, to represent the polarity of the projection, either excitatory or inhibitory, respectively. . Circles located on the bottom of the figure overlap many P-units, to represent the pyramidal cell receptive fields Only a few cells are depicted in each structure to represent numerous populations. See main text for acronyms.

those segments, preserving the topographic alignment of the electroreceptors.

The segments have distinct input processing properties [23, 29], but each possess an identical structure. A schematic of the ELL circuitry involved in the encoding of P-units afferents is illustrated in Fig. 5.5.1. Similarly to the retina, each of the ELL segments is organized in a laminar fashion, and the information propagates upward. The Deep Fiber Layer (DFL) and the Deep Neuropil Layer

(DNL) contains the receptor afferent (RA) axons and the axonal connections with the granular interneurons, located in the Granular Cells Layer (GCL). P-units synapses are glutamatergic, so that the output from the electroceptors is excitatory. The interneurons (GC1-2) invert the polarity of the afferent input and project an inhibitory signal to the pyramidal cells (BP). They are also responsible for the inhibitory surround structure of the pyramidal cell's receptive fields. All pyramidal cells are grouped in the Pyramidal Cells Layer (PCL); those that synapse directly with the glutamatergic afferents are labelled E-cells, while those that connect with the granular interneurons are labelled I-cells. When the input voltage increases, E cells increase their firing rate, while I cells are inhibited and reduce their firing rate. These cells can be identified with ON and OFF cells found in the visual system. These two cell types are responsible for a divergence in the upward stream in sensory information processing, resulting in the ON and OFF parallel pathways. Both E and I pyramidal cells project excitatorily to the Nucleus Praementialis Dorsalis (Pd), built of stellate (SC), bipolar (BC) and multipolar cells (MPC). Stellate and bipolar cells project back to the PCL, creating a direct feedback pathway [94, 22]. Stellate cell projections are glutamatergic, and further are spatially localized, meaning that their synaptic terminations end very close to the site where the initial signal was emitted by the pyramidal cells. Bipolar cells feedback is GABAergic but is not spatially profiled, and affects many pyramidal cells. Both stellate and bipolar signals from the Pd propagate back to the pyramidal cells via the Stratum Fibrosum (StF), and synapse in the Ventral Molecular Layer (VML). An indirect feedback pathway also exists. Multipolar cells of the Pd project excitatorily to the Eminentia Granularis Pars Posterior (EGp). Via the Parallel Fibers (PF), a glutamatergic feedback signal ends in the Deep Molecular Layer (DML), and affects the discharge pattern of the pyramidal cells.

In this thesis, we will be interested in modelling the dynamics of the pyramidal cells, were our network architecture will closely follow the one we just described.

Chapter 2

Model Derivation

The goal of our model is to analyze the sensory processing features of a neural microcircuit corresponding to the electrosensory lateral line lobe (ELL) of the weakly electric fish. This is done by describing the behavior of the cells populating the pyramidal cell layer, when the system is subject to spatio-temporal stimulation. In this section, we will derive the model we study in Chapter 3, 4, 5 and 6, based on physiology of the ELL. We will thus follow Section 5.5.1 closely, along with the relevant references which will be cited along with the text. In Section 2.1, we will build our model step by step, including the most salient features of the ELL circuitry. In Section 2.2, we will outline the calculations used in determining the equilibrium states and their stability.

2.1 Model

As outlined in Section 5.5.1, the ELL is subdivided into three sensory processing segments: CMS, CLS and LS. Although each of these shows different frequency tuning properties and receptive field geometry, they all share an equivalent morphology, where the skin electroreceptors are topographically represented [35, 23, 29]. Sensory afferents trifurcate and project in each of the segments. Our model comprises a single segment, corresponding to a one-dimensional man-

ifold Ω, taken as a subset of $\mathbb{R}^1$. We are thus mapping the 2D surface of the skin to a one-dimensional line, and it is natural to take this line in the rostro-caudal direction, i.e. in the head-to-tail direction in which the fish swims. The parameter $x \in \Omega$ determines the spatial location of recordings on the segment within the pyramidal cell layer. On the perspective of large scale nets (see Section 1.3.3), each site contains a sub-network (or units) of cells, within which a very large number of dendrites, synapses and cellular bodies are found. These units line up to form to whole domain, so that the neural tissue forms a continuous medium [71, 72, 74, 68].

According to the receptive fields modalities, p-units afferents project to the pyramidal cell layer via a parallel path from the skin electroreceptors up to the sensory layer. For simplicity, we assume that the sensory signals are stimulating the pyramidal cells directly for ON cells and via an interneuron for OFF cells (see below). The response of a pyramidal cell is monitored by looking at the time evolution and spatial distribution of the mean somatic membrane potential or activity, across the domain Ω. This quantity corresponds to the scalar field $u(x,t)$.

The pyramidal cell layer is populated by ON and OFF cells. These correspond to E- and I-type cells found in the literature. The respective fraction of ON and OFF cells in the network is denoted by α_{on} and α_{off}, such that $\alpha_{on} + \alpha_{off} = 1$. Stimuli are processed by two parallel sensory pathways. ON pyramidal cells are post-synaptic to p-units afferents. They respond to excitatory (resp. inhibitory) inputs by increasing (resp. decreasing) their firing rate. In contrast, OFF pyramidal cells are innerved by interneurons located downstream in the granular cell layer. These interneurons relay the afferent signals up to the OFF cells by inverting the polarity of the stimulus; OFF cells are excited (resp. inhibited) by inhibitory (resp. excitatory) signals. Aside from input response, ON and OFF cells have equivalent dynamics. Given some pre-synaptic stimulus $I(x,t)$, the post-synaptic potentials PSP_j for $j = ON, OFF$ at the pyramidal cell layer are

given by

$$PSP_{on}(x,t) = \eta_{on} * I(x,t)$$

$$PSP_{off}(x,t) = \eta_{off} * \mathcal{I}[I(x,t)],$$

where $*$ is a temporal convolution as in Eq. 1.9 and $\mathcal{I}$ stands as the interneuronal operator, specific to the OFF pathway. The pre-synaptic filtering made by the interneuron is here omitted. The synaptic response functions are labelled with respect to the pathway they are in, namely by $\eta_{on}(t)$ and $\eta_{off}(t)$ for ON and OFF pathways respectively. Many cells in the visual system respond maximally in the dark [91, 47]. Experimental results in the ELL have shown that E and I cells do not always share the same baseline firing rate [35, 23, 29]. Consequently, we make the hypothesis that the operator $\mathcal{I}$ is linear to first order such that it may be approximated by $\mathcal{I}(u) \approx V_o - u$, where V_o is the spontaneous activity of the OFF cells. This parameter accounts for the difference in baseline activities of ON and OFF cells.

The state variables of our model are $u_{on}(x,t)$ and $u_{off}(x,t)$, corresponding to the activity of ON and OFF cells at location x and time t. It has been shown that very few lateral connections exist within the pyramidal cell layer, where the activity propagates upstream in a parallel fashion to higher nuclei [22]. Thus, no activity propagates laterally between neural sites. To this point, the activity of the ON and OFF pyramidal cells is structured by sensory stimuli:

$$\begin{aligned} u_{on}(x,t) &= \eta_{on} * I(x,t) \\ u_{off}(x,t) &= \eta_{off} * [V_o - I(x,t)]. \end{aligned} \tag{2.1}$$

As shown in Fig. 2.1, pyramidal cells project to higher nuclei (Pd and EGp), from which they receive delayed feedback. We focus on the direct feedback pathway from the Pd as in [32] . As illustrated in Figure 5.5.1, the direct feedback pathway is divided into two components: pyramidal cell projections to bipolar cells feedback to the sensory layer with inhibitory synaptic connections,

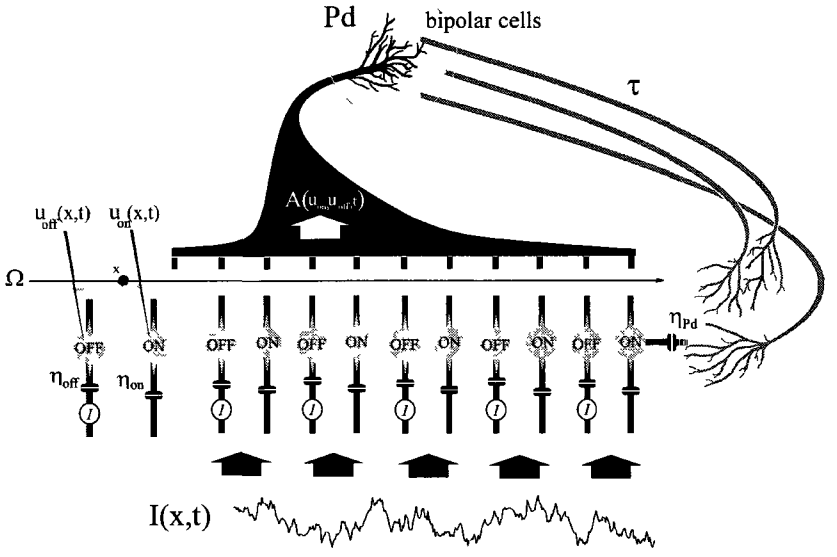

Figure 2.1: **Idealized circuitry of the ELL.** The sensory layer is populated by ON and OFF pyramidal cells across the spatial extent Ω of the segment. ON cells receive the input directly, while OFF cells receive a mirror image of the input, inverted with respect to their baseline activity V_o. ON and OFF cells activity are denoted by $u_{on}(x,t)$ and $u_{off}(x,t)$, respectively. Pyramidal cells receive and relay spatio-temporal stimuli up to a higher nucleus, where single site activities are lumped into a neural aggregate $A(u_{on}, u_{off}, t)$. Bipolar cells synapse back to the pyramidal cell layer via delayed connections.

while stellate cells feedback is glutamatergic and thus excitatory. The feedback from the bipolar cells is spatially diffuse, and will be the focus of our study. From the pyramidal cell layer up to the Pd, the firing activity of ON and OFF populations across the network is lumped into a single neural component,

$$A(t) = \int_\Omega dy \Sigma_{N_{on}(y)} s_{on}(y)(t) + \int_\Omega dy \Sigma_{N_{off}(y)} s_{off}(y)(t), \qquad (2.2)$$

where $N_{on}(x)$ and $N_{off}(x)$ are the number of ON and OFF cells at location x. $s_{on}(x)(t)$ and $s_{off}(x)(t)$ are the ON and OFF cell's spike trains at location x. The Σ symbol represents the sum over all the spike trains of all the cells at a given spatial location. The domain being continuous, we use here an integral

instead of a series to sum over the sub-units.

Aggregated activities are synaptically transferred back to the pyramidal cell layer via the SfF, without spatial modulation and after a time lap τ. This time interval accounts for the finite axonal propagation speed of action potential, and for the processing of signals by the bipolar cells. The time delay τ and synaptic time scales are considered to be large compared to the individual action potential durations, so that the spiking activity may be replaced by a smooth firing rate function of the mean membrane voltage i.e. $s(t) = f(u)$. Thus, Eq. (2.2) may be written as a non-weighted sum over the relative proportions α_{on} and α_{off} of ON and OFF cells

$$A(u_{on}, u_{off}, t) = \alpha_{on} \int_{\Omega} dy f[u_{on}(y,t)] + \alpha_{off} \int_{\Omega} dy f[u_{off}(y,t)]. \tag{2.3}$$

The firing rate function f determines the frequency tuning properties of single neural sites. It maps the firing frequency response to input currents. In this thesis, it is defined by

$$f(u) = \frac{1}{1 + e^{-\beta(u-h)}}, \tag{2.4}$$

with a gain of β and threshold h. As opposed to many studies on continuous domains, Eq. (2.3) is spatially independent; no integration kernel modulates the projection of feedback activity. Thus, our model has a "global" or "all-to-all" feedback profile.

The recurrent component is branched to the pyramidal cells somata with either GABAergic ($k = -1$) or glutamatergic ($k = 1$) connections. The bipolar and stellate projections are mediated by the response function η_{Pd}, through which we obtain the post-synaptic potential according to the signal initiated at the Pd. Combining Eq. (2.1) and Eq. (2.3) we obtain

$$\begin{aligned} u_{on}(x,t) &= \eta_{on} * [I(x,t)] + \eta_{Pd} * [kA(u_{on}, u_{off}, t-\tau)] \\ u_{off}(x,t) &= \eta_{off} * [V_o - I(x,t)] + \eta_{Pd} * [kA(u_{on}, u_{off}, t-\tau)]. \end{aligned} \tag{2.5}$$

Note that the aggregate A is here multiplied by the feedback polarity k, to represent the inhibitory or excitatory nature of the Pd-ELL connections. By changing the value of k within the interval $[-1, 1]$, we are modifying the amount of excitatory versus inhibitory feedback (See Chapter 3). Excitatory and inhibitory recurrent connections lead to completely different behavior, which are summarized in Section 2.3 (see also Chapter 4). The inhibitory case (i.e. $k = -1$) will be the focus of most this study because of the dominance of the bipolar inhibitory feedback, but we nevertheless keep the parameter open here.

If we assume that all synapses involved in this circuit are identical and obey the same dynamics i.e. $\eta_{on} = \eta_{off} = \eta_{Pd} = \eta$, Eq. (2.5) becomes

$$\begin{aligned} u_{on}(x,t) &= \eta * [I(x,t) + kA(u_{on}, u_{off}, t-\tau)] \\ u_{off}(x,t) &= \eta * [V_o - I(x,t) + kA(u_{on}, u_{off}, t-\tau)] \end{aligned} \tag{2.6}$$

For exponential synapses i.e. $\eta(t) = ae^{-at}$, $a \in \mathbb{R}$, applying Liebnitz rule as in Section 1.3.3 yields network dynamics in integro-differential form

$$\boxed{\begin{aligned} (1 + a^{-1}\partial_t)u_{on}(x,t) &= kA(u_{on}, u_{off}, t-\tau) + I(x,t) \\ (1 + a^{-1}\partial_t)u_{off}(x,t) &= kA(u_{on}, u_{off}, t-\tau) + V_o - I(x,t) \end{aligned}} \tag{2.7}$$

This is the model that will be analyzed in this thesis.

2.2 Steady State Analysis

ON and OFF populations reach steady activities whenever $\partial_t u_{on}(x,t) = \partial_t u_{off}(x,t) = 0$. Without stimulation, Eq. (2.7) becomes spatially independent. Steady states

$(\bar{u}_{on}(x), \bar{u}_{off}(x))$ are implicitely determined by

$$\begin{aligned} \bar{u}_{on}(x) &= kA(\bar{u}_{on}, \bar{u}_{off}) \\ \bar{u}_{off}(x) &= kA(\bar{u}_{on}, \bar{u}_{off}) + V_o. \end{aligned} \tag{2.8}$$

If the firing threshold h is high, then the feedback connection are weakly recruited in absence of sensory inputs. Thus, we may suppose that ON cells are not firing and that OFF cells respond according to their spontaneous firing rate i.e. $(\bar{u}_{on}(x), \bar{u}_{off}(x)) = (0, V_o)$. Note that this is just a choice, and an actual experimental situation can be mimicked by adjusting V_o. As the activity profiles are spatially homogeneous, $A(\bar{u}_{on}, \bar{u}_{off}) = \Omega(\alpha_{on} f[\bar{u}_{on}] + \alpha_{off} f[\bar{u}_{off}])$, and we obtain

$$\begin{aligned} \bar{u}_{on}(x) &= \Omega k(\alpha_{on} f[\bar{u}_{on}] + \alpha_{off} f[\bar{u}_{off}]) \\ \bar{u}_{off}(x) &= \bar{u}_{on} + V_o. \end{aligned} \tag{2.9}$$

We see that the activity of the OFF cells is greater that the activity ON cells whenever $V_o > 0$. This particular solution corresponds to OFF cells firing in absence of input, while ON cells are quiescent. The stability of steady states is determined by linearizing Eq. 2.7 around Eq. 2.9. For spatially homogeneous eigenstates i.e. $u_j(x,t) = \bar{u}_j(x) + \tilde{u}e^{\lambda t}$, we obtain

$$\begin{aligned} (1 + a^{-1}\lambda)\tilde{u} &= k\{\alpha_{on} \int_\Omega dy f'[\bar{u}_{on}(x)]e^{-\lambda\tau} + \alpha_{off} \int_\Omega dy f'[\bar{u}_{off}(x)]e^{-\lambda\tau}\}\tilde{u} \\ (1 + a^{-1}\lambda)\tilde{u} &= k\{\alpha_{on} \int_\Omega dy f'[\bar{u}_{on}(x)]e^{-\lambda\tau} + \alpha_{off} \int_\Omega dy f'[\bar{u}_{off}(x)]e^{-\lambda\tau}\}\tilde{u}. \end{aligned} \tag{2.10}$$

Define

$$R = R(\bar{u}_{on}, \bar{u}_{off}) \equiv \alpha_{on} \int_\Omega dy f'[\bar{u}_{on}(x)] + \alpha_{off} \int_\Omega dy f'[\bar{u}_{off}(x)]. \tag{2.11}$$

For spatially homogeneous solutions, $R = \Omega(\alpha_{on} f'[\bar{u}_{on}] + \alpha_{off} f'[\bar{u}_{off}])$. With this notation, the transcendental characteristic equation for this problem be-

comes

$$1 + a^{-1}\lambda = kRe^{-\lambda\tau}, \tag{2.12}$$

where $\lambda \in \mathbb{C}$. Note that this equation is scalar, so that the elements of the eigenspectrum σ determine the stability of the two population activities simultaneously. This is also coherent with the nature of the coupling, which connects all members of the network with the same weight. Static spatially profiled inputs $I(x,t) = I(x)$ break the symmetry of the solutions, which are then no longer spatially homogenenous. Steady states now satisfy

$$\begin{aligned} \bar{u}_{on}(x) &= kA(\bar{u}_{on}, \bar{u}_{off}) + I(x) \\ \bar{u}_{off}(x) &= \bar{u}_{on} + V_o - 2I(x). \end{aligned} \tag{2.13}$$

If we assume that the eigenmodes are spatially homogeneous, we obtain the same linearized problem as for $I(x,t) = 0$, where the characteristic equation is given by Eq. 2.12. Even if the equations share a similar shape, the case $I(x) \neq 0$ is more difficult to analyze. This is because the function R in this case depends on spatially-dependent steady states and is consequently more difficult to compute.

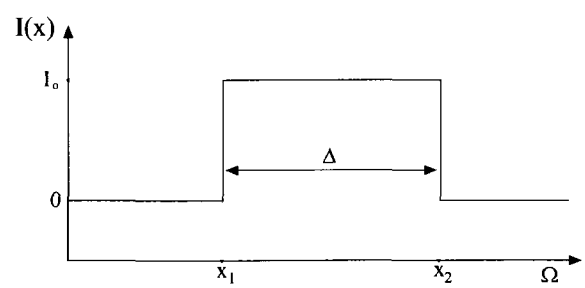

Figure 2.2: **Spatial profile of a pulse stimulus.** It is defined by $I(x,t) = I_o$ for $x \in [x_1, x_2]$ and $t_1 < t < t_2$ and zero otherwise.

It is nevertheless possible to gain some insight by considering piecewise homogeneous stimuli. Pulses only drive a fraction of the cells, as illustrated in

Figure 2.2. In this case, the function R may be computed easily, so that the stability of ON and OFF activity states may be formulated as a function of the input width $\Delta = |x_1 - x_2|$ and amplitude I_o. Furthermore, the spatial separation between external stimulation and autonomous dynamics makes pulses ideal input choices to observe the effect of stimulation on the behavior of delayed feedback connections. Another strong argument behind the use of pulses is their great relevance towards physiology. Studies motivating our work have illustrated how the spatial profile of external inputs alters the system activity states [95, 96, 34, 97, 98, 99]. In particular, the impact of a transition between spatially local and global input profiles has been linked to the stability of global oscillations [32, 27, 26, 100]. In this context, the use of static pulses or "bumps" allows us to control the input spatial contiguity as well as its strength, in order to formulate the criteria behind network stability analytically. Thus, the analysis presented in Chapter 3 and 5 deals with the response of the neural populations to pulses, but numerical results on input bumps are also presented in Chapter 4 .

2.3 Bifurcation Analysis

Bifurcations are spontaneous state transitions occuring in topologicaly unstable dynamical systems, initiated by perturbations in the system's parameters. They are of particular relevance in biological systems, where they characterize the mechanisms by which equilibria undergo qualitative changes in their behavior and/or stability. Bifurcations are fundamental for the understanding of physical phenomena occuring in fluctuating environments, like multistability, oscillations and phase transitions.

Consider the case of a network composed of an even number of ON and OFF cells by setting $\alpha_{on} = \alpha_{off} = 1/2$. We fix the synaptic response time constant to $a = 1$. For a feedback polarity k and without stimulation i.e. $I(x,t) = 0$, our system becomes a scalar delay-differential equation. If we further set the

baseline activity of OFF cells to zero (i e $V_o = 0$), Eq 2 7 may be written as

$$\begin{aligned} u_{on}(t) &= -u_{on}(t) + k\Omega[\frac{1}{2}f(u_{on}(t)) + \frac{1}{2}f(u_{off}(t))] \\ u_{off}(t) &= -u_{off}(t) + k\Omega[\frac{1}{2}f(u_{on}(t)) + \frac{1}{2}f(u_{off}(t))] \end{aligned} \tag{2 14}$$

From a mathematical standpoint, local bifurcations correspond to changes in stability of so-called non-hyperbolic fixed points for which eigenvalues have a zero real part Equation (2 8) is non-hyperbolic if $Re(\lambda) = 0$, where $\lambda = Re(\lambda) + iw$ where $w \in \mathbb{R}$ The characteristic equation may then be written as

$$1 + a^{-1}iw = kRe^{-iw\tau} \tag{2 15}$$

A in-debt analysis of Eq (2 15) is given in Chapter 4 Let us here present the calculations involved for $k = 1$ and $k = -1$ without stimulation Further details concerning the stimulated case are detailed in Chapter 3 and 4

i) **k=1** For excitatory feedback, Eq 2 14 may be writen as

$$\begin{aligned} u_{on}(t) &= -u_{on}(t) + \Omega[\frac{1}{2}f(u_{on}(t)) + \frac{1}{2}f(u_{off}(t))] \\ u_{off}(t) &= -u_{off}(t) + \Omega[\frac{1}{2}f(u_{on}(t)) + \frac{1}{2}f(u_{off}(t))] \end{aligned} \tag{2 16}$$

Note that we have $\bar{u}_{on} = \bar{u}_{off} \equiv \bar{u}$ so that we may write Eq (2 8)

$$u = \Omega[\frac{1}{2}f(\bar{u}) + \frac{1}{2}f(u)] = \frac{\Omega}{1 + e^{-\beta((\bar{u})-h)}}, \tag{2 17}$$

where Eq (2 4) was used The common fixed point $\bar{u}$ for ON and OFF activities is defined implicitly For $k = 1$, eigenvalues can be shown to have a zero imaginary part, so that damped oscillations and periodic solutions are not possible Substituting $|\lambda = 0|$ into Eq 2 15 may be simplified to

$$1 = R = \frac{\Omega\beta e^{-\beta(\bar{u}-h)}}{(1 + exp{-}\beta(\bar{u} - h))^2} \tag{2 18}$$

Combining Eq. (2.17) and (2.18), we may write

$$1 = \Omega\beta(\frac{\Omega}{\bar{u}} - 1)(\frac{\bar{u}}{\Omega})^2, \tag{2.19}$$

which corresponds to the tangancy condition for a saddle-node bifurcation by taking the derivative with respect to u on all sides of Eq. (2.17). A saddle-node bifurcation is a codimension 1 bifurcation in which a pair of equilibria of opposed stability merge and disapear. Equation (2.19) has the roots

$$\bar{u}_{1.2}(\beta) = \frac{1}{2}\frac{\beta\Omega \pm \sqrt{\beta^2\Omega^2 - 4\beta\Omega}}{\beta},$$

where the steady states are function of the feedback response gain β and the network size Ω at the instability. The threshold h may also be expressed as a function of β at saddle node points where Eq. (2.18) and (2.17) hold simultaneously. The saddle-node curve in (h, β) parameter space is thus

$$h(\beta) = \frac{\beta\Omega + \sqrt{\beta^2\Omega^2 - 4\beta\Omega} + 2ln(\frac{\beta\Omega - \sqrt{\beta^2\Omega^2 - 4\beta\Omega}}{\beta\Omega + \sqrt{\beta^2\Omega^2 - 4\beta\Omega}})}{2\beta}. \tag{2.20}$$

It is of interest to consider the particular case where $\bar{u} = h$, for which Eq. (2.20) reduces to

$$h(\beta) = \frac{\Omega}{2}.$$

At this precise point in parameter space, the steady state $\bar{u} = h = \frac{\Omega}{2}$ undergoes a pitchfork bifurcation beyond the value $\beta = \beta^* \equiv 4/\Omega$. This bifurcation involves the loss of stability of a fixed point and the appearance of two new stable fixed points symmetrically positionned on each side of it. The bifurcation is supercritical since $\frac{\partial^3 f}{\partial u^3}(\bar{u}, \beta^*) < 0$. As the condition is relaxed, the system undergoes saddle-node bifurcations along the curve $h(\beta)$. Hence, the presence of the threshold h leads the system into a cusp-shaped birfurcation portrait [101]. The presence of pitchfork bifurcations implies that excitatory feedback is characterized by multistability, where oscillatory solutions are not possible.

When the spontaneous activity of ON and OFF populations is not the same i.e. $V_o \neq 0$, the new equilibria become

$$\bar{u}_{on} = \frac{\Omega}{2}[f(\bar{u}_{on}) + f(\bar{u}_{off})],$$

$$\bar{u}_{off} = \frac{\Omega}{2}[f(\bar{u}_{on}) + f(\bar{u}_{off})] + V_o, \tag{2.21}$$

where we now have $\bar{u}_{on} = \bar{u}_{off} - V_o$. Fixed points of the system may thus be found by solving the scalar equation

$$\bar{u} = \frac{\Omega}{2}[f(\bar{u}) + f(\bar{u} + V_o)], \tag{2.22}$$

for $\bar{u} = \bar{u}_{on}$. Saddle-node instabilities are characterized by the relationship

$$1 = \frac{\Omega}{2}[f'(\bar{u}) + f'(\bar{u} + V_o)], \tag{2.23}$$

for which $|\lambda = 0|$. We can solve (2.22) and (2.23) numerically, and identify the sets in (h, V_o) parameter space for which there exists a solution. The result is a combination of saddle-nodes and pitchforks, as illustrated in Figure 2.3.

ii) **k=-1** For inhibitory feedback, mutistability (i.e. the coexistence of two or more stable equilibria) is not possible since Eq. (2.9) only has a single root. Andronov-Hopf instabilties occur whenever $\lambda = \pm iw$, for $\mathbb{R} \ni w \neq 0$, where a limit cycle solution becomes stable. In this case, the eigenvalue problem becomes

$$1 + iw = -Re^{-\imath w\tau}, \tag{2.24}$$

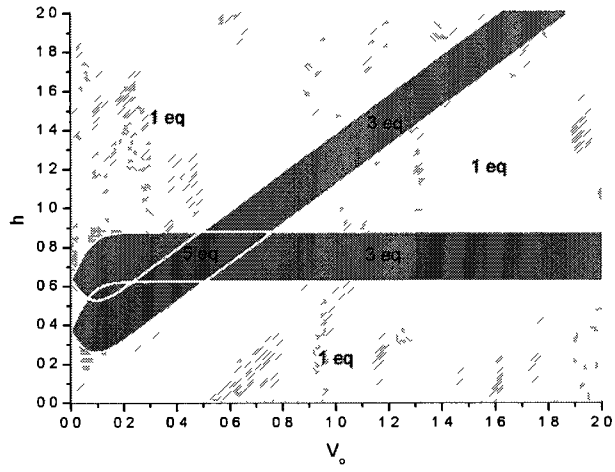

Figure 2.3: **Bifurcation diagram in (h, V_o) parameter space.** Saddle-node curves delimit regions where multiple fixed points (eq) coexist. Here, $\beta = 25$.

where R is defined in Eq. (2.11). Separating this equation into imaginary and real parts, we obtain

$$0 = 1 + R\cos(w\tau) \tag{2.25}$$

$$0 = w - R\sin(w\tau), \tag{2.26}$$

The ratio of these equations gives the following:

$$w = -\tan(w\tau) \Leftrightarrow w\tau = -\arctan(w).$$

Since $\cos(arctan(x)) = \frac{1}{\sqrt{1+x^2}}$, we obtain

$$0 = 1 - \frac{R}{\sqrt{1+w^2}}.$$

Solving this second order polynomial gives

$$w_{1\,2} = \pm\sqrt{R^2 - 1}$$

$$\tau = \frac{1}{w} \arctan(w).$$

This determines the critical delay and frequency for which the eigenvalue λ has zero real part. Thus Ω is the frequency of the temporally oscillating solution born at this bifurcation; this frequency will generally change as the system moves further past this bifurcation point. The case $V_o = 0$ and $V_o \neq 0$ may be analyzed in the same way, although the function R will contain the ON and OFF steady states.

Chapter 3

Oscillatory response in a sensory network of ON and OFF cells with instantaneous and delayed recurrent connections

Lefebvre J., Longtin A., LeBlanc V.G. (2009), Phys. Trans. Roy. Soc. A. 28 vol. 368 no. 1911, pp. 455-467, doi:10.1098/rsta.2009.0229

Abstract

A neural field model with multiple cell-to-cell feedback connections is investigated. Our model incorporates populations of ON and OFF cells, receiving sensory inputs with direct and inverted polarity, respectively. Oscillatory responses to spatially localized stimuli are found to occur via Andronov-Hopf bifurcations of stationary activity. We explore the impact of multiple delayed feedback components as well as additional excitatory and/or inhibitory non-delayed recurrent signals on the instability threshold. Paradoxally, instantaneous excitatory recurrent terms are found to enhance network responsiveness by reducing the oscillatory response threshold, allowing smaller inputs to trigger oscillatory activity. Instantaneous inhibitory components do the opposite. The frequency of these response oscillations is further shaped by the polarity of the non-delayed terms.

3.1 Introduction

Rhythmic activity in the brain is commonly associated with the processing of neural information. Such oscillatory patterns are ubiquitous in many areas of the cortex, where they take part in higher brain functions and memory, displaying a vast range of frequencies. They are found in the thalamus, the thalamo-cortical system, and in many sensory pathways like vision [95, 102, 103], electroreception [33] and audition [104]. Oscillatory behaviour in sensory systems has been proposed to be one of the basic mechanisms of input selection and detection, where oscillatory activity is triggered on the basis of stimulus properties. Specifically, oscillatory response has been observed in various sensory networks under spatially non-homogeneous stimulation. Excitatory populations are known to enter states of rhythmic activity when the input shows sufficient spatial contiguity ("binding stimulus") [95, 96, 97, 99], or is noisy but which shows sufficient spatial correlation [33].

Aside from sensory stimuli structure, specific circuit geometry plays a crucial

role in the presence of rhythmic activity Network oscillations in sensory systems typically refer to synchronous states achieved by the means of Andronov-Hopf type instabilities commonly observed in inhibitory networks [2, 105, 106] However, the effect of multiple recurrent connections blurs the notion of what causes oscillatory behavior, as the combined actions of local and global signals is poorly understood Models in electroreception commonly incorporate global i e all-to-all recurrent connections In vision, models introduce an elaborate mixture of global and local recurrent circuitry to mimic sensory information processes and exhibit oscillatory activity, a feature which can be amplified by feedback connections [103] Generically, sensory pathways incorporate sets of recurrent connections with distinct polarities, i e either excitatory or inhibitory, where these are associated to excitatory and inhibitory synaptic connections, respectively For example, [107] studied oscillations thresholds for paired excitatory and inhibitory delayed feedback where delays were either fixed or distributed Further, [108] suggested that combined positive and negative feedback may describe attention modulation in cortical networks

Most sensory systems exhibiting oscillatory activity also involve ON and OFF cells [47, 109, 110] While the connection between rhythms and sensory inputs has been partially established, there is currently no consideration of the distinct ON and OFF cells behaviors in the treatment of sensory information and the genesis of temporal activity oscillations We ask the question as to how these populations might behave in a feedback system under stimulation can oscillations still be observed? Does the system have the same oscillation threshold?

In a previous work from the authors [111], precise conditions on which oscillatory input responses are seen in a general ON/OFF system with a unique global inhibitory delayed feedback were established, along with a study of network responses to periodic forcing as well as the gain of the system in the equilibrium regime Here, we want to investigate the more generic case of a mixture of local and global recurrent connections, and investigate how this change in the

network architecture influences the genesis of oscillatory activity. Our aim is to understand generic properties beyond those studied for the standardly studied equivalent ON cell system, where local circuitry reinforces global oscillations [96] or vice versa [103]. To do so, we will first present our model in Section 2, and review in Section 3 the conditions on which oscillatory instabilities occur in a model with delayed inhibitory feedback components and how the interplay between ON and OFF populations input responses results in oscillatory activity. In Section 4, we introduce a mixture of instantaneous and delayed recurrent connections and demonstrate how the mixed feedback profile alters the instability threshold and the response frequency to spatially localized pulses.

3.2 Model

Our analysis is particularly motivated by electroreception, but applies also to other senses. The architecture considered in Fig. 3.1 is inspired from the physiology of the electrosensory lateral lobe (ELL) found in the brains of the weakly electric fish (*Apteronotus leptorhynchus*), acting as the primary operator in stimuli encoding (for an exhaustive physiological discussion see [22]). The sensory layer is populated by ON and OFF pyramidal cells which feed forward their activity vertically to higher brain center, these in turn integrate ON and OFF activity and feed it back to the sensory layer via delayed interactions of different polarities. Here, these higher brain centers do not contribute to spatial encoding, but merely act as activity accumulators. This fact distinguishes our approach from typical neural fields models that usually exhibit spatial connectivity profiles. Non-delayed recurrent connections are nevertheless added to mimic local anatomy, connections which are weak in the ELL of the electric fish. As there are very few lateral connections between units in the sensory layer in electrosensory systems, these connections are typically neglected, the dynamics of the system being described using delayed feedback components.

As in many sensory pathways, spatio-temporal inputs are processed through

the interplay of ON and OFF neural populations. The distinct input response mechanism between these cell types is mainly due to the presence of extra pre-processing within the OFF pathway, where an intermediate cellular body called an *interneuron* transfers an inverted image of received inputs to the OFF cells, while ON cells receive the input directly, with preserved polarity. Thus, when the input stimulus increases, ON cell activity increases while that of OFF cells decreases. Given the synaptic response functions η_{on} and η_{off} and some applied pre-synaptic input $I(x,t)$, the post synaptic potentials PSP_j for $j = ON, OFF$ at the sensory layer are given by

$$PSP_{on}(x,t) = \eta_{on} * I(x,t)$$

$$PSP_{off}(x,t) = \eta_{off} * \mathcal{I}[I(x,t)]$$

where $*$ is a temporal convolution and $\mathcal{I}$ stands as the interneuronal process. We make the hypothesis that the operator $\mathcal{I}$ is linear to first order such that it may be approximated by $\mathcal{I}(u) \approx -u$. Thus for simplicity we consider the situation where, without sensory inputs $I(x,t) = 0$ and in open loop, stationary activity states correspond to both dormant ON and OFF populations $\bar{u}_{on} = \bar{u}_{off} \approx 0$.

The system is composed of N distinct feedback loops where the delay $\tau > 0$ accounts for processing and axonal conduction times and is assumed to be identical for all delayed circuits. The mean somatic membrane potentials, or *activities*,

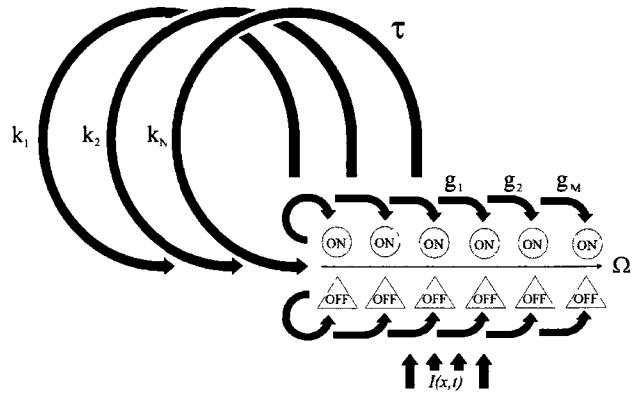

Figure 3.1: **Schematic of the multi-loop feedback circuit.** The system consists of a layer of ON and OFF pyramidal cells. These integrate spatio temporal inputs $I(x,t)$ and project their output activity to higher brain centers, which process and feed back the signal via multiple feedback loops, after some time delay τ and with polarity k_i. Instantaneous i.e non-delayed feedback loops mimic local connectivity with polarities g_j.

$u_{on}(x,t)$ and $u_{off}(x,t)$, at the sensory layer obey the following dynamics:

$$\begin{aligned}(1+a_{on}^{-1}\partial_t)u_{on}(x,t) &= \sum_{i=1}^{N} k_i S(u_{on},u_{off},t-\tau) \\ &\quad + \sum_{j=1}^{M} g_j S(u_{on},u_{off},t) + I(x,t) \\ (1+a_{off}^{-1}\partial_t)u_{off}(x,t) &= \sum_{i=1}^{N} k_i S(u_{on},u_{off},t-\tau) \\ &\quad + \sum_{j=1}^{M} g_j S(u_{on},u_{off},t) - I(x,t)\end{aligned} \tag{3.1}$$

where we chose exponential synapses i.e. $\eta_p(s) = a_p e^{-a_p s}$, $p = ON, OFF$. We use k for delayed feedback strengh, and g for n*on-delayed*, or *instantaneous* feedback strength. Polarities of the recurrent connections are individually weighted by $k_i, g_j > 0$ for excitatory and $k_i, g_j < 0$ for inhibitory feedback, where $i = [1,N]$ and $j = [1,M]$. A spatio-temporal stimulus $I(x,t)$ with arbitrary polarity (either excitatory or inhibitory) is presented with inverted polarity

to the OFF layer, while ON cells receive the input directly. The recurrent term

$$S(u_{on}, u_{off}, t) = \int_{\Omega} dy[\alpha_{on} f_{on}(u_{on}(y,t)) + \alpha_{off} f_{off}(u_{off}(y,t))] \qquad (3.2)$$

corresponds to global i.e. all-to-all coupling, for which $f_j(u) \equiv (1+e^{-\beta(u-h_j)})^{-1}$ (j=ON,OFF) is a smooth sigmoidal firing rate function with threshold h_j and gain β. The finite spatial domain is Ω, while α_j is the relative proportion of j type cells in the population. ON and OFF populations project evenly to all cells in the system via the multiple feedback connections, irrespective of their polarity, which might be either excitatory or inhibitory, or both.

3.3 Oscillatory Activity and Stimulation

Let us first consider the non-stimulated case i.e. $I(x,t) = 0$ and the regions in parameter space where global oscillations may be found. We will neglect all non-delayed recurrent signals i.e. $g_j = 0$, $\forall j$, and describe the evolution of activity in the context of multiple delayed loops. Oscillatory activity is typically characterized by determining Andronov-Hopf instability thresholds. The solutions $\bar{u}_{on}$ and $\bar{u}_{off}$ of Eq.(3.1) for $g_j = 0$ are spatially uniform and can be implicitly written as

$$\begin{aligned} \bar{u}_{on} &= K\frac{\Omega}{2}[f(\bar{u}_{on}) + f(\bar{u}_{off})] \qquad (3.3) \\ \bar{u}_{off} &= K\frac{\Omega}{2}[f(\bar{u}_{on}) + f(\bar{u}_{off})] \end{aligned}$$

where $K \equiv \sum_{i=1}^{N} k_i$. For simplicity, we chose $\alpha_{on} = \alpha_{off} = 1/2$, $a_{on} = a_{off} = 1$ and $h_{on} = h_{off} \equiv h$. We further fixed the response gain $\beta = 25$, so that the firing rate function f is smooth.

Since all the delays in Eq.(3.1) are identical, the multiple feedback components of Fig.3.1 are analogous to the single delayed connection case with gain K. In Fig. 3.2, whenever $K > 0$, no oscillatory solutions are possible, as exci-

tatory connections dominate the dynamics and bring the system in a regime of multistability. However, if $K < 0$, linearizing the system around Eq.(3.3) indicates that an supercritical Andronov-Hopf bifurcation occurs for smaller values of the delay as K decreases, meaning that a dominant number of inhibitory components versus excitatory components first makes possible oscillatory activity, and further encourages the stability of global oscillations by decreasing the magnitude of the critical delay. Consequently, additional delayed feedback components with identical delays but different polarities do not alter the dynamics qualitatively, if the condition $K < 0$ is fulfilled.

The stimulated case i.e. $I(x,t) \neq 0$ can be analyzed in a similar fashion,

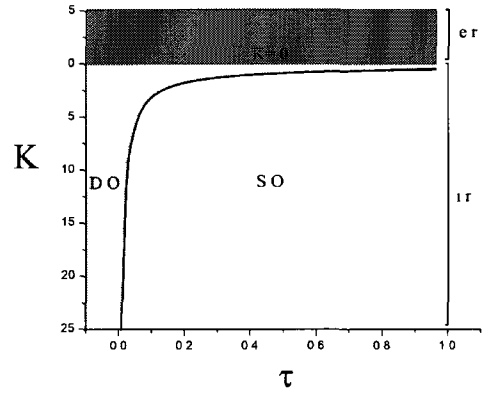

Figure 3.2 **Andronov-Hopf curve in (K,τ) parameter space.** The horizontal line $K = 0$ separates the parameter space between excitatory and inhibitory regimes The bifurcation curve delimits regions of damped oscillations and regions where global oscillations are stable As the number of inhibitory delayed components increases (K decreases), smaller delays are needed to stabilize oscillatory solutions, reducing the instability threshold S O refers to stable oscillations, while D O refers to damped oscillations .

to determine the effect of distributed input on the genesis of rhythmic activity. We will assume from now on that a single inhibitory delayed connection is present, weighted at $K = k_1 = -1$, which we now know is analogous to the case of several delayed feedback connections dominated by inhibition, treated previously A spatially distributed stimuli of the form $I(x,t) = I(x)$ induces a

non-homogeneous solution, determined from (3.1) by

$$\begin{aligned} \bar{u}_{on}(x) &= S(\bar{u}_{on}, \bar{u}_{off}) + I(x) \\ \bar{u}_{off}(x) &= \bar{u}_{on}(x) - 2I(x) \end{aligned} \tag{3.4}$$

Oscillatory response corresponds to an input-triggered supercritricial Andronov-Hopf bifurcation. We can isolate the instability and specify the input response threshold by linearizing Eq. (3.1) around (3.4) for $\bar{u}_{on.off}(x,t) = \bar{u}_{on.off}(x) + u_\lambda(x)e^{\lambda t}$, $\lambda \in \mathbb{C}$. This particular choice of ansatz restricts our stability analysis to spatially homogeneous modes. We obtain the characteristic equation

$$\lambda + 1 + Re^{-\lambda\tau} = 0 \tag{3.5}$$

An input is expected to cause a Andronov-Hopf bifurcation if $Re(\lambda) = 0$ for $\lambda = a + iw$, $w \neq 0$, which occurs whenever the parameter R satisfies

$$\tan(\omega(R)\tau) + \omega(R) = 0 \tag{3.6}$$

where $\omega(R) = \sqrt{R^2 - 1}$ is the frequency at the bifurcation. The parameter R is defined by

$$R = [\alpha_{on} \int_\Omega dy f'(\bar{u}_{on}(y)) + \alpha_{off} \int_\Omega dy f'(\bar{u}_{off}(y))] \tag{3.7}$$

The parameter R arises from linear stability considerations, and is an integral over the solutions $\bar{u}_{on}(x)$ and $\bar{u}_{off}(x)$, measuring how close these are to the feedback activation threshold h. Spatially distributed inputs $I(x,t)$ are expected to bring the solutions either closer or away from h, subsequently changing the value of R and triggering oscillatory solutions via Andronov Hopf instabilities whenever $R = R_c$, where R_c satisfies Eq. (3.6). As opposed to the non-stimulated case where an increase of the delay τ was causing the oscillations for $K < 0$, spatially profiled stimulation alone is triggering oscillatory activity by balanc-

ing local excitation and recurrent inhibition at some critical feedback amplitude, specified by h, which will be fixed throughout the analysis. [111] studies the exact dynamical impact of a modification of h.

For concreteness, we numerically test these results with a pulse stimulus defined by $I(x,t) = I_o$ for $x \in \Delta = [x_1, x_2]$ and $t_o < t < t_1$ while $I(x,t) = 0$ otherwise. The width of the pulse is defined by $\Delta = |x_1 - x_2|$. This input distribution is ideal for separating local and global dynamics and identifying feedback effects, and is coherent with many stimulation patterns studied experimentally in spatially extended system. From Fig. 3.3, stationary uniform activity states $\bar{u}_{on}$ and $\bar{u}_{off}$ are stable on the basis of well chosen parameters until $t = t_o$. The equilibrium (3.4) becomes unstable for the duration of the pulse and recovers stability at the offset of stimulation, delimiting the oscillatory response time of the combined ON and OFF population. Fig. 3.4 illustrates the condition Eq.(3.6) fullfilled at the onset of the stimulus $t = t_o$ and again at the offset $t = t_1$ for $R_c \approx 1.823$ and $\tau = 2.0$, where the eigenvalues cross back and forth the imaginary axis

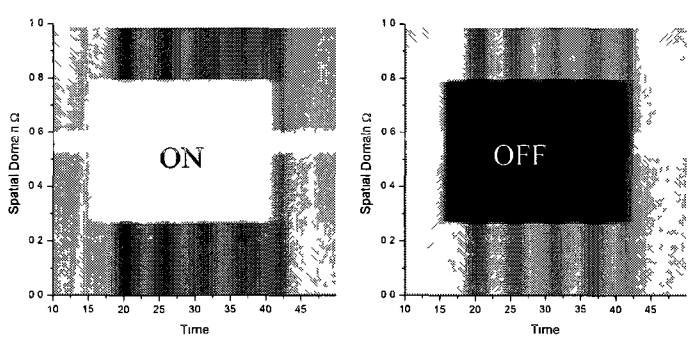

Figure 3.3: **ON/OFF network oscillatory response to a localized pulse.** Parameters are $\tau = 2.0$, $\Omega = 1$, and $h = 0.25$ The input has the amplitude $I_o = 0.4$ between $x_1 = 0.25$ and $x_2 = 0.75$, and 0 otherwise for $15 < t < 40$

This behavior is coherent with many findings on recurrent neural networks,

where a spatially localized pulse generates global oscillations when the input width is sufficiently large [97], even though no delay is present. Further findings seem also to agree for stochastic Integrate-and-Fire models with delayed feedback, where the input spatial correlation must meet a critical value to trigger oscillatory response [32, 33], or require the use of dynamic synapses to establish the required level of non-linearity [99]. Our results incorporate distinct ON/OFF population responses, and indicates that oscillatory activity as a response mechanism is possible even when individual cell responses to external inputs are not purely excitatory. The dynamic distinctiveness and sensitivity of ON/OFF networks as compared to the purely excitatory case i.e. ON /ON networks will be studied elsewhere (see Chapter 5).

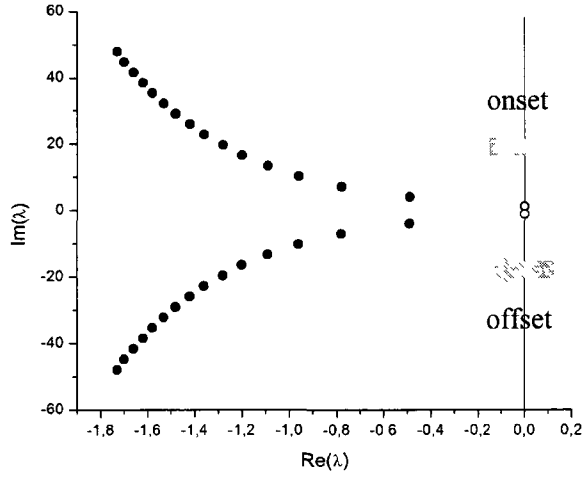

Figure 3.4: **Eigenvalues crossing the imaginary axis as the critical parameter R_c is met.** At the onset of the pulse stimulus, the Andronov-Hopf curve (3.6) is crossed for the chosen delay $\tau = 2.0$ where the parameters are such that the solutions enter a regime of stable oscillations. Unstable eigenvalues cross the imaginary axis accordingly. At the offset of the bump, the opposite process takes place and the stationary activity states recover their stability and the oscillations disappear at the same time as the stimulus.

3.4 Instantaneous and Delayed Feedback Dynamics

Although delayed feedback connections have been studied extensively (In particular, see [112, 32, 105] and references therein), little is known about *mixed* feedback profiles, where non-delayed ("local") and delayed ("global") recurrent terms are combined. This setup is further complicated by the presence of distinct ON and OFF populations. This raises the important question as to how robust are the dynamics seen in delayed feedback system when additional recurrent terms are considered. *Non-delayed*, or *Instantaneous recurrent* components account for local signals, mimicking local spatial connectivity and lateral activity propagation. Eventually, we would like to understand the role of spatial connectivity profiles (which greatly complicates the analysis), but this knowledge will build on the simpler all-to-all instantaneous plus delayed coupling studied here.

Of particular interest is how delayed and non-delayed components combine and alter the oscillatory activity threshold. For simplicity, we set $M = 1$ and look at the case where a single non-delayed recurrent component of polarity g is present. Eq.(3.1) becomes

$$\begin{aligned}(1 + a_{on}^{-1}\partial_t)u_{on}(x,t) &= -S(u_{on}, u_{off}, t-\tau) + gS(u_{on}, u_{off}, t) + I(x,t) \\ (1 + a_{off}^{-1}\partial_t)u_{off}(x,t) &= -S(u_{on}, u_{off}, t-\tau) + gS(u_{on}, u_{off}, t) - I(x,t)\end{aligned} \tag{3.8}$$

where we set $\alpha_{on} = \alpha_{off} = 1/2$, $a_{on} = a_{off} = 1$, $h_{on} = h_{off} \equiv h$ and $\beta = 25$. Note the first terms on the r.h.s. are delayed, while the second ones are not. As before, we assumed here that we have a predominantly inhibitory feedback

loop, weighted by $K = k = -1$. Fixed points of Eq.(3.8) are now given by

$$\begin{aligned} \bar{u}_{on}(x) &= (g-1)S(\bar{u}_{on}, \bar{u}_{off}) + I(x) \\ \bar{u}_{off}(x) &= \bar{u}_{on}(x) - 2I(x) \end{aligned} \tag{3.9}$$

Similarly to the purely delayed case above, linearizing the system around (3.9)

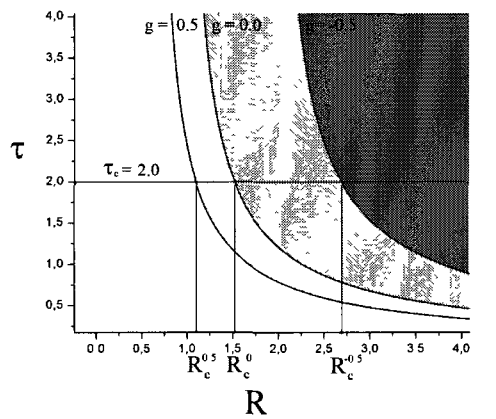

Figure 3.5: **Andronov-Hopf curve (3.11) for** $g = 0.5$, 0 **and** -0.5. Shaded regions corresponds to parameter sets where oscillatory solutions are stable. These regions are delimited by Andronov-Hopf curves as in Eq. (3.11) for different values of g. The instability thresholds for $\tau = 2.0$ are such that $R_c^{0.5} < R_c^0 < R_c^{-0.5}$, indicating that the additional non-delayed excitatory component ($g = 0.5$) increases the "oscillatory" sensitivity of the system, promoting oscillatory responses to pulse inputs.

for the ansatz $\bar{u}_{on.off}(x,t) = \bar{u}_{on.off}(x) + u_\lambda(x)e^{\lambda t}$, $\lambda \in \mathbb{C}$, yields a perturbed version of the previous eigenvalue problem

$$\lambda + 1 + Re^{-\lambda\tau} - gR = 0 \tag{3.10}$$

where R is given in Eq.(6.8). The instantaneous recurrent term is expected to shift the spectrum, according to the magnitude of g. Oscillatory solutions are stable in parameter space in a region delimited by the curve

$$w(R)(-\cos(w(R)\tau) + g) = \sin(w(R)\tau) \tag{3.11}$$

where the frequency is now given by $w(R,g) = \sqrt{(R^2 - 1 + 2Rg - R^2g^2)}$.

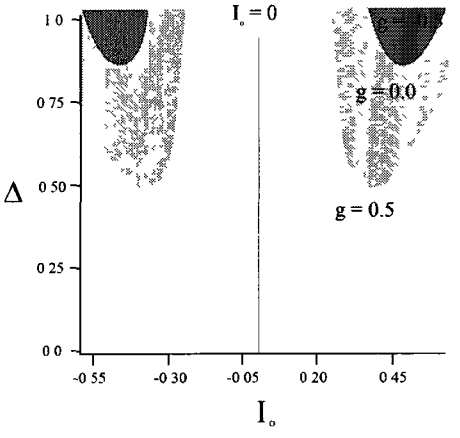

Figure 3.6: **Pulse widths Δ and amplitudes I_o generating oscillatory responses.** Shaded regions correspond to the input configurations where oscillatory responses to a localized pulse are observed, for either $g = -0.5$, 0 or 0.5. The response threshold changes induced by additional non-delayed connections, on top of the global delayed inhibitory feedback, alter the criterions imposed on the input in order to trigger an Andronov-Hopf instability in the system. Parameters are $\Omega = 1$, $\tau = 2.0$ and $h = 0.25$

The parameter R can be treated as a functional of the instantaneous recurrent strength i.e. $R = R(g)$, so that we may identify the oscillatory response threshold by solving Eq.(3.11) for $R_c(g) \equiv R_c^g$. **Surprisingly, the response threshold is found to be inversely proportional to g, indicating that increasingly excitatory non-delayed components decrease the value of the threshold R_c^g and facilitates the genesis of oscillation.** Fig. 3.5 shows this by comparing the values of $R_c^{-0\,5}$, $R_c^{0\,5}$ and R_c^0, the latter value corresponding to the purely delayed case i.e. without any instantaneous recurrent term. Excitatory non-delayed interactions ($g = 0.5$) reduce the oscillatory response threshold, so that $R_c^{0\,5} < R_c^0$. The opposite occurs for inhibitory non-delayed interactions ($g = -0.5$), where $R_c^{-0\,5} > R_c^0$. This implies that minimal input distribution requirements are relaxed when $g > 0$, increasing the system sensitivity to pulse inputs that cause oscillations. In the case of a localized pulse (Fig. 3.6), the minimal pulse spatial width $\Delta = |x_1 - x_2|$ causing oscillations

is significantly smaller, while the interval of amplitudes I_o generating oscillations is greatly enlarged. We also note the characteristic symmetry between excitatory($I_o > 0$) and inhibitory inputs($I_o < 0$), due to combined ON and OFF responses, indicating that evenly distributed inputs of opposed polarity will generate the same network response.

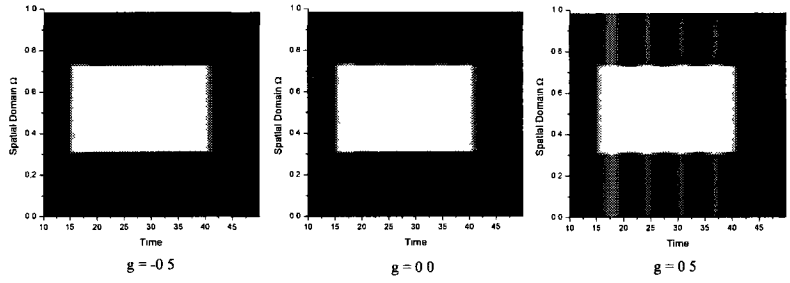

Figure 3.7: **ON population responses to a localized pulse when** $g = -0.5$, 0 **and** 0.5. Parameters in Eq. (3.8) are $\Omega = 1$, $I_o = 0.3$, $\Delta = 0.4$, $h = 0.25$ and $\tau = 2.0$

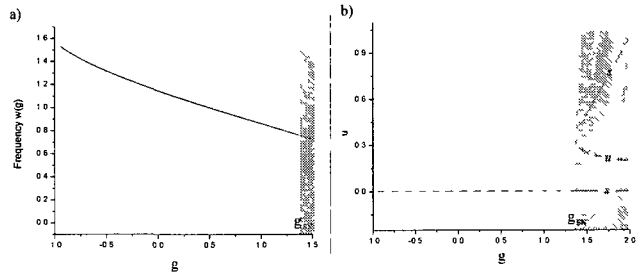

Figure 3.8: Frequency and equilibria stability for increasing local feedback gains. a. Input response frequency as a function of the instantaneous recurrent signal polarity g. The input response frequency at the threshold decreases as the non-delayed recurrent signal becomes more and more excitatory. b Saddle-node bifurcation occurring at $g_{SN} \approx 1.375$, delimiting the region investigated. Parameters $\tau = 2.0$ and $h = 0.25$.

In order to test this prediction, we stimulate the network response in Fig. 3.7 with a pulse-shaped stimulus with different strengths i.e $g = -0.5$, 0 and 0.5. The system exhibits small damped oscillations for $g = -0.5$, indicating that the input width and amplitude are not sufficient to trigger stable oscillations. When g is increased to 0, damped oscillations are still observed, although with

longer decay rate, indicating that the system is closer to the oscillation threshold. When $g = 0.5$, the input triggers stable oscillations. In all these cases, the same input distribution was used. The extension to multiple instantaneous feedback connections may be done in a similar way as in the case of delayed connections, setting $G = \sum_{j=1}^{M} g_j$, yielding similar quantitative results (not shown).

We can identify the values of R satisfying Eq.(3.11) and consider how the response frequency $w(R_c, g)$ varies as a function of g, at the threshold. As Fig. 3.8a shows, an increasing instantaneous recurrent strength g decreases the response frequency, indicating that local signals shape oscillatory patterns, even in the case where global inhibitory delayed connections are present. Throughout this work, we restricted our analysis to the strength interval $g \in [-1, g_{SN}]$. For $g < -1$, the frequency $w(R, g)$ becomes imaginary and oscillatory activity disappears inside the associated region of parameter space. At g_{SN}, a saddle-node bifurcation occurs as shown in Fig. 3.8b. At this point, network oscillations collide with the basin of attraction of the new fixed points, and multistability is observed. The saddle-node bifurcation point is determined by the firing rate threshold h and response gain β, fixed earlier.

3.5 Conclusion

In this paper, we first demonstrated how oscillations appear in a delayed feedback network of ON and OFF cells with external stimuli, and investigated the issue of multiple delayed feedback loops. We then analyzed the effects of a mixture of delayed and non-delayed recurrent connections and demonstrated how the stability of the input-induced oscillations depends on the strength of non-delayed connections. When a delayed inhibitory term is present, instantaneous excitatory connections increase the network oscillatory responsiveness by decreasing the response threshold and allowing a greater range of pulse inputs to trigger oscillatory activity. Non-delayed inhibitory connections do the opposite by increasing the oscillatory response threshold. Further, the response

frequency decreases when g increases.

Acknowledgments

Special thanks to A. Hutt, L. Maler and W. Nesse. We thank NSERC and FQRNT for funding.

Chapter 4

Dynamics of driven recurrent networks of ON and OFF cells

Lefebvre J., Longtin A., LeBlanc V.G. (2009), Phys. Rev. E., 80, 041912, doi: 10.1103/PhysRevE.80.041912. Selected for the Virtual Journal of Biological Physics Research.

Abstract

A globally-coupled network of ON and OFF cells is studied using neural field theory. Theory predicts that, without input, multiple transitions to oscillations can occur, depending on feedback delay and the difference between ON and OFF resting states. Static spatial stimuli can induce or suppress global oscillations via a Andronov-Hopf bifurcation. This is the case for either polarity of such stimuli. In contrast, only excitatory inputs can induce or suppress oscillations in an equivalent network built of ON cells only, even though oscillations are more prevalent in such systems. Novel non-monotonic responses to local stimuli occur, where responses lateral to the stimulus switch from excitatory to inhibitory as the input amplitude increases. With local time-periodic forcing, the unforced cells oscillate at twice the driving frequency via full-wave rectification mediated by the feedback. Our results agree with simulations of the neural field model, and further, qualitative agreement is found with the behavior of a network of spiking stochastic integrate and fire model neurons.

4.1 Introduction

Autonomous and driven responses of networks are a focus of much current research in biological physics. The interplay of feedforward and feedback connections, of both excitatory and inhibitory type, are strong determinants of dynamical behaviors [113, 114]. In particular, the modeling of spatially extended neural systems with such connections has received increasing attention as they exhibit a host of interesting dynamical phenomena. Mechanisms have been found for transitions between equilibria and non-homogeneous states in space and/or in time (see e.g. [85] and references therein). Propagation and processing delays in biological networks further expand the range of dynamical possibilities [106, 105, 2]. Responses to simple localized inputs can lead to localized structures such as bumps and breathers [85, 44]. A main challenge lies on modeling responses to static [86] or moving spatial stimuli [80] which are relevant to neural networks. Stochastic spatio-temporal stimuli with vary-

ing degrees of spatial correlation, as they occur in naturalistic situations, have also begun to receive attention [32, 33]. Another is the inclusion of multiple types of cells, which complicates the bifurcation analysis greatly. For example, two-population systems are under study [85, 69, 88, 87, 115], where cells in one population have similar properties and connections to other cells.

Sensory systems are a common context in which to model responses of networks to localized spatio-temporal inputs. In many sensory systems however, the cells are divided into ON and OFF-type cells. The effect of this division on the aforementioned dynamical phenomena has not been studied. ON and OFF cells can similarly drive other cells further along the sensory pathway, but external input to OFF cells is inverted (e.g. by interneurons) in comparison to ON cells. For example, ON (OFF) pyramidal cells (also called E and I cells, respectively) in the electrosensory lateral line lobe (ELL) of weakly electric fish, which provide the prime motivation for our model below, increase (decrease) their firing rate when the electric field at the primary receptors in their receptive field increases (decreases) [22, 116]. ON and OFF cells also occur in many other sensory pathways including visual [47], auditory [110] and pain processing pathways [109], where they further shape receptive fields.

All these pathways further involve recurrent connections from higher nuclei back to ON and OFF cells [32, 103]. The role of feedback is a major question in neuroscience, and its answer is likely complicated even by most basic ON/OFF cell properties. In particular, oscillatory activity has been reported in the ELL when there is sufficient spatial correlation in stimuli. This is thought [33, 32] to be important for categorical coding, where spatially correlated stimuli are caused by the presence of other fish (and oscillations ensue) while spatially uncorrelated stimuli relate more to prey (and oscillations do not ensue). It has further been shown [117] that such gamma-range oscillations enhance the directional sensitivity of neurons in the electrosensory system. Since very few lateral connections exist within ELL, the interplay between rhythmic activity and recurrent signals

from higher nuclei back to ELL is of prime importance to understand how such inputs generate oscillations. As this component of feedback circuitry is part of many senses, our analysis provides a picture of the dynamical effects that can be attributed to this basic skeleton of those sensory systems, as opposed to other pieces of circuitry specific to different senses, such as local connections.

Thus our analysis on driven recurrent networks of ON and OFF cells is particularly motivated by experiments in electroreception, where an increase in the spatial correlation of a stimulus causes oscillatory firing activity, an effect requiring feedback and successfully modeled using ON cells only without local connectivity [32, 33]. The fact that OFF cells are equally involved means that an increase in stimulation does not necessarily increase the feedback signal, since ON and OFF cells respond in opposite directions to that input. This raises the question of whether transitions between fixed points and oscillations can still occur, and what specific dynamical effects this arrangement might lead to. Our results below show that transitions to oscillatory activity for constant inputs can indeed occur when both ON and OFF cells are present. Further, we predict novel, and even paradoxical autonomous and driven responses of delayed feedback networks of ON and OFF cells.

4.2 Model

We focus on the simplest case of a 1D layer of intercalated ON and OFF cells. We follow the basic connectivity scheme of the electrosensory system, in which each cell, regardless of type, is coupled identically to every other cell via global delayed feedback [22]. This feedback is provided in reality by a distant population to which the ON and OFF cells project; we assume for simplicity that this population sustains the same activity without further processing and feeds it back to all cells in the 1D layer. Since the delayed coupling connectivity is

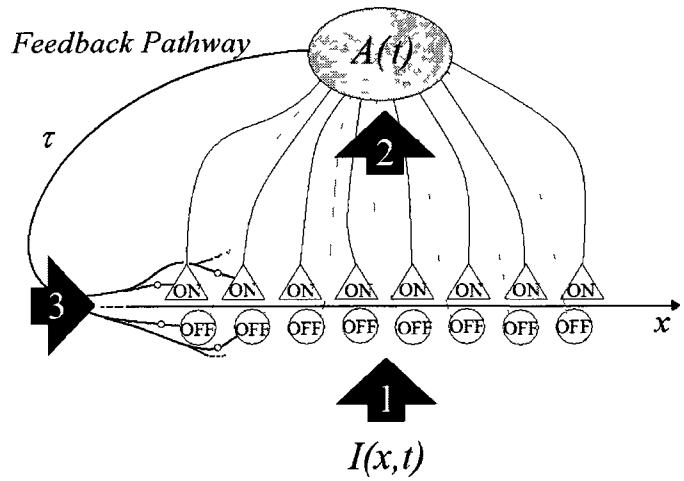

Figure 4.1: **Sensory processing with feedback. 1.** For simplicity, ON cells receive external input $I(x,t)$ directly; OFF cells are identical but receive inverted input via an interneuron (not shown). Apart from feedback, there are no connections between neighboring or distant cells, inspired from the architecture on the electrosensory lateral line lobe. **2.** ON/OFF activity projects to higher brain. **3.** The summed activity $A(t)$ drives ON/OFF cells after a delay τ.

all-to-all, there is no spatial dimension in the autonomous model. However, the spatial stimulus will impose a spatial dimension, i.e. a topology. Our analysis quantifies how opposing responses of these populations to spatiotemporal input $I(x,t)$ affects activity patterns in the ON-OFF layer. The mean somatic membrane potentials or "activities" $u_{on}(x,t)$ and $u_{off}(x,t)$ obey:

$$\begin{aligned} \hat{D}_{on} u_{on}(x,t) &= A(t-\tau) + I(x,t) \\ \hat{D}_{off} u_{off}(x,t) &= A(t-\tau) + V_o - I(x,t) \end{aligned} \tag{4.1}$$

where $\hat{D}_j = (1 + a_j^{-1}\partial_t)$ with synaptic response time a_j^{-1}. $V_o \in \mathbb{R}$ sets the asymmetry between ON and OFF spontaneous rates. ON and OFF cells produce the same feedback (strength and polarity) to all cells [32]. This global delayed

feedback which acts at "3" in Fig.4.1 is

$$A(t-\tau) = k \int_\Omega dy[\alpha_{on} f_{on}(u_{on}(y,t-\tau))$$

$$+\alpha_{off} f_{off}(u_{off}(y,t-\tau))]$$

where, for j =ON,OFF,

$$f_j(u) \equiv (1+e^{-\beta(u-h_j)})^{-1} \tag{4.2}$$

is the firing rate function with threshold h_j and gain β. The finite spatial domain is Ω, while α_j is the relative proportion of j type cells in the population. The delay $\tau > 0$ accounts for processing and axonal conduction times. We set $k = 1$ for excitatory and $k = -1$ for inhibitory feedback. Specific ON/OFF neural systems will deviate more or less from this generic configuration, but understanding their driven recurrent dynamics requires first analyzing this generic case. Further elaborations on this basic circuitry, such as the presence of local connectivity seen in other senses, are briefly discussed below.

4.3 Steady state analysis

To set the stage, we examine the case where, with $I(x,t) = 0$ and no feedback, ON units do not fire ($\bar{u}_{on} \approx 0$) while OFF units do ($\bar{u}_{off} \approx V_o$). This can be adjusted with V_o to suit specific systems. Note however that this information on V_o is difficult to obtain *in vivo*, since the observed firing rate is a combination of the spontaneous activity of the cell and the feedback onto this cell from all cells. The spontaneous rate can be obtained in certain experiments if the feedback can be turned off, e.g. either surgically or pharmacologically, and this "open-loop" knowledge will help calibrate the neural model by adjusting its bias V_o.

The asymmetry V_o plays an important role, seen by performing a bifurcation analysis of (6.1) in the (β, h) parameter space, as well as a function of the delay τ, for the homogeneous and autonomous case $I(x,t) = 0$. Solutions of (6.1) are spatially uniform and implicitly determined by

$$\begin{aligned} \bar{u}_{on} &= k\frac{\Omega}{2}[f(\bar{u}_{on}) + f(\bar{u}_{off})] \\ \bar{u}_{off} &= k\frac{\Omega}{2}[f(\bar{u}_{on}) + f(\bar{u}_{off})] + V_o \end{aligned} \tag{4.3}$$

For simplicity, we chose $\alpha_{on} = \alpha_{off} = 1/2$, $a_{on} = a_{off} = 1$ and $h_{on} = h_{off} \equiv h$ so that we may write the firing rate functions f without subscripts.

4.3.1 Excitatory feedback k=1

For excitatory feedback $k = 1$, no oscillatory solutions are possible. In this case, for $V_o = 0$, varying β passed the value $4/\Omega$ causes a supercritical pitchfork bifurcation only when $\bar{u}_{on} = \bar{u}_{off} = h = \Omega/2$. Otherwise, if $h \neq \Omega/2$, saddle-node bifurcations occur. The dynamics are thus organized around a cusp point. However, when $V_o \neq 0$ with β fixed, multistability ensues as the activation threshold h is varied, with new fixed points arising via saddle node bifurcations. We do not analyze this case is greater detail since our main focus below is on inhibitory feedback.

4.3.2 Inhibitory feedback k=-1

For inhibitory feedback $k = -1$, and for $V_o = 0$, the unique fixed point can bifurcate to a stable limit cycle at an appropriate delay [105, 2] (see Fig.4.2a). Letting $V_o \neq 0$ introduces two distinct instability domains instead of one, as

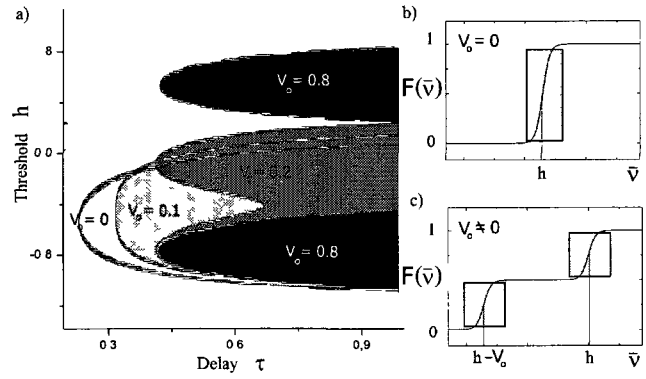

Figure 4.2: **Oscillatory regimes in the threshold-delay parameter space.** Shaded regions, delimited by instability curves, correspond to global temporal oscillations. The shape of these regions is changed by the asymmetry V_o between ON and OFF subpopulations, introducing two effective thresholds in the system (b-c); the shaded boxes mark limit cycle behavior. Parameters are $k = -1$, $\beta = 25$, $\alpha_J = 0.5$ and $\Omega = 1$.

seen in Fig.4.2a in the $h - \tau$ space. Thus multiple transitions to oscillations are possible. In fact, defining $\bar{u}_{on} = \bar{u}_{off} - V_o \equiv \bar{\nu}$ allows us to recast Eq.(4.3) more simply as $\bar{\nu} = F(\bar{\nu}) \equiv k\frac{\Omega}{2}\left[f_{on}(\bar{\nu}) + f_{off}(\bar{\nu})\right]$. Thus, $V_o \neq 0$ amounts to introducing two effective thresholds $h_{on}(V_o, I_o = 0) = h$ and $h_{off}(V_o, I_o = 0) = h - V_o$ (Fig.4.2b,c). The presence of asymmetry $V_o > 0$ creates two distinct spontaneous firing rates for ON and OFF populations, but does not alter the system threshold per se. This change of variable above is used to represent these different activities by a single state, resulting in a one-dimensional fixed point, but which exhibits two "effective" thresholds. The input breaks locally the symmetry introduced by this change of variable and the ON and OFF activities cannot be represented by a single point. From this perspective, plotting stationary firing rate F versus stationary activity $\bar{\nu}$ reveals two distinct regions where oscillations emerge through Hopf bifurcations, surrounded by fixed points (plateaus). Steep regions correspond to oscillations of the activity of the ON and OFF population around their respective thresholds h_{on} and h_{off}. Given a fixed point $\bar{\nu}$, each population will respond to input with a different sensitivity, and be driven in and out of oscillation by inputs of different amplitude. Oscil-

lations always reach all cells due to feedback.

4.4 Responses to static inputs

The results of the last Section lay the foundation for understanding how ON and OFF units integrate spatiotemporal signals. From now on, we set $k = -1$, and illustrate novel responses, first in a regime near the Hopf (large τ), then in the fixed point regime (small τ). Stimuli are always applied to ON and OFF cells evenly.

Spatially uniform input $I(x) = I_o$ linearly shifts the steady state defined by (4.3). This is equivalent to threshold modifications, $h_{on} = h - I_o$ and $h_{off} = h - V_o + I_o$, such that $h_{on} = h_{off} - V_o + 2I_o$. More importantly, a static non-uniform input $I(x,t) = I(x)$ induces in the steady state a non-homogeneous solution that satisfies:

$$\begin{aligned} \bar{u}_{on}(x) &= A(\bar{u}_{on}, \bar{u}_{off}) + I(x) \\ \bar{u}_{off}(x) &= \bar{u}_{on}(x) + V_o - 2I(x) \end{aligned} \tag{4.4}$$

where we have made the dependence on u_{on} and u_{off} explicit. An input may induce a transition from fixed point to oscillations (Hopf) by moving the variable R across its critical value R_c at the bifurcation defined by:

$$tan(\omega(R_c)\tau) + \omega(R_c) = 0 \tag{4.5}$$

for $\omega(R) = \sqrt{R^2 - 1}$ where $R = [\alpha_{on} \int_\Omega dy f'(\bar{u}_{on}(y)) + \alpha_{off} \int_\Omega dy f'(\bar{u}_{off}(y))]$; if $|R| > 1$, $\omega(R)$ corresponds to the frequency at the bifurcation. The network allows the transition from fixed point to global oscillation as a response to an input of sufficient amplitude. Transition to oscillatory behavior is caused by local units approaching the neighborhood of the feedback activation threshold h represented by the shaded area in Fig. 4.2b,c), leading to higher values of the

variable R.

Figure 4.3a demonstrates the effect of the amplitude of a pulse on the variable R defined above. The pulse is a piecewise homogeneous signal that has an amplitude of I_o over a spatial width $\Delta = |x_2 - x_1|$ but is set to 0 elsewhere. For $I_o = 0$, R sits in a local minima for which $R < R_c$ and ON and OFF populations have stationary firing rates. When a localized input drives the system, R increases as the locally excited units approach the activity level h.

Figure 4.3b illustrates the activity increase of both ON and OFF sub-units for some stimulated site located at $x = y$ with respect to the activation curve f, in the spirit of Fig. 4.2b,c. Fig. 4.3c illustrates the same for ON units only. In each case, the stimulated ON population increases its activity towards the threshold, resulting in an increase in the value of R. According to this picture, if the pulse amplitude is high enough, the curve $R(I_o)$ crosses the critical value defined by Eq.(4.5) and oscillatory activity appears throughout the network. Note that if the pulse amplitude increases further, the value of R decreases. Thus, if the pulse amplitude is too high, no oscillatory response will be seen.

Our analysis also reveals that oscillations are less prevalent in an ON/OFF system compared to one with ON cells exclusively (labelled thereafter as ON/ON), in the sense that they occur over a smaller volume of pulse amplitudes and widths. This can be seen in Fig.4.3a by the larger area occupied by the curve above the critical line $R = R_c$ in the ON/ON case compared to the ON/OFF case. Further, ON/OFF nets can exhibit oscillations for either positive and negative inputs. As one can see in Fig. 4.3a, the ON/OFF network allows R to cross the instability threshold R_c for both positive and negative pulse amplitudes, while the ON/ON network only does so for positive amplitudes. This result is intuitively expected given the distinct rectification properties of ON and OFF cells.

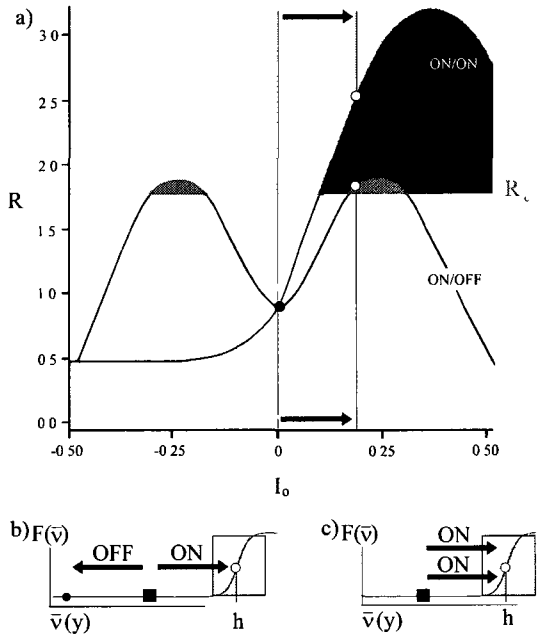

Figure 4.3: **Impact of local stimulation.** a) Variable R as a function of a localized pulse amplitude. The amplitude of the pulse is I_o over a spatial width of $\Delta = 0.6$ and is zero otherwise. Increasing the amplitude will cause the value of R to change, for a network made of equal numbers of ON and OFF cells (ON/OFF) and one built uniquely of ON cells (denoted by ON/ON). In both cases, crossing the critical value R_c causes a Andronov-Hopf bifurcation and the resulting limit cycle becomes stable. Other parameters are $V_o = 0.0$, $h = 0.1$, $\beta = 25$, $\alpha_j = 0.5$. b) Schematic of local effects of excitatory stimulation in the activity for some driven site $x = y$ in a ON/OFF network. In this example, prior to the input, both ON and OFF units have the same activity denoted by the dark square. Local inputs shift activity states towards (resp. away from) the threshold h for the case of ON units (resp. OFF) units. Changes in the variable R, and thus the resulting oscillations, are essentially due here to the change in activity of the ON cells (open circle), since the activity of the OFF cells is negligible (dark circle). c) Similar behavior occurs in a ON/ON network, but the activities simultaneously approach the threshold, resulting in a greater increase in R, as shown in part a). The opposite occurs for inhibitory pulses.

Interestingly, for some parameters, global oscillations are stable for $I(x) = 0$, and the reverse transition is observed, as shown in Fig. 4.5. We emphasize that distinct ON and OFF populations allow such an instability to occur even if their effective thresholds are not identical. Furthermore, letting an input spatial profile tend to a constant recovers the homogeneous problem described

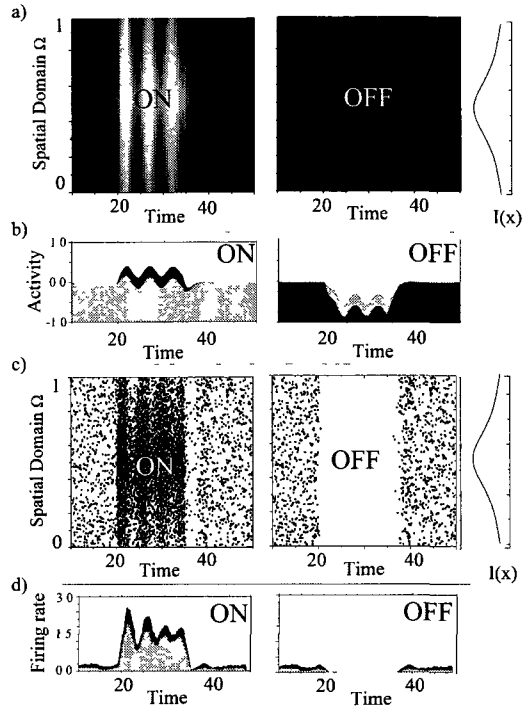

Figure 4.4: **Oscillatory response triggered by a static input bump.** ON (left) and OFF (right) populations responding to a localized positive bump. Grey shading encodes relative activity amplitudes. b) Central(black) and lateral(grey) response of ON and OFF populations, showing the time evolution of the solutions inside and outside the pulse. The input triggers oscillations from stationary activity states. Parameters are $V_o = 0.0$, $\tau = 1.8$, $h = 0.12$, $\beta = 25$ and $\alpha_j = 0.5$. The bump has an amplitude $I_o = 0.6$ for $t \in [20, 35]$, and is set at 0 otherwise. c) Equivalent phenomenon in a stochastic spiking network of $N = 1000$ integrate-and-fire neurons equally spaced on the "spatial" interval $[0, 1]$ (see Eq. (4.6)). ON cells demonstrate oscillatory firing rates, while OFF cells are inhibited in the subthreshold regime. Parameters are $V_o = 0$, $\alpha_j = 0.5$, $\tau = 1.8$, $D = 2.0$, $h_{on} = h_{off} = 1$, with $\mu = 0.2$ and $g = -0.05$. The refractory period is $\tau_{ref} = 0.1$. The membrane and synaptic time constants are $a = \tau_m = 1$. The input amplitude is 2.0 for $20 < t < 35$ and 0 otherwise. The bump length scale is set at $\sigma = 0.6$. d) Mean firing rate variations in time of ON and OFF cells from LIF simulations. Changes in the cell mean firing rate are shown both inside (black) and outside (grey) the bump. Mean firing rate is stationary prior to stimulation. The bump triggers global firing rate oscillations. A time window of 10 integrating steps was taken to approximate the frequencies. Note that time, here and in the following figures, is in arbitrary units which can be mapped to physiological time scales. The firing rate is expressed in spike/τ_m.

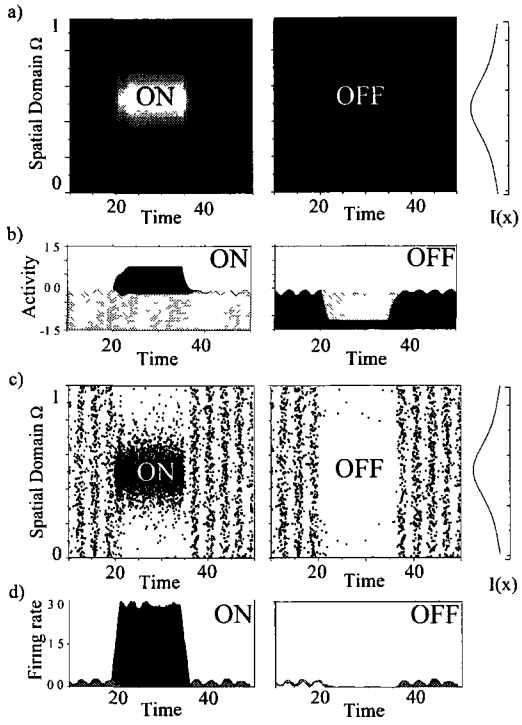

Figure 4.5: **Bump-shaped stimulus removing global oscillations.** a) As in Fig. 4.5, ON (left) and OFF (right) cells responses to a localized positive bump are shown. b) Central(black) and lateral(grey) dynamics shows the damping of the oscillations as the input is turned on. Parameters are $V_o = 0.0$, $\tau = 1.1$, $h = -0.05$, $\beta = 25$ and $\alpha_j = 0.5$. The bump has an amplitude $I_o = 0.2$ for $t \in [20, 35]$, and is set at 0 otherwise. The bump length scale is set here at $\sigma = 0.1$ c) Equivalent phenomenon in a stochastic spiking network of $N = 1000$ integrate-and-fire neurons equally spaced on the "spatial" interval $[0, 1]$. Other parameters are $V_o = 0$, $\alpha_j = 0.5$, $\tau = 1.1$, $D = 1.0$, $h_{on} = h_{off} = 1$,$\tau_{ref} = 0.1$ with $\mu = 0.8$ and $g = -0.06$. The membrane and synaptic time constants are $a = \tau_m = 1$. The input amplitude is 0.5 for $20 < t < 35$ and 0 otherwise. d) Mean firing rate as a function of time for both ON and OFF cells, inside(black) and outside(grey) the input bump. A time window of 10 integrating steps was taken here as well. The firing rate is expressed in spike/τ_m.

by asymmetry-induced instabilities as in Fig.4.2, where limit cycles are only allowed in restricted regions of the $(h(V_o, I_o), \tau)$ parameter space.

4.4.1 Numerical Simulations

We numerically test these predictions using spatially localized bump stimuli which are biophysically relevant. In Fig.4.4 and 4.5 we consider the response of Eq. (6.1) to $I(x,t) = I_o(2\sigma)^{-1}exp[-|x-x_o|\sigma^{-1}]$ if $t_1 < t < t_2$ and 0 elsewhere. In Fig. 4.4, the bump drives the sensory layer for $t > t_1$, and stationary activities lose their stability when the variable R satisfies Eq.(4.5). Global oscillations appear across the network, modulating the structure of the bump-shaped responses. The reverse mechanism occurs at $t = t_2$ when the bump disappears, and where ON and OFF stationary activities recover their stable fixed point behavior. In Fig. 4.5a, the opposite phenomenon is observed. Prior to the bump, limit cycles are stable for the chosen parameters, until $t = t_1$. The global equilibrium (4.4) becomes stable during the input, and loses stability at input offset as the boundary defined by Eq.(4.5) is crossed again.

This behavior is further qualitatively reproduced in simulations of noisy spiking networks of Integrate and Fire neurons (LIF) with all-to-all coupling. Our aim is to show that a simple generic form of this model adapted to the ON/OFF context can show qualitatively similar behavior to that of the neural field model. Our goal is not to provide a detailed representation of experimental data, nor a detailed correspondence between the LIF and the neural field formulation. The respective ON and OFF membrane potentials v_j^{on} and v_j^{off} in a population of N cells obey

$$\tau_m \frac{dv_j^{on}}{dt} = -v_j^{on} + g\sum_{t_i} \eta(t_i - \tau) + \mu + \xi(t) + I(j,t)$$

$$\tau_m \frac{dv_j^{off}}{dt} = -v_j^{off} + g\sum_{t_i} \eta(t_i - \tau) + \mu + \xi(t) + V_o - I(j,t) \qquad (4.6)$$

with Gaussian white noise $\xi(t)$ of intensity D, feedback gain g, spiking times of all neurons $\{t_i\}$ and bias current μ. The synaptic response function is given by $\eta(s) = ae^{-as}$ whenever $s > 0$ and zero otherwise. The synaptic time constant a is here set to 1. The membrane time constant τ_m is also fixed to 1. The

asymmetry V_o and input amplitude I_o must be tuned in order to reach the appropriate membrane potential correspondence between the neural field and LIF formulations of network dynamics. Indeed, our numerical experiments suggest that a close relationship exists between both model formulations, but its full determination is not the aim of the current work. Figure 4.5b shows that the firing rate oscillations vanish across the domain as the input is turned on. The input causes the feedback to reach a critical amplitude, bringing cells subthreshold and thus inhibiting network activity. Pyramidal cells in the electrosensory system can increase their firing rates more than tenfold in response to a stimulus, so large variations are physiological. The specific mean firing rates observed in our simulations, as well as the frequency of the emerging firing rate oscillation via the Hopf bifurcation, are consequences of the specific choices of the synaptic time constant (set throughout to $a = 1$) as well as the membrane time constant (set throughout to $\tau_m = 1$) and the delay. For example, lower firing rate oscillation frequencies are observed for larger delay values (not shown). If time units are scaled such that 1 (time unit) = 10msec, as the physiologically relevant delay range suggests, one obtains firing rate oscillation frequencies around 50 Hz, as observed in experimental studies on the electrosensory system [32, 33, 34].

4.4.2 Central and lateral responses

We next consider network responses to input for smaller delays, i.e. in the fixed point regime. For $V_o \neq 0$, the response to a local pulse, where $I(x,t) = I_o$ for $x \in [x_1, x_2]$ if $t_o < t < t_1$ and $I_o = 0$ otherwise, might alter feedback in non-intuitive ways. Indeed, asymmetry between ON and OFF populations induces, lateral to the pulse, a non-monotonic response as I_o increases (Fig. 4.6a). As input increases, the contribution of the stimulated cells to the global feedback is first reduced, then enhanced. The behavior of both ON and OFF cells shown in Fig.4.7a,b illustrates the phenomenon in Fig.4.6a,b. For a small pulse, the magnitude of global feedback drops: lateral activity goes up. For a larger pulse, ON activity increases further, OFF activity remains low as for

the small pulse, and global feedback is stronger: lateral activity is now less than before the pulse. This is a consequence of the feedback component $A(t)$ varying non-monotonically with respect to I_o, which is reflected by the lateral response behavior plotted in Fig. 4.6a. The magnitude of this effect depends on the choice of parameters, especially the feedback gain, which can be adjusted to amplify the excitatory and inhibitory responses. The central response will, however, always be more important than the lateral response. This phenomenon is also observed in our integrate-and-fire network, where the lateral firing rate first increases then decreases when the input amplitude is augmented, as shown in Fig. 4.8. We further note that excitatory feedback ($k = +1$) alone brings solutions away from the threshold; response curves are monotonic. Small excitatory feedback in parallel with dominant inhibitory feedback is equivalent to a small change in the gain k, as long as solutions maintain their stability properties for $k < 0$ (not shown).

4.5 Response to time periodic stimuli

More paradoxical effects are seen in the fixed point regime with stimuli of the form $I(x,t) = I(x)sin(\omega_o t)$, where $2\pi/\omega_o$ is large compared to the synaptic $(1/a_j)$ and feedback (τ) time scales. For a local pulse $I(x) = I_o$ for $x \in [x_1, x_2]$ and $I(x) = 0$ elsewhere, we observe a lateral discrepancy in the dominant frequencies of the population activity (Fig.4.9). *Interestingly, this is a spatial change in oscillatory mode, but without any space dependent connectivity.* The feedback integrates input from both ON $(+I(x,t))$ and OFF $(V_o - I(x,t))$ cell populations which, for periodic input, are in antiphase. Given the form of the firing rate function, each of these feedback components is roughly a half wave-rectified version of the input oscillating at frequency ω_o. The sum of these two components produces a feedback that fullfills the role of a second forcing term, driving the system globally at frequency $2w_o$ as a full-wave rectified version of

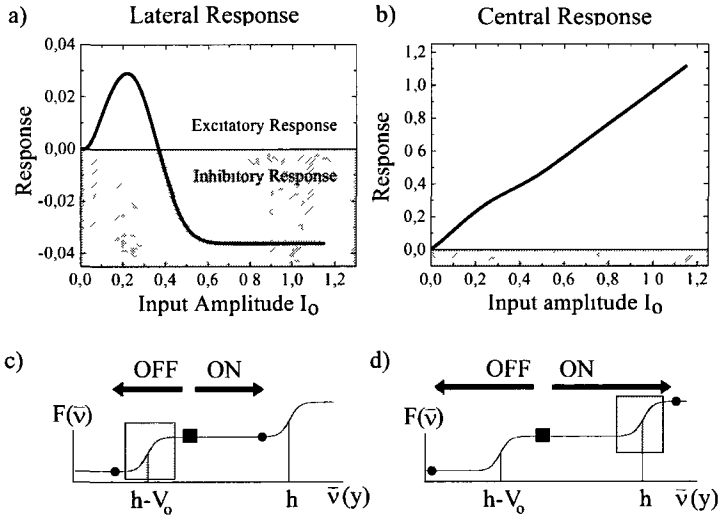

Figure 4.6: **Response vs I_o outside the pulse is non-monotonic.** Inhibitory feedback decreases, as OFF activity massively decreases, but then increases, as ON cells are locally recruited by the pulse and continue to increase their rate. Note that the magnitude of the response depends on the choice of parameters, especially the feedback gain $|k|$ (here set to 1), but is smaller than that in the central response. b) Response vs I_o inside the pulse (central ON cell) is monotonic, but with two slopes. The same non-monotonic feedback effect as in (a) occurs, but is compensated by I_o. The difference between the curves in (a) and (b) is simply I_o. Note that for central OFF cells, the response curve is monotonically decreasing, due to the inhibitory effect of the incoming pulse. The pulse amplitude is I_o for $x \in [0.35, 0.75]$ and $t \in [20, 25]$, and 0 otherwise, $V_o = 0.3$, $h = 0.05$, $\beta = 25$, $\tau = 0.2$ and $\alpha_j = 0.5$, with random initial conditions. c) Schematic description of local effects of stimulation for some driven site x=y, resulting in non-monotonic lateral response. The variable used here is $\bar{\nu}$, in order to represent the asymmetrical solutions u_{on} and u_{off} by a single state with two distinct thresholds. Given the parameters considered, the fixed point $\bar{\nu} = F(\bar{\nu})$ before the pulse (dark square) is located in the plateau between $h_{off} = h - V_o$ and $h_{on} = h$ but closer to h_{off}. By analogy to the initial formulation (i.e. without $\bar{\nu}$), the stimulation puts u_{onf} and u_{off} in different parts of the response curve. As the input drives the units, the activity of the OFF cells (dark circle to the left) is inhibited and crosses the threshold h_{off}, while ON cells (dark circle to the right) are not excited sufficiently to reach their response threshold h_{on}. The cumulative effect across all stimulated sites generates a decrease in the amplitude of the inhibitory feedback, and lateral activity increases. d) As the input amplitude increases further, the activity of the ON cells crosses h_{on} and augments the amplitude of the inhibitory feedback, leading to a lateral decrease in activity.

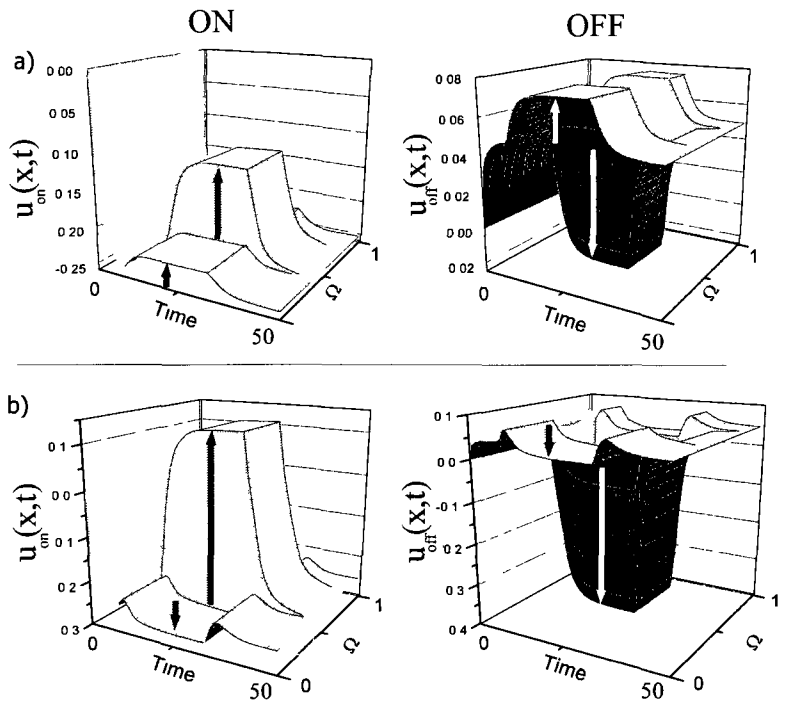

Figure 4 7· **Response of the ON and OFF cells to a localized discontinuous pulse of amplitude I_o in the fixed point regime**. Here, for $I_o = 0$, OFF cells are firing and ON cells are almost silent. The initial decay seen in the time course of the ON cells is caused by this choice of initial conditions. a) ON(left) and OFF(right) populations activity in response to the pulse. Here $I_o = 0\,1 < V_o$. Activity of all cells increases. b) The pulse amplitude is increased to $I_o = 0.4 > V_o$; lateral activity now decreases The pulse is identical as in Fig. 4 6.

the input. This rhythm always appears, regardless of whether the periodic pulse drive is local or global. However, inside the pulse, the direct input competes with the feedback, producing a dominant rhythm at ω_o for sufficiently large I_o. Outside the pulse, only the global feedback-driven rhythm at $2\omega_o$ is seen.

Further, near to the Hopf regime (e g. for larger delays), a time-periodic pulse of large amplitude and/or spatial extent will induce a sequence of Hopf bifurcations as the condition in Eq.(4.5) is cyclically fullfilled. The result is a complex waveform that includes bursts relating to the Hopf-induced limit cycles

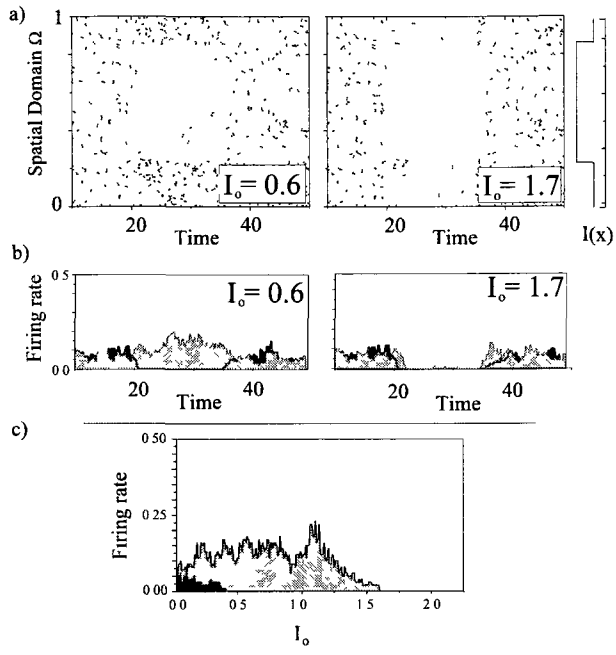

Figure 4.8: **Non-monotonic lateral response of OFF cells to a spatially localized pulse in a LIF network.** a) A spike plot of a network of $N = 1000$ cells, qualitatively reproducing the results shown in Fig. 4.6 and 4.7 is shown. Smaller input amplitudes(left) generate an excitatory lateral response, while the response for larger amplitudes becomes inhibitory(right). b) Time evolution of the firing rate both inside(black) and outside(grey) the pulse. As the input amplitude increases from 0.6 to 1.7, the lateral response changes from excitatory to inhibitory, and the firing rate first increases and then decreases. c) Central(black) and lateral(grey) firing rate as a function of the input amplitude I_o, qualitatively reproducing the results shown in Fig. 4.6a,b. The lateral response exhibits the same non-monotonicity, while the central response is monotonically decreasing, as expected from center OFF cells. Given this parameter set, OFF cells are in the suprathreshold regime due to the choice of a high value of V_o, while the ON cells are maintained in the subthreshold regime where they fire at a very low rate (not shown). The non-monotonic response of the ON cells can be appreciated in the neural field model (Fig. 4.7) because the "activity" is plotted (rather than spike times), and this activity can take values below the threshold. Parameters are $V_o = 1.2$, $\alpha_j = 0.5$, $\tau = 0.1$, $D = 1.0$, $\tau_{ref} = 0.1$. $\mu = 0.1$, $h = 1.0$ and $g = -0.9$. The input has an amplitude of I_o between $[0.25, 0.85]$ for $20 < t < 35$ and zero otherwise. A time window of 10 integrating steps was taken to compute the firing rates. The firing rate is expressed in spike/τ_m.

(not shown). Their analysis will be presented elsewhere.

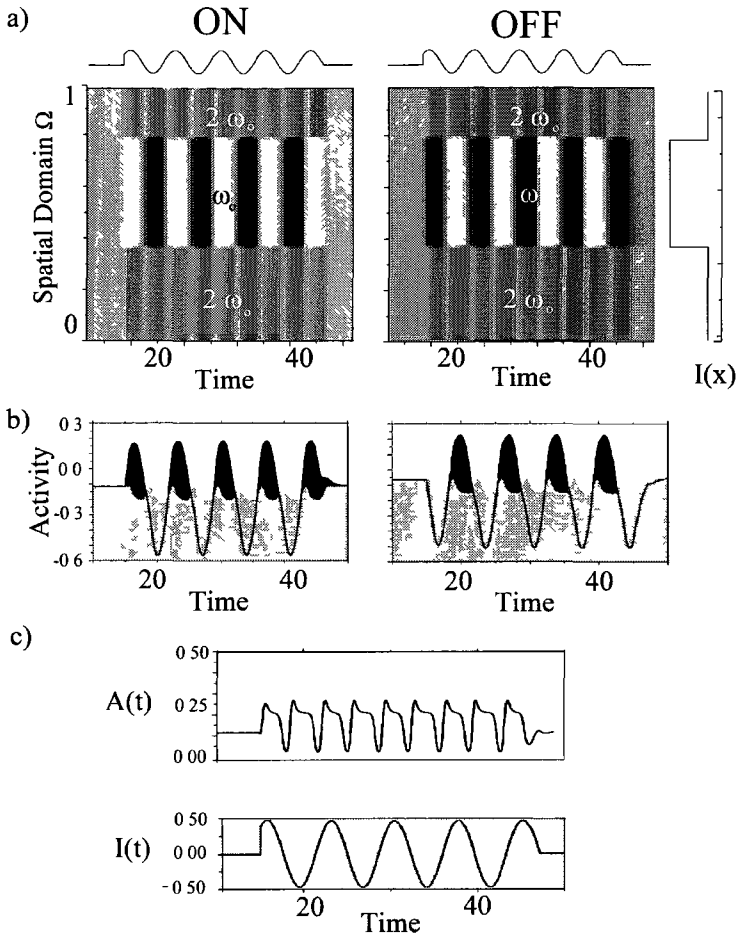

Figure 4 9: **Lateral frequency doubling effect**. a) Spatially inhomogeneous response of ON(left) and OFF(right) populations to local periodic forcing with $I_o = 0.5$ over the region $x \in [0.35, 0.75]$ and zero elsewhere for $15 < t < 45$. b) Time evolution of the activity of ON and OFF cells inside(black) and outside(grey) the time-periodic pulse, showing the central-lateral response discrepancy. c) Associated time evolution of the feedback signal $A(t)$, showing that combined ON and OFF contributions make the recurrent component oscillate at twice the input frequency. Parameters are $\omega_o = 0.9$, $V_o = 0\,05$, $h = 0.0$, $\beta = 25$, $\tau = 0.4$ and $\alpha_j = 0.5$.

4.6 Discussion

We have performed a bifurcation analysis of a neural field of ON and OFF cells with all-to-all delayed coupling. For excitatory coupling we have found multi-stability between homogeneous fixed point states. Novel and even paradoxical effects are predicted to occur in such networks with inhibitory coupling, on which we have put more emphasis. Our work was directly inspired by the configuration of the electrosensory system in which local connections are weak compared to delayed feedback connections. Localized inputs near the Hopf regime can turn oscillations on or off. Compared to equivalent networks made fully of ON cells, we have shown that such nets exhibit transitions to oscillations over a narrower range of parameters that characterize the pulse input - namely its width and strength. However, the ON/OFF network is shown to exhibit such transitions for both stimulus polarities. Our work supports the observation of oscillations in the electrosensory system seen with spatially correlated inputs [32, 33] when both ON and OFF cells are present. A next step is to extend our analysis to stochastic spatiotemporal stimuli to show how, as in those studies, the spatial correlation of a stochastic input can bring on gamma-range oscillations, and whether the Hopf curve behaves as shown here for localized pulse inputs.

In the fixed point regime, localized inputs produce monotonic or non-monotonic input-output relations. Local time-periodic forcing leads to co-existing network oscillations at different frequencies, in the sense that we can see one gamma frequency centrally, where cells are in the receptive field of primary receptors (such as electroreceptors projecting to ELL) receiving the pulse stimulation, while another frequency is measured laterally to the pulse. In fact, experiments have been proposed [118] to measure these non-monotonic lateral as well as frequency doubling effects, especially to see the spread in the range of gamma frequencies that ensues.

Another direction of interest is to consider how local connectivity interacts with the global delayed loop considered here. Our results are qualitatively and

numerically unchanged (not shown) if non-delayed inhibitory feedback is also present, mimicking local connectivity. The same is true when moderate positive delayed feedback is present at the same time as the negative all-to-all delayed feedback considered here. A deeper analysis of the dynamical effects caused by such additional circuitry is beyond the scope of our study and is left for future work. Local connectivity makes the system truly spatial to begin with, rather than only in the presence of a stimulus as is the case in the present study.

We note that all-to-all networks of stochastic LIF neurons have been analyzed using a mean field analysis [119] in which the field contributed by all cells affects the mean bias and the noise level of each cell. They have found oscillatory behavior when inhibition is sufficiently strong, which is in line with our findings using neural field theory and with our numerics on the neural field and the LIF's. Because of the all-to-all coupling, including sparse random coupling, their theory is also without space, as is ours. Although we consider only excitatory or inhibitory connections in isolation, our work goes beyond their study by considering that ON and OFF cells both receive external input and respond in opposite directions to it. Further we consider the effects of time-varying inputs. It will be of interest to develop their theory or that in [33] to see how the noise influences the effects that we describe. It will also be of interest to see what are the prime determinants of the oscillation frequency in delayed nets of all-to-all coupled ON and OFF cells as a function of the balance of excitation and inhibition, the noise level and of the relative time scales of excitatory and inhibitory networks, as has been investigated for autonomous networks in [120].

As mentioned in the introduction, ON and OFF cells are found in most sensory pathways and in conjunction with feedback. The simple circuit investigated here can thus serve as a stepping stone towards understanding responses to inputs, including the onset of oscillations, in other senses, since the oscillation mechanism discussed here is accessible to these senses. Oscillations in the visual system induced by spatially correlated stimuli have been argued to rely mainly

on local circuitry in cortex. Further, locally generated oscillations can be amplified by a recurrent loop such as the thalamo-cortical loop [103]. This is clearly different from the electrosensory system where the feedback loop is important (see also work on the nucleus isthmi in the visual tectum by Wessel et al.[112]) As these resulting temporal oscillations are thought to be of particular significance for higher cognitive functions [96, 98], their continued dynamical analysis in the context of more biophysically detailed driven networks of ON and OFF cells is further warranted.

Acknowledgments

We thank A. Hutt, L. Maler and W. Nesse for discussions and NSERC Canada and FQRNT for support.

Chapter 5

Responses of recurrent nets of asymmetric ON and OFF cells

Lefebvre J., Longtin A., LeBlanc V.G. (2010) Journal of Biological Physics, in press

Abstract

A neural field model of ON and OFF cells with all-to-all inhibitory feedback is investigated. External spatio-temporal stimuli drive the ON and OFF cells with, respectively, direct and inverted polarity. The dynamic differences between networks built of ON and OFF cells ("ON/OFF") and those having only ON cells ("ON/ON") are described for the general case where ON and OFF cells can have different spontaneous firing rates; this asymmetric case is generic. Neural responses to non-homogeneous static and time-periodic inputs are analyzed in regimes close to and away from self-oscillation. Static stimuli can cause oscillatory behavior for certain asymmetry levels. Time-periodic stimuli expose dynamical differences between ON/OFF and ON/ON nets. Outside the stimulated region, we show that ON/OFF nets exhibit frequency doubling, while ON/ON nets can not. On the other hand, ON/ON networks show antiphase responses between stimulated and unstimulated regions, an effect that does not rely on specific receptive field circuitry. An analysis of the resonance properties of both net types reveals that ON/OFF nets exhibit larger response amplitude. Numerical simulations of the neural field models agree with theoretical predictions for localized static and time-periodic forcing. This is also the case for simulations of a network of noisy Integrate-and-Fire neurons. We finally discuss the application of the model to the electrosensory system and to frequency doubling effects in retina.

5.1 Introduction

Information processing along sensory pathways relies both on single cell properties and network geometry. A dominant feature of these pathways is feedback between successive anatomically distinct neural populations or nuclei, as well as connections within each nuclei. At some point along a sensory pathway, feedback appears, and shapes the integration and processing of spatio-temporal inputs in ways that are yet to be fully understood. Much experimental and theoretical research is in fact devoted to this issue. In particular, feedback may underlie the

appearance of oscillatory activity when the input has certain attributes. Such oscillations, which have been linked to information processing tasks in many areas of the nervous system, often emerge via inhibitory feedback connections [121, 122, 2, 105, 106], and especially when delays are present [56, 2, 97]. Large delays can even produce multistability [2, 123].

Localized inputs are known to cause localized increases in activity or "bumps" that can be maintained as long as the input is on. Oscillatory responses to static input can also occur because the spatial profile of the input induces an Andronov-Hopf bifurcation in the recurrent network [98, 99]. In other cases, the degree of spatial correlation in an otherwise stochastic input determines the onset of oscillation [56, 33]. Such oscillations, however, are not always triggered by a static stimulus. Time-periodic inputs also recruit the temporal integration properties of the sensory pathway, and drive recurrent connections. Investigations of these issues has also moved on to more realistic two-population systems [85, 88], where all cells respond the same way to external input.

In fact, the bulk of the research on driven neural networks considers that all cells respond in the same manner to the external stimulus. However, most sensory systems are made up, at some point along the way, of two subpopulations, namely ON and OFF cells [47, 110, 109, 124]. This is true for the visual, auditory, pain, and electrosensory systems. The ON and OFF populations are distinguished by their response to inputs. ON cells receive input directly, and increase their firing activity when the input increases. In contrast, OFF cells receive an inverted image of incoming stimuli, transmitted via inhibitory interneurons [47]. Secondly, ON and OFF cells will generally fire at different mean rates even in the absence of an external input stimulus. Examples of such asymmetrical zero-input activity between ON and OFF populations have been observed in the electrosensory system [35] and the visual system [125], where the distribution of firing rates for ON cells has a different mean than that for OFF cells.

The distinct responses of ON and OFF populations with different intrinsic spontaneous rates is the focus of our paper. We characterize this rate difference as an "asymmetry". This situation is usually described as one wherein the two populations have distinct firing rates, where "spontaneous" refers to the fact that there is no external stimulation. But this is to be distinguished from another common use of the term "spontaneous" where the context is one in which the cell is isolated from both the external stimulus and the feedback. The firing of the cells at different mean rates is usually attributed to the fact that there is either local circuitry that produces different net currents into the cells, or that the intrinsic physiological characteristics such as leak conductance are different, or both. It is already an interesting question to infer these "intrinsic spontaneous" rates from the spontaneous rates measured when the feedback is intact (with zero-input in both cases). In some settings, it is possible to pharmocalogically or surgically impair the feedback to reveal the intrinsic spontaneous rates.

In this article, we propose a comprehensive comparative study of input response dynamics of networks built of ON and Off cell populations (ON/OFF nets) to those of networks built solely of excitatory cells (ON/ON nets). In [111], a variety of stimulus responses in a ON/OFF net have been presented in the context of a neural field model, with much additional support from simulations of networks of noisy leaky integrate-and-fire neurons. The parameters that influenced the number of steady states of the network dynamics and their stability were analyzed. In particular, it was shown that unequal spontaneous firing rates or "asymmetr" can strongly influence the number of steady states and their stability, but without demonstrating stronger implications of this asymmetry as we do here. Further, the response features discussed in [111] gave little information about the sensory processing differences and benefits enabled by the combined action of multiple neural populations. It is especially important to determine whether a recurrent symmetric ON/OFF net, which our previous study showed is less likely to exhibit self-sustained oscillations in response to a static input,

is still less likely to do so when the symmetry condition is relaxed Our results below show that, surprisingly, this is not the case, i e asymmetric ON/OFF nets can be more prone to oscillate

To address the fundamental questions of the advantages versus disadvantages of an ON/OFF organization, a systematic comparison of stimulus-induced states in networks with and without OFF cells is essential This will enable us to distinguish response features due to feedback nonlinearities from those caused solely by the characteristic inhibitory responses of OFF cells to input Our paper builds on the recent results on recurrent networks of ON and OFF cells in [111] and can be seen as the natural extension of that work It first extends its predictions by investigating enlarged regions of parameter space (with special attention paid to the delay and the asymmetry), and further identifies an array of novel effects The enlarged region is particularly explored in the context of the response of both ON/ON and ON/OFF networks to stimuli (static as well as time-periodic) close to and away from the Andronov-Hopf regime, our previous work was limited to the regime away from the Andronov-Hopf bifurcation It compares the propensity to oscillate of asymmetric ON/OFF nets to that of symmetric ON/OFF nets and of ON nets Further, it contrasts the input-output characteristics of such recurrent networks in the time and frequency domains, enabling a comparison of their resonance properties The paper also presents novels results on a newly found discrepancy between the response of ON cells in the central region (i e where external forcing is applied) in ON/ON nets versus ON/OFF nets in the context of periodic input, and exposes the subtle role of asymmetry and of feedback in this effect and in frequency doubling in general Finally, we study the response of ON/OFF nets to periodic gratings, i e periodic forcing in both space and time, and discuss how these results can shed light on certain aspects of frequency-doubling phenomenon known to occur in the retina under conditions of periodic spatiotemporal illumination [126, 127]

In Section 5 3, we review the mechanism by which a static spatially localized

pulse triggers global oscillations, and investigate the instability threshold as a function of the activity asymmetry between ON and OFF populations. We then study in Section 5.4 the effect of time-periodic stimulation to see how a lateral response frequency discrepancy is generated, and proves that it can only be seen in ON/OFF systems. In each of these cases, we focus on the role played by asymmetrical firing rates on the behavior of neural populations. Lastly, in Section 5.5, we use the properties of the feedback connections to qualitatively reproduce results on frequency doubling in the retina. Throughout our work, we systematically compare our model predictions based on a neural field formulation with numerical simulations of an network of noisy leaky integrate-and-fire (LIF) neurons with all-to-all (i.e. global) delayed feedback.

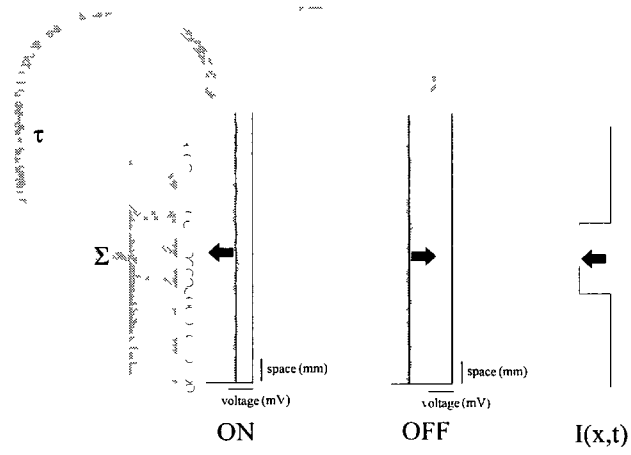

Figure 5 1 Schematic of the driven ON/OFF network The spatial extent of the network is shown vertically, while the mean somatic membrane potential, or activity, across the domain is drawn horizontally The system is composed of a layer of intercalated ON and OFF pyramidal cells As an example, here OFF cells (right) have a higher activity level than ON cells (left) When the input $I(x,t)$ increases and is applied to both cell types, ON cells become more excited, and OFF cells have a reduced activity All activities are summed (Σ) across the network and sent back to the pyramidal cell layer with all-to-all delayed feedback coupling Lateral connections between neural sites are considered weak and negligible

5.2 Model

Figure 6.1 illustrates the neural field model built of ON and OFF cells, connected globally via inhibitory delayed feedback only. Both populations are homogeneously distributed along a spatial domain of size Ω. Activities of the ON and OFF populations propagate to a higher brain center. This center integrates the activity and feeds it back inhibitorily to the sensory layer, i.e. to all ON and OFF cells after some propagation time lag $\tau > 0$. The feedback activity to ON and OFF cells also goes through the same synaptic response function (see below). The parallel sensory pathways of ON and OFF cells are thus identical. The only difference is an interneuronal relay between the external stimulus and the OFF cell, which inverts the polarity of incoming sensory signals. For simplicity we have omitted the dynamics of any primary sensory receptor cell, as well as the connectivity between these cells and the ON and OFF cells that would determine the receptive field. In the visual system, such primary cells also include many classes of retinal ON and OFF cells, which project to thalamic ON and OFF cells. In contrast, in the electric sense the receptors are only of the ON type, and project to ON and OFF pyramidal cells (known as E and I cells, respectively). No lateral connections between cells are assumed, although spatially localized sensory stimuli drive localized ON and OFF populations, with direct and inverted polarity, respectively. Local perturbations are nevertheless propagated throughout the network via the recurrent loop, where they generate linear effects, as well as non-linear effects resulting from bifurcations.

The architecture considered here, although common to many early sensory systems, is inspired by the layout of the electrosensory lateral line lobe (ELL), found in the weakly electric fish, where very few lateral connections exist [22]. This point distinguishes our approach from most neural field models, which typically incorporate spatial kernels. Local circuitry has indeed an important impact on the generation and stability of spatial patterns [44, 86, 78, 74], but we focus here on the effects of delayed interactions. Nevertheless, our previous work [128] has shown that moderate instantaneous recurrent connections, mimicking

local anatomy, influence only quantitatively the tendency of a dominantly inhibitory delayed feedback system to oscillate by altering the oscillatory response threshold and frequency. These effects have further been shown to not change the dynamics of this model qualitatively. Note that while the model set-up is inspired from the electrosensory system, it also applies to any recurrent network in which the cells receiving global feedback can be split into two groups: ones that respond to external input changes with activity changes of similar and opposed polarity.

The mean somatic membrane potential, or *activity*, of the sub-populations $u_{on}(x,t)$ and $u_{off}(x,t)$ evolves according to the dynamics

$$\begin{aligned}(1+a^{-1}\partial_t)u_{on}(x,t) &= -A(t-\tau)+I(x,t) \\ (1+a^{-1}\partial_t)u_{off}(x,t) &= -A(t-\tau)+V_o+sI(x,t),\end{aligned} \tag{5.1}$$

where a is the time constant of the synapse, whose response to a delta-function spike is of the form $\eta(t) = ae^{-at}$. We will fix at $a = 1$ throughout our work. The sensory signal $I(x,t)$ is added to the activity of an ON cell with preserved polarity, while an OFF cell receives the input with inverted polarity ($s = -1$). Also, the OFF cell generally fires at a different rate in absence of input ($I = 0$) and feedback ($A = 0$); without loss of generality we consider $V_o \geq 0$. We will make comparisons between ON/OFF networks and ON/ON networks. Thus we parameterize ON/OFF networks by setting $s = -1$, and ON/ON networks by setting $s = +1$. The recurrent feedback term A integrates the activity of each population across the network

$$A(t-\tau) = G\int_\Omega dy[\alpha_{on}f(u_{on}(y,t-\tau)) + \alpha_{off}f(u_{off}(y,t-\tau))], \tag{5.2}$$

where $f(u) \equiv (1+e^{-\beta(u-h)})^{-1}$ is a sigmoidal firing rate function, with threshold h and gain β. The network full spatial extent is here $\Omega = 1$ and remains fixed throughout. α_j for $j = (on, off)$ corresponds to the proportion of j type cells amongst the total population. These will be fixed at $\alpha_{on} = \alpha_{off} =$

0.5, so that our network contains an even number of ON and OFF cells. The feedback gain G will be fixed to 1 for the rest of the analysis. We further set $\beta = 25$, so that our firing rate functions are relatively smooth sigmoids. The feedback is nevertheless a nonlinear function of its input u, which makes the whole system nonlinear. In our comparative study, we frequently present the alternative description provided by a noisy leaky Integrate-and-Fire network. The evolution of the membrane potential of the j-th LIF neuron obeys

$$\begin{aligned} \frac{dv_j^{on}}{dt} &= -v_j^{on} + g\sum_{t_i} \eta(t_i - \tau) + \mu + \xi(t) + I(j,t) \\ \frac{dv_j^{off}}{dt} &= -v_j^{off} + g\sum_{t_i} \eta(t_i - \tau) + \mu + \xi(t) + V_o + sI(j,t), \end{aligned} \tag{5.3}$$

with Gaussian white noise $\xi(t)$ of intensity D, i.e. the autocorrelation is $\langle \xi(t)\xi(t') \rangle = 2D\delta(t-t')$. The feedback gain is denoted by g, the spiking times of all neurons by t_i, and the bias current by μ. V_o is here again the asymmetry parameter. This setup is analogous to the neural field description given in Eq.(6.1), where only mean somatic membrane potentials are taken into account.

5.3 Responses to Static Stimuli

The type of response generated by a static (time-independent) sensory input depends on the proximity of the selected parameter set to the Andronov-Hopf curve, which separates equilibrium (fixed point) solutions from oscillatory solutions. There are two cases to consider: the Andronov-Hopf regime and the fixed point regime. The fixed point regime is typically reached by selecting small or zero delays. In this regime, only feedback dynamics provides nonlinear effects in response to sensory driving, although not of the oscillatory type. This case is ideal to examine basic effects of recurrent connections. Larger delays bring the system closer to the Andronov-Hopf regime where intrinsic oscillations emerge. In this case an increase in a static input will cause a transition to oscillatory activity. Nonlinear properties of the feedback are also present in this region

of parameter space, but often difficult to separate from the oscillatory component of the solutions. Below we investigate the dynamical impact of static and spatially non-homogeneous driving in each of these regimes, by selecting an appropriate small/large delay.

5.3.1 Oscillatory dynamics

Oscillations appear in inhibitory recurrent systems by increasing the delay or the feedback gain. Steady states of Eq.(6.1) for some time-independent stimulus $I(x,t) = I(x)$ are non-homogeneous functions, implicitly determined by

$$\begin{aligned} \bar{u}_{on}(x) &= A(\bar{u}_{on}, \bar{u}_{off}) + I(x) \\ \bar{u}_{off}(x) &= \bar{u}_{on}(x) + V_o + (s-1)I(x). \end{aligned} \tag{5.4}$$

Setting $u_j(x,t) = \bar{u}_j(x) + \tilde{u}e^{\lambda t}$, $\tilde{u} \in \mathbb{R}$, $\lambda \in \mathbb{C}$, yields the characteristic equation

$$\lambda + 1 + Re^{-\lambda\tau} = 0. \tag{5.5}$$

Andronov-Hopf bifurcations occur for $Re(\lambda) = 0$ with $\lambda = a + iw$, $w \neq 0$, where the parameter R is defined by

$$R = \frac{1}{2}[\int_\Omega dy f'(\bar{u}_{on}(y)) + \int_\Omega dy f'(\bar{u}_{off}(y))]. \tag{5.6}$$

This function corresponds to the amplitude of the linear component of the feedback, and thus determines the impact of the feedback term on the steady state linear stability. It is the first coefficient of the taylor expansion of A near the fixed point $(\bar{u}_{on}, \bar{u}_{off})$. Note that R depends on the response polarity s, since it is a function of the steady states $\bar{u}_{on,off} = \bar{u}_{on.off}(s)$. As a result, the eigenvalue dependence on the network type (ON/OFF and ON/ON) is embedded within the last expression. The parameter R is an integral of the steady states over the domain Ω, and is maximized when the activities u_{on} and u_{off} are in the neighbourhood of the threshold h. Oscillations will be triggered by external

inputs that allow steady states $\bar{u}_{on\ off}$ to approach h sufficiently closely, such that R crosses the instability threshold $R = R_c$. This critical value is defined by:

$$tan(\omega(R_c)\tau) + \omega(R_c) = 0. \tag{5.7}$$

This linear analysis predicts that the frequency of the oscillation right at the Andronov-Hopf bifurcation is $\omega(R) = \sqrt{R^2 - 1}$.

Transitions to oscillatory behavior are function of asymmetry. These transitions depend on the spatial distribution of the sensory signals. External sensory driving has to generate a sufficient change in the value of R to cause $R > R_c$ and trigger stable oscillations in the whole network, that is, excite or inhibit a sufficiently large fraction of ON and/or OFF population to activity levels near the feedback threshold h, where R is maximal. The further the activities are from threshold, the larger the input must be to cross the critical value. A typical example of input driven oscillatory response, occurring via an Andronov-Hopf instability in an ON/OFF network ($s = -1$) is illustrated in Fig. 5.2. We compare Integrate-and-fire and neural field descriptions. The stimulus considered is a pulse, which is defined by $I(x,t) = I_o$ for $x \in \Delta = [x_1, x_2]$ and $t_o < t < t_1$ while $I(x,t) = 0$ otherwise. At the onset of the input, OFF cells are inhibited and ON cells are excited. The resulting excursion of the parameter R across the instability threshold R_c is here caused by the ON cells, whose activity reaches the neighbourhood of the threshold h, while the activity of the OFF cells decreases far below. In this example, $V_o = 0$, and thus both ON and OFF populations show the same activity level prior to and after the stimulation. The range of spatial widths $\Delta \equiv |x_2 - x_1|$ and amplitudes I_o triggering stable oscillations in this context have already been established [128]. A question remains: how are transitions to oscillations affected if the spontaneous firing rates were different i.e. $V_o > 0$?

The asymmetry level between ON and OFF populations increases the response possibilities, as the feedback does not operate in a all-or-none fashion. Without any stimulation, V_o introduces two distinct *effective* feedback thresholds,

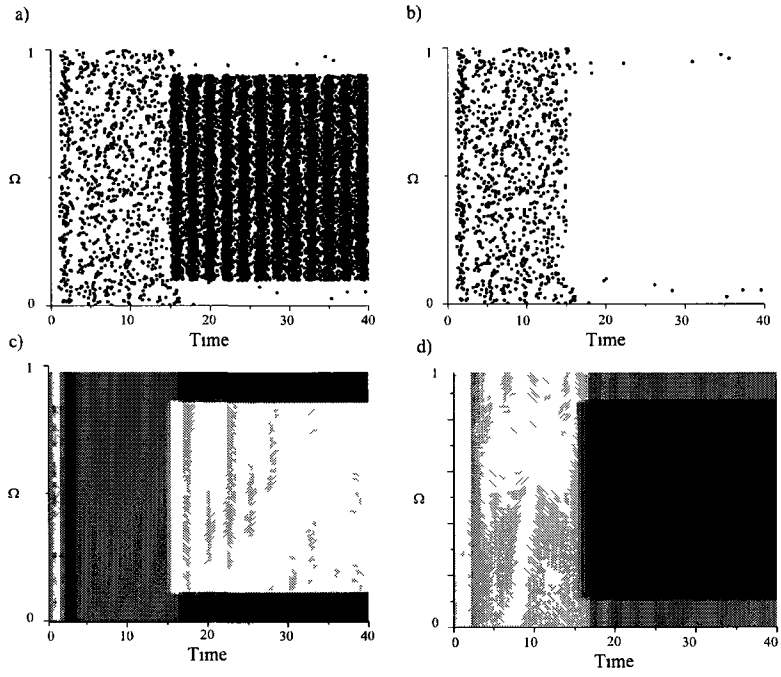

Figure 5.2. Localized pulse generating oscillatory activity in a ON/OFF network for both the neural field and integrate-and-fire descriptions. The activity of ON cells is shown on the left, and of the OFF cells on the right. As the input is turned on, the activity of stimulated ON(resp. OFF) cells increases(resp. decreases); te resulting change in the feedback causes a bifurcation. The neural field model (a-b) shows the ON and OFF populations reaching a stable limit cycle after a short transient. The global oscillations in the LIF model (c-d), shown in the lower panels, take the form of periodic firing rate modulations. Parameters are $I_o = 0.5$, $V_o = 0\,0$, $\Delta = 0\,8$, $h = 0.25$ and $\tau = 0.8$ for the neural field description. The LIF model parameters are $I_o = 1.9$, $h = 1$, $\mu = 0.4$, $g = -0.07$, $D = 2.0$ for $N = 1000$ cells with Gaussian white noise; parameters have been scaled to closely match the response frequency in the neural field case. The input has an amplitude I_o and a width of $\Delta = 0.8$ for $t > 15$. Throughout the paper we set $\alpha = 1, \beta = 25$ and $\Omega = 1$.

$h_{on} = h$ and $h_{off} = h + V_o$, causing two possible Andronov-Hopf transitions in parameter space. This phenomenon can be seen in Fig. 5.3 where are plotted the regions in (τ, h)-parameter space where oscillations are stable, for different levels of asymmetry and without any input i.e. $I(x,t) = 0$. As V_o increases, the stable domain splits into two regions, corresponding to the predominant

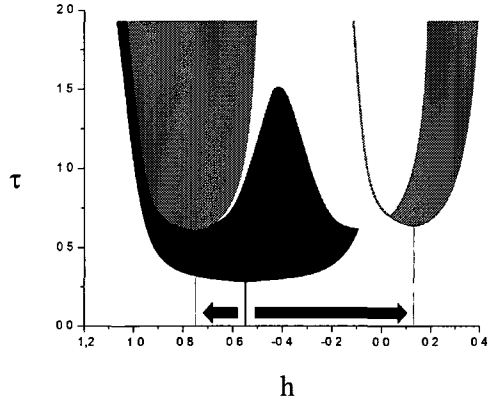

Figure 5.3: Regions in the (τ, h) subspace of parameter space where global oscillations are stable for $I(x,t) = 0$ and various asymmetry levels (adapted from [111]) . For $V_o = 0$ (black shaded region), ON and OFF populations share the same spontaneous firing rates, and thus have the same activity relative to the feedback threshold. The resulting Andronov-Hopf region has the shape of a parabola, as in an ON/ON system. If V_o is increased to 0.2 (gray shaded region), the stable domain starts to split into two distinct regions, showing that ON and OFF population do not have the same activity level with respect to the threshold of the system, and thus, that their relative Andronov-Hopf domains (where cyclic solutions becomes stable) are becoming distinct. The separation becomes even more appreciable with respect to initial case when V_o reaches the value of 0.4 (dark gray shaded region) as indicated by the black arrows. Parameters are as in Fig. 5.2 with $I(x,t) = 0$.

response of either ON or OFF populations and according to the new effective thresholds. This steady state property of the system illustrates that transitions to stable oscillations occurs within two regimes, as a consequence of different effective ON and OFF feedback activation thresholds.A positive pulse moves the activity of ON and OFF cells towards critical levels, located at h_{on} and h_{off}, around which the value R increases significantly.

A brief comparison between ON/ON and ON/OFF nets responses(i.e. the cases s=+1 and -1) with respect to the proximity of the Andronov-Hopf regime has been presented in [111]. There, it has been shown that input driven oscillatory activity is more prevalent in ON/ON nets. However, the presence of asymmetrical firing rates i.e. $V_o \neq 0$ is expected to significantly alter this result. Figure

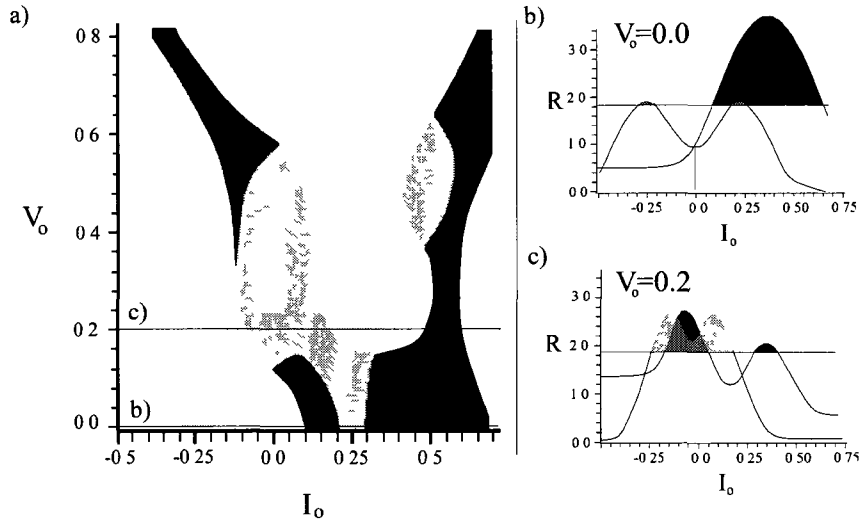

Figure 5.4: a) Regions in (I_o, V_o) space where oscillatory response occurs, for ON/ON (dark grey) and ON/OFF(light grey) network configurations. These points are such that $R > R_c$ in each case. For small asymmetry values, the ON/OFF configuration can respond to both excitatory and inhibitory inputs, the oscillatory response region being symmetrical with respect to the vertical line $I_o = 0$. ON/OFF nets can oscillate for both positive and negative inputs. ON/ON nets have a larger interval of I_o values that cause oscillation compared to ON/OFF nets. An ON/ON net can oscillate in response to both positive and negative inputs only if V_o is large. b) Slice of the graph shown in panel a) for $V_o = 0.0$, illustrating how the parameter R in Eq. (5.6) changes as a function of I_o. Shaded areas correspond to the parameter sets are such that $R > R_c$. c) For larger asymmetry $V_o = 0.2$, an ON/OFF net now has a larger range of inputs that cause oscillations; and ON/ON nets now show two distinct intervals of inputs amplitudes. Parameters are $R_c \approx 1.83$, $\tau = 1\ 4$, $\Delta = 0.6$, $h = 0\ 1$.

5.4a shows the effect of an increasing asymmetry V_o on the ability of a pulse of amplitude I_o to trigger stable oscillations. This is shown for both network configurations. This complex structure represents points in parameter space for which $R > R_c$. It becomes quite hard to give an intuitive interpretation of what is going on, given the complex forms of the oscillatory zones, but we may still state general results.

For V_o small, asymmetrical firing rates have a radically different impact on ON/OFF and ON/ON network responses. In the ON/ON case, there is an os-

cillatory response sensitivity shift towards inhibitory signals, while the opposite occurs for ON/OFF configurations. Given a broader interval of inputs causing oscillation, these are more prevalent in ON/ON networks for the weakly asymmetrical cases $V_o \lesssim 0.15$. This confirms the property of our two-population system: *ON/OFF nets have symmetrical behavior w.r.t. excitatory and inhibitory inputs, while ON/ON nets do not.* This result holds over a large range of asymmetry values; beyond this, the ON/ON configuration surprisingly starts to respond to both input polarities with oscillations, as one can see in Fig.5.4c. Further, the opposite occurs in the ON/OFF case, where the system no longer responds to both polarities. We emphasize that these results are dependent on the input spatial width. Larger pulses are responsible for greater variations of the parameter R, which implies that smaller amplitudes are required to reach the oscillation threshold R_c.

5.3.2 Steady state dynamics

For small delays, a static input does not trigger an oscillatory response. This is because the threshold R_c exceeds the maximal bound of Eq.(5.6). Nonlinear effects are nevertheless generated through the interaction of the input with the feedback, since ON and OFF populations activate the recurrent connections differently depending on their activity prior to receiving input. Spatially localized pulses, in particular, are ideal to study these effects, as the sharp spatial separation between stimulated and non-stimulated sites emphasizes feedback dynamics. The system may then display distinct activity patterns inside (central) and outside (lateral) the pulse. Previous studies [111] of central/lateral discrepancies in ON/OFF nets were not compared to ON/ON networks, nor explored as a function of asymmetry. This is our task here.

We consider the case of equal spontaneous activities $V_o = 0$, in which both ON and OFF cells are subthreshold. We focus again on spatially localized stimuli. We also focus on the differences between the activity of both cell types in

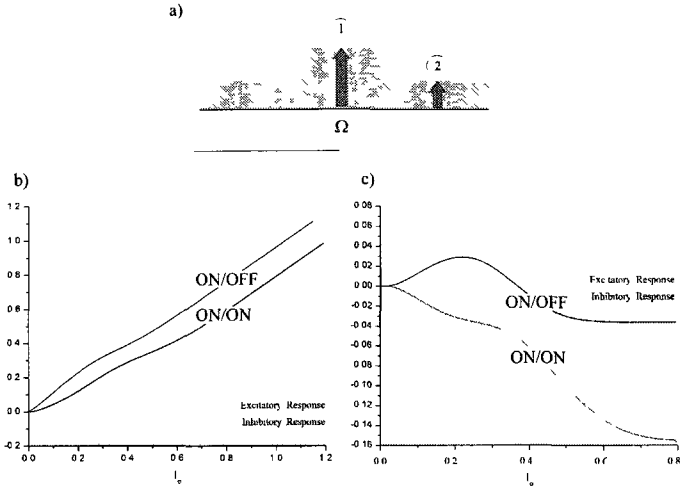

Figure 5.5: Central and lateral responses to a spatially localized pulse of amplitude I_o and width $\Delta = |x_1 - x_2|$ far from the Andronov-Hopf regime, for both ON/OFF and ON/ON network configurations. ON/OFF nets lateral response is non-monotonic, while it is not so in the ON/ON case. a) Local regions correspond to the neural sites located inside the pulse i.e. for $x \in [x_1, x_2]$, which are directly stimulated. Lateral sites do not receive the input, but are driven only by the feedback. b) The activity difference between stimulated and non-stimulated states are plotted versus I_o. The central response is monotonic for both configurations, although two slopes distinguish the curves. c) Lateral responses are radically different for ON/ON and ON/OFF nets. The ON/OFF response to the pulse is non-monotonic as a function of pulse height I_o, while the ON/ON response is monotonically decreasing. The difference between the curves in (b) and (c) is I_o in both cases. Parameters are $V_o = 0.3$, $h = 0.05$, $\tau = 0.2$.

stimulated regions and non-stimulated regions; this difference is likely important for decoding at a higher level Static positive inputs locally increase (resp. decrease) the activity of the ON (resp. OFF) cells. The resulting response curve is monotonic (not shown). As the input increases further, so does feedback, leading in both ON/OFF and ON/ON cases to a lateral decrease in activity. ON/OFF systems will have the same global network response for inhibitory inputs, while ON/ON systems, in contrast, will not show any modulation of the feedback.

For asymmetrical cases $V_o > 0$, the response of OFF cells allows the system

to modulate the polarity of the response as a function of the stimulus amplitude. Central/lateral responses to an excitatory localized pulse in the fixed point regime are shown in Fig. 5.5. OFF cells, here maintained at supra-threshold activity because $V_o \neq 0$, are locally inhibited by the incoming pulse, reducing the feedback and thus generating a global increase in activity. If the input amplitude increases, ON cells locally reactivate the feedback amplitude by crossing the threshold, now leading to a global decrease in activity. In contrast, in the case where no OFF cells are present, the only consequence of increasing the stimulus amplitude is an increased feedback inhibition. Consequently, our analysis predicts that *ON/OFF systems exhibit non-monotonic lateral response curves, while ON/ON systems are restricted to inhibitory lateral responses.* Note that these steady state effects at small delays, caused by input-feedback interactions, are also at work in the larger delay regime of the previous subsection. There, they influenced the distance to threshold and thus transitions to oscillations caused by static inputs; but their role is somewhat masked by these more dramatic transitions to oscillatory activity.

Finally we note that some ON and OFF cells respond to steady input currents by showing bursts of spikes at the onset and offset of stimulation - thus lending another meaning to an "off response" cell. These transient effects have been linked to various neural mechanisms like post-inhibitory rebound in many sensory systems (see [129]) where they play an important functional role. They are typically reproduced by models in which the neuron state is dependent on the time derivative of the input, where sudden changes in the input temporal structure result in important membrane voltage changes. We have not yet drawn attention to the fact that recurrent connections do reproduce similar responses under certain conditions. For example, in [111], Fig.7, both ON and OFF cells outside the stimulation zone exhibit a sudden increase in activity at both onset and offset of the pulse. In our model the effect is most pronounced for lateral cells, and is a consequence of the non-monotonic response shown in Fig. 5.5 - which itself is a consequence of the asymmetry $V_o \neq 0$. Central units do not

show this behavior as clearly, as the amplitude of this excursion is relatively smaller than the amplitude of the stimulus itself. The effect is nevertheless present as a gentle slope change exists in the response curve. Thus, the variety of transient on and off responses seen experimentally in a variety of systems may in some cases have a contribution from feedback effects.

5.4 Time-Periodic Stimuli

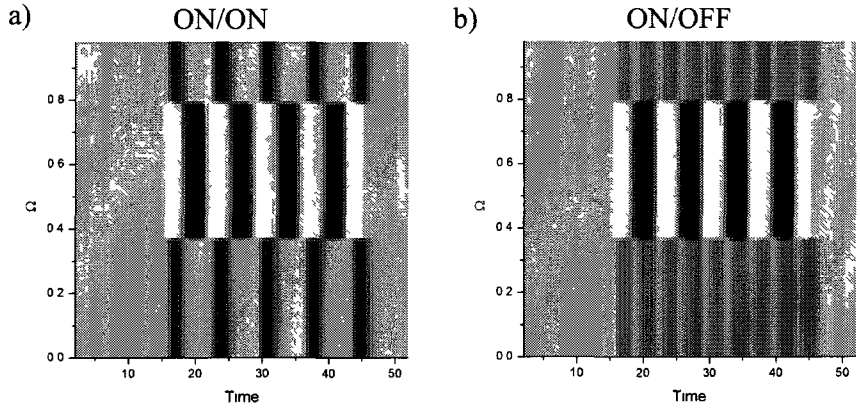

Figure 5.6: ON cell response to a sinusoidally modulated localized pulse. a) The ON/ON response is characterized by a central response in phase with the input, while the lateral response is antiphasic with respect to the central response b) The ON/OFF response exhibits a lateral frequency doubling effect, where the activity oscillates at twice the input frequency, while centrally the activity is in phase with the input and oscillates at the driving frequency Furthermore, the amplitude of the central response is higher than in the ON/ON case Parameters are $\Omega = 1$, $\tau = 0.3$, $h = 0.0$, $I_o = 0.5$ for $x \in [0.35\ 0.75]$ and $t > 15$, $w_o = 0.9$, $V_o = 0.05$

Oscillations in neural systems can also be triggered by time-periodic stimuli. Such non-autonomous components of the input determine the main features of the system's response, but additional nonlinear effects can be generated via the recurrent interactions. Non-autonomous problems, however, pose an important analytical challenge, as dynamical systems theory has few tools to determine the shape and stability of the resulting non-stationary solutions Results have nevertheless been obtained in specific input shapes, like linear ramps [130], lat-

erally drifting bumps [80], and global periodically-forced spiking models [131]. In our context, the absence of spatial kernel simplifies the analysis greatly, as the dynamics can be essentially described by the interaction between the stimulus and its "image" propagated via feedback. We thus analyze the response patterns close to and away from the Andronov-Hopf regime by selecting the appropriate delay.

In Fig.5.6, we show the response of ON cells to a spatially localized pulse with a sinusoidally modulated amplitude, in both ON/ON or ON/OFF network configurations. Two main results are obtained when one analyzes in detail the distinction between these two responses: 1) second harmonic or frequency-doubled response (laterally), and 2) sustained amplitude response (centrally). We will analyze each of these cases separately. Further, in this section, we restrict our analysis to inputs which possess the following spatio-temporal structure: $I(x,t) = I_o sin(w_o t)$ for $x \in \Delta = [x_1, x_2]$ and $t_o < t < t_1$ while $I(x,t) = 0$ otherwise.

5.4.1 Frequency doubling

[111] showed that periodic driving, in the case of small delays, results in a lateral frequency doubling effect in ON/OFF networks. This effect is caused by the combined responses of ON and OFF populations, resulting in the feedback being modulated at twice the input frequency. Underlying this effect is the fact that the recurrent feedback loop acts as a full-wave rectifier, getting a boost from both positive and negative going phases of the input. This effect was found in ON/OFF nets; here we contrast it with the behavior of an ON/ON net with similar forcing. We further show that it can occur in a LIF network. Our aim is to characterize the functional differences between this type of behavior, which appears to be specific to ON/OFF networks, and the antiphasic lateral response seen in ON/ON networks, as seen in Fig. 5.6. Further here we explore the effect of increasing delay times on the structure of the response. As a result,

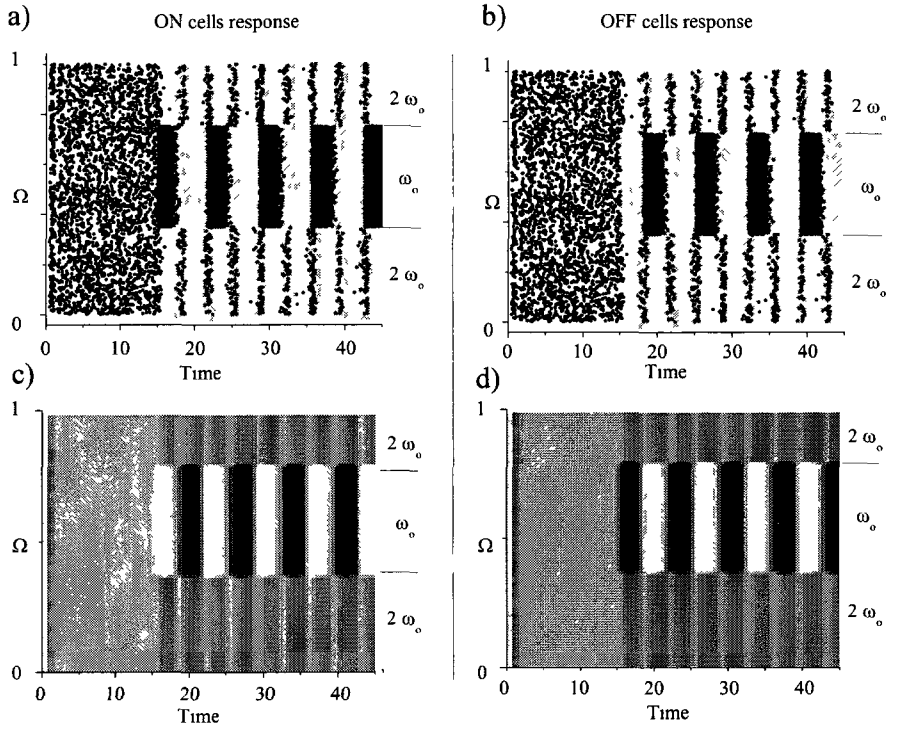

Figure 5.7: Sinusoidally modulated localized pulse generating a lateral frequency doubling effect in a ON/OFF net ON and OFF population responses are presented, for both neural field(a-b) and spiking(c-d) approaches. The parameters for the neural field description are identical as in Fig. 5.6 while for the LIF Integrate-And-Fire description these are $\tau = 0.3$, $h = 1$, $I_o = 5.5$, $\mu = 1.05$, $V_o = 0.05$ and $g = -0.06$ for Gaussian white noise

this problem must be considered both close and away from the Andronov-Hopf regime.

Away from Andronov-Hopf bifurcation in the fixed point regime, when the delay is small, the input cannot trigger a bifurcation as the spectrum of eigenvalues is bounded to the left of the imaginary axis. As Fig. 5.7 shows for both the neural field and LIF models, ON and OFF populations respond to localized signals with opposed polarity. In the case of sinusoidally modulated amplitudes, the reversed OFF response constitutes an antiphasic (i.e. 180 degree phase shifted) image of the signal transmitted to the ON cells. The combined responses of ON

and OFF cells results in a signal oscillating at twice the input frequency.

Frequency doubling might be explained when one looks at the interaction of

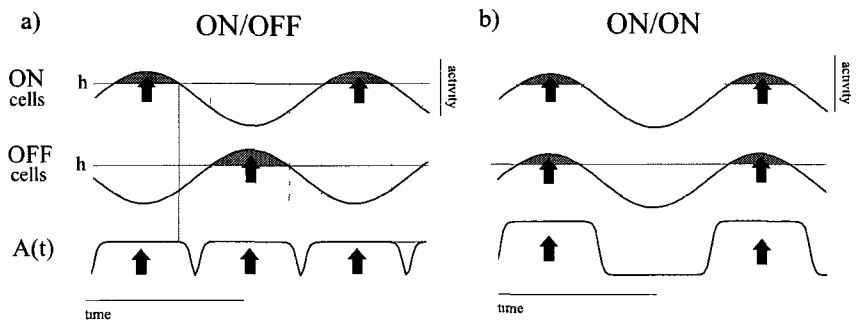

Figure 5.8: Schematic representation of the time evolution of the activity of cells in ON/OFF and ON/ON nets. a) As the activity of either ON and OFF cells increases beyond the threshold h (shaded areas), the amplitude of the feedback increases. In ON/OFF nets, stimulated ON and OFF cells never activate the feedback simultaneously, the resulting recurrent signals oscillates at twice the input frequency. b) Stimulated cells in an ON/ON net activate the feedback simultaneously, which then oscillates with the same frequency as the input. The profile of the feedback term $A(t)$ as in Eq. (5.2) is also shown in the two cases.

the ON and OFF cell activity with the feedback activation threshold h. Figure 5.8 a illustrates the sequence of events leading to feedback oscillations. Before the stimulus is applied, steady firing rates states are reached by both ON and OFF populations. As the sinusoidally modulated pulse is turned on at $t = t_1$, $I(x) > 0$ for $x \in [x_1, x_2]$, and ON cell activity increases until the feedback activation threshold is met. This increases the amplitude of the feedback, resulting in a lateral decrease in activity. As the first half of the input cycle ends and where $I(x,t) \approx 0$, the ON population decreases its activity below the threshold, which deactivates the feedback. The activity then increases laterally. Now OFF cells become excited, due to their reversed response, and activate the feedback again. The lateral activity decreases once more. This sequence of events is not instantaneous, and the lateral response shows two small bumps of activity for every input period, caused by two feedback activation/deactivation sequences. This process repeats itself until the input is turned off. The resulting lateral activity behavior corresponds to the time evolution of the feedback term $A(t)$, which oscillates at twice the input frequency.

Of particular significance is that our analysis predicts that lateral double frequency responses in only possible when ON and OFF populations are present. As Fig. 5.8b illustrates, ON/ON type networks do not exhibit this behavior. This is because ON/ON systems only activate and deactivate the feedback once per input cycle. The lateral response then corresponds to a sequence of steady activity plateaus, corresponding to successive feedback changes in amplitude caused by ON cells reaching the threshold. The resulting effect is a central-lateral response phase shift of 180 degrees. One might characterize the response of ON/OFF networks by comparing the input contrast curves generated by this configuration to those for the ON/ON systems. Frequency doubling and lateral phase shift can be seen as outcomes of global feedback driving, but seen predominantly in regions where the input has smaller or zero amplitude.

Figure 5.9a,b shows the central and lateral responses for small delays. In the case of large delays, a similar behavior occurs, but the input makes the parameter R cross back and forth the critical value R_c. For large delays, R_c is also much smaller. As we can see from Fig. 5.9c,d, the variations of R generate periodic epochs of Andronov-Hopf cycles, or bursts, superimposed to the activity profile provided by the input. This makes the network response look even more nonlinear. The temporary transitions to oscillatory activity are caused by the activity levels getting closer to and away from the threshold h, changing the value of R accordingly.

In a ON/OFF configuration (Fig. 5.9c), only one stimulated population at a time approaches h, as explained in Fig. 5.8. The variation of R is thus much smaller than in the ON/ON case, where the two populations simultaneously interact with the feedback. The excursion of the parameter R in the ON/OFF case takes place in the vicinity of the bifurcation, causing relatively small oscillations. In contrast, oscillations in the ON/ON case are much larger, as the excursion of the parameter R takes place further into the Andronov-Hopf regime. We note that this effect is apparent mainly for small input frequencies, as the stimulus

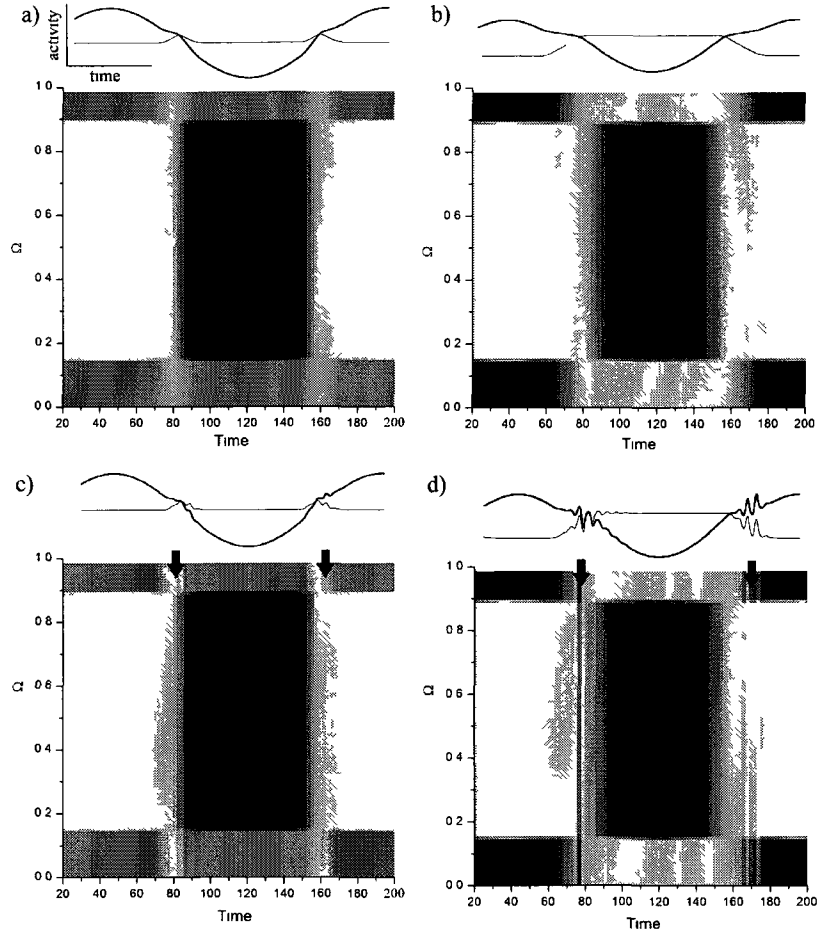

Figure 5 9 ON cell responses to a time periodic stimulus in ON/OFF and ON/ON nets far(a,b) and close$(c\ d)$ to the Andronov-Hopf regime Andronov-Hopf cycles appear whenever ON or OFF cells activity is near the feedback threshold h, making the parameter R cross the critical value R_c A small frequency of $w_o = 0\ 04$ allows those cycles to gain sufficient amplitude to be seen The ON/OFF net is shown on the left (a,c) and ON/ON on the right (b,d) On the top of each panel, bold lines describe the central temporal evolution of the solutions, while thin lines describe lateral dynamics Other parameters are $\Omega = 1$ $I_o = 1\ 1$ for $x \in [0\ 15\ 0\ 85]$ and 0 elsewhere, $V_o = 0\ 05$ and $h = 0\ 0$ The delay chosen in the fixed point regime is $\tau = 0\ 5$ while $\tau = 1\ 8$ near the Andronov Hopf regime

has enough time to gain the required amplitude to generate a bifurcation

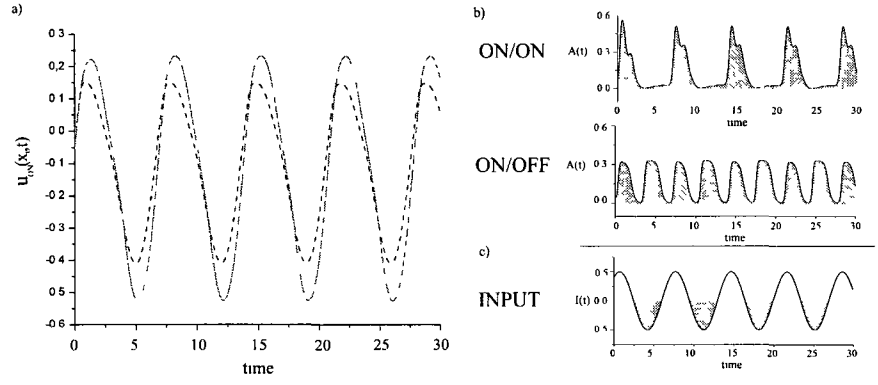

Figure 5.10: Response amplitude discrepancy of central ON cells in ON/ON and ON/OFF networks. a) Evolution of the activity of sinusoidally driven ON cells, for central locations i.e. $x_i \in \Delta$. Activity oscillations in a ON/OFF network(solid line) are larger than in a ON/ON network (dashed line). b) Resulting evolution of the feedback $A(t)$ according to a sinusoidal stimulus, in the ON/ON and ON/OFF cases. In the ON/ON case, the sudden activation of the feedback caused by the two populations is such that $A(t)$ makes high amplitude excursions away from the resting value, resulting in a strong inhibitory effect on the network. This decreases the amplitude of the response, but only when the amplitude of the input is positive. In the ON/OFF case, the simultaneous and antiphase responses of ON and OFF cells result in a full-wave rectification across the feedback loop. The variations of the feedback amplitude are much smaller, meaning that less inhibition affects the response at the sensory layer. Further, the activation of the negative feedback by the OFF cells during the negative components of the input results in a amplification of the response. The input temporal structure in plotted in c). Parameters are $\Omega = 1$, $\tau = 0.3$, $h = 0.0$, $I_o = 0.5$ for $x \in [0.35\ 0.75]$ and $t > 15$, $w_o = 0.9$, $V_o = 0.05$.

5.4.2 Amplitude of Sustained ON/OFF Response

We now consider the amplitude of responses to periodic forcing. The behavior illustrated in Fig. 5.6 also puts forward another novel effect, namely a central response amplitude difference between purely excitatory networks and those built of both ON and OFF cells. Indeed, the central response of the ON cells has significantly greater amplitude in an ON/OFF setup. This behavior can be explained when one considers the temporal structure of the feedback in the ON/ON and ON/OFF cases. Figure 5.10a illustrates the central response patterns in both configurations, as well as the feedback time course $A(t)$ in as in Eq.5.2(b)) when a sinusoidal input is present (which is also plotted in panel c).

In an ON/ON network, whenever the input amplitude increases, both populations recruit the feedback simultaneously, which results in a sudden and high

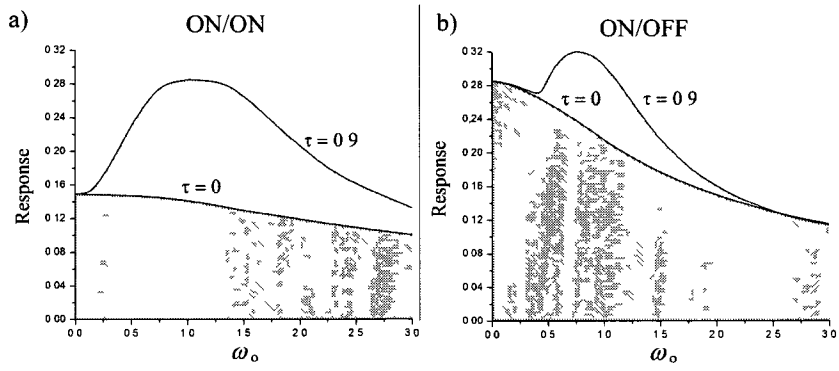

Figure 5.11: Response amplitude of central ON cells in ON/ON and ON/OFF nets as a function of input frequency A sinusoidally modulated pulse of fixed amplitude $Io = 0\ 25$ and width $\Delta = 0\ 4$ generates distinct frequency tuning properties if the system incorporates OFF cells a) For $\tau = 0$, ON/ON nets response is relatively constant over the range of frequencies considered The units recruit the feedback pathway, which in turn reduce the amplitude of the cells response For $\tau = 0\ 9$, the curve shows the resonance due to the Andronov-Hopf frequency The response amplitude diminishes as the frequency becomes larger, because the input becomes too fast compared to the system's dynamics b) In ON/OFF nets, the response curve is lowpass For $\tau = 0$, the response is maximal at low frequencies due to the feedback amplification, where the amplitude is larger compated to the case shown in a) Increasing the delay to $\tau = 0\ 9$ makes the system closer to the Andronov-Hopf regime a resonant peaks becomes visible near the Hopf frequency

amplitude increase of $A(t)$. The resulting strong inhibitory signal reduces the amplitude of the cell's response. As the input amplitude then decreases, both populations reduce their activity below the threshold, resulting in a sudden and complete deactivation of the feedback. The remaining negative part of the input is not altered by the feedback, which is not activated.

In a ON/OFF network however, the feedback $A(t)$ does not reach as high an amplitude, because only one population at a time, either ON or OFF cells, can recruit recurrent connections. As the input amplitude increases, only ON cells activate the feedback, resulting in a relatively smaller inhibitory signal. This allows the response of the stimulated ON cells to reach higher amplitudes than in the ON/ON case. And as the amplitude of the stimulus becomes negative, *the negative feedback acts as a amplifier, and sustains the response of the stimulated cells.* This is because the negative part of the input makes the OFF cells activate the feedback once again: the feedback amplifies the cellular response.

The response amplitude deviation shown in Figure 5.10 further shapes the frequency tuning properties of ON/ON and ON/OFF nets. In Figure 5.11, the response amplitude of driven units is plotted with respect to stimulus frequency for small and large delays. Panel a) shows that ON/ON nets response is band-pass. For zero delays ($\tau = 0$), the response curve is flat over the range of input frequencies. Increasing the delay to a higher value ($\tau = 0.9$), the resonance peak appears as the system gets closer to the Andronov-Hopf regime and exhibits stronger oscillatory behavior near the characteristic Hopf frequency. In the ON/OFF case (plotted in panel b)), the response is low pass, where stimuli with smaller frequencies trigger responses of amplitudes much larger than in the ON/ON case. If the feedback delay is changed from $\tau = 0$ to $\tau = 0.9$, the Andronov-Hopf resonance peaks appears.

5.5 Application to Sensory Systems

The model under study here, which incorporates ON and OFF populations with global recurrent connections, can shed light on recent experimental findings, in both the electrosensory and visual systems. These two systems use ON and OFF cells to integrate sensory inputs, and have feedback. We show that some experimental data are reproduced by our generic model, thus providing a simple caricature of the dynamics at work when both populations operate together, and 2) that known results obtained in ON/ON networks still hold when more realism is put in the models by incorporating OFF cells.

5.5.1 Electrosensation

The electrosensory system is endowed with ON and OFF cells, known respectively as E and I pyramidal cells. These cells receive direct input from primary sensory neurons, the electroreceptors, which cover the body of the animal. It

is known that E and I cells project back to themselves via the nucleus preeminentialis (nP) after a minimal delay of approximately 10 msec [22]. It is also known that stochastic inputs in time cause oscillatory activity in the gamma band (around 40 Hz) when the inputs are strongly correlated in space [32, 33]. In the context of our model here, spatial correlation is proportional to the number of neurons receiving common input. No such oscillatory activity was seen when neighbouring patches of electroreceptors receive independent stochastic forcing. This experimental result was reproduced by a computational modeling of a network of E cells projecting to themselves with inhibitory delayed feedback of the type considered here. This was the case for LIF type nets with intrinsic noise driven by the external correlated noise [32] as well as for a linear fluctuation theory using stochastic LIF neurons with delayed feedback [33, 34]. The outstanding question is whether the inclusion of OFF cells known to be present in approximately equal numbers as ON cells can alter our understanding of this picture.

In [111] we showed that ON/OFF networks can also oscillate when a sufficient number of neurons receives a static input, enabling the parameter R to cross the critical value R_c. Further we showed that the range of inputs that cause this transition was more limited than for ON/ON nets. While the deterministic localized "step input" stimulation used in that paper (and here) differs from the stochastic zero-mean stimulus used in [32, 33], the lower propensity of the ON/OFF network to oscillate when an input bump is applied suggests that OFF cells could counteract the genesis of gamma oscillations. However, that result was obtained for a symmetric network ($V_o = 0$). Our new results here for the asymmetric case now show that the situation is more complex. The ability to oscillated really depends on V_o (see Fig.5.4). In some cases, the ON/OFF network may in fact have a greater propensity to show an oscillatory response to a static input. This question could be ultimately settled by knowing the spontaneous activities, which can be done by opening the feedback loop surgically or temporarily using pharmacological agents. So it may be that the oscillations

seen experimentally in the electrosensory system were in fact supported, and maybe even strengthened, by the presence of the OFF cells

5.5.2 Response to Periodic Grating and Retinal Frequency Doubling

In this subsection we consider the response of our recurrent network of ON and OFF cells to forcing that is periodic in both space and time This type of forcing is common in research on the visual system, where it is referred to as contrast-reversed periodic stimulation For simplicity we consider sinusoidal gratings Note however that we do not consider sinusoidal drifting gratings which are also often used in vision research (we only comment briefly on the resulting dynamics below) Here, the modulation is fixed in space Hence there is a discrete set of points in space, at the local minima of the spatial modulation, that never receive any stimulation beyond the background stimulation on which the periodic grating is applied Parameters of this stimulation are the spatial frequency, the temporal frequency, and the spatial and temporal modulation amplitudes, which can be combined into one amplitude factor I_o

$$I(x,t) = I_o sin(w_o t)[1 + \cos(\gamma x)] \tag{5 8}$$

where w_o is the temporal frequency and γ the spatial frequency The response of our one-dimensional array of ON cells to the sinusoidal grating is shown in Fig 5 12 The temporal part of this forcing, turned on at $t = 15$, is shown above the plot, while the spatial part is shown to the right This set-up is similar to that studied in Section 5 4 1 on periodically modulated pulses, except that here the pulses have a sinusoidally repeating profile in space The activity in the regions receiving more illumination is seen to oscillate at the temporal driving frequency w_o On the other hand, the activity of regions receiving less illumination are found to oscillate at twice the input frequency even though the input is weak in those regions The frequency-doubling effect is maximal

at positions $x_n = (2n+1)\pi(\gamma)^{-1}$ where $I(x_n, t) = 0$. The frequency doubling observed here occurs because the combined responses of ON and OFF populations propagate back through the network via the recurrent connection. Illuminated locations oscillate predominantly at the input frequency, even though the frequency-doubled component is globally driving the system via the feedback - this latter component is just weaker than the direct driving frequency component in the illuminated region. The relative strength of the fundamental and frequency-doubled components thus changes in a continual manner from regions of zero illumination to regions of maximal illumination from the grating.

The addition of OFF cells to our recurrent sensory pathway may be used to shed some light on phenomena occurring in the visual system. Frequency doubling has been observed in many experimental studies of retinal ganglion cell responding to periodic illumination gratings (see [127] and references therein). These observations have also been reproduced computationally [126]. In [127], experiments were carried out in guinea pig retina, where both ON and OFF pathways are present. Lateral responses (outside the illuminated bars) at twice the stimulus frequency were reported, and attributed to the presence of non-linearities in the ON and OFF pathways, and to the dimension of the receptive field of amacrine cells. In the experiments, illumination grating stimuli were drifted or reverse-contrasted periodically in time, while the activities of central (sites of maximal illumination) and lateral (position of zero-illumination) ganglion cells were simultaneously recorded and compared (see [127] for details). For gratings with a low spatial frequency, the activity was shown to track the input temporal modulation in regions of maximal illumination (labelled "F1" behavior). In contrast, in regions of zero-illumination, the activity of the ganglion cells oscillated at twice the temporal input frequency (labelled "F2" or "non-linear" behavior). In [126], this phenomenon has been reproduced by a complex computational model of a retinal sub-circuit in which frequency doubling, also called "second harmonic response", has been linked to photoreceptor non-linearities and amacrine wide-field effects. The model, developed for the

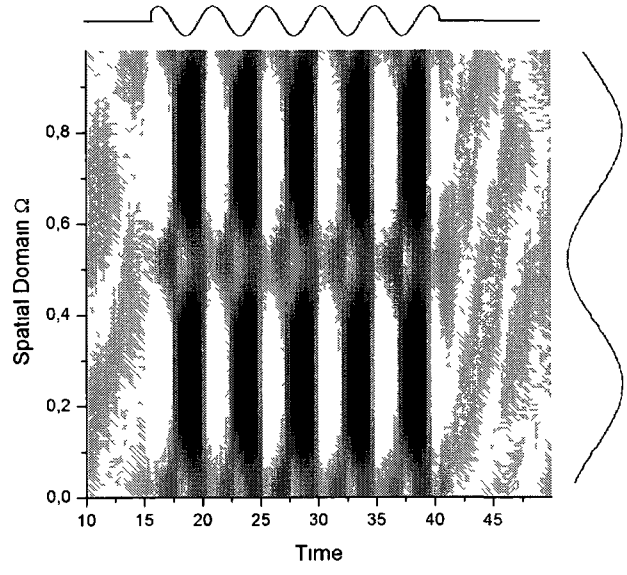

Figure 5.12: Frequency doubling caused by a spatially and temporally sinusoidal input, mimicking an illumination grating stimulus This input is presented here to a one-dimensional retina Parameters are $\Omega = 1$, $\tau = 0\ 4$, $h = 0\ 0$, $I_o = 0\ 5$, $w_o = 1\ 3$, $V_o = 0\ 05$ and $\gamma = 13\ 0$

ON pathway because the data on the off pathway are more scarce, includes the properties of subtypes of photoreceptors, horizontal cells, bipolar cells, ganglion cells as well as two classes of amacrine cells: narrow field ("nested" amacrine cells) and wide field amacrine cells. The complex wiring diagram involves feed-forward inhibition and recurrent negative feedback loops.

The setting of the experiment described in [127] and the work in [126] suggests that our model might be used to reproduce certain features of the observed dynamics. Those authors state that F2 non-linear responses - qualitatively similar to our lateral frequency doubling behavior - is due to the ganglion cell's "non-linear" receptive field, which possesses quite distinct spatial summation properties in comparison to the more familiar center-surround "linear" receptive field. F2 responses are not sensitive to the recording position within the spatial grating, and thus do not appear to be the determined or influenced by local spatial connectivity. While the F2 responses are constant over all grating

phases, the F1 responses (due to the standard center-surround receptive field) are proportional to the illumination in the grating. This is qualitatively similar to what is seen in Fig. 5.12.
Further, the F1 and F2 responses show similar dependencies on the spatial frequency of the grating, and this dependency is preserved over the receptive field of the ganglion cells. Also, [127] reports that non-linear receptive field effects are caused by the spatial summation of independent "sub-unit" responses that populate a wide area around the ganglion cell's dendritic field. The range of these connections is supposedly a consequence of the presence of wide-field amacrine cells. As a result, F2 responses measured across the receptive field were shown to sum up linearly at the ganglion cells.

Thus the interplay of the activation of ON and OFF cone pathways involves weakly interconnected sub-units distributed across the receptive field. Their activity is integrated via the wide-field amacrine cells, which is analogous to a large scale feedback pathway with weak lateral connectivity, as in our model and in the ELL discussed in Section 5.5.1. Thus, although retinal sub-circuits are not spatially homogeneous, and our model lacks the complexity to reproduce the full range of phenomena described in [127], we argue that the qualitative behavior of the non-linear responses of ganglion cells to a periodic grating can be reproduced without spatial connectivity considerations, by including globally summed inhibitory effects. In this context, our model proposes a mechanism which is responsible for input rectification, which relies on the non-linearity of both the ON and OFF recurrent pathways.

We have considered here only contrast-reversed gratings, as opposed to drifting gratings. Preliminary results with drifting sinusoidal gratings do not reveal frequency doubling in our one-dimensional array (not shown). The difference with the retinal data under these conditions may be due to the fact that two-dimensions are needed to reproduce the basic observations, or that more intricate circuitry has to be included. Also, the frequency doubling exhibited by our

model is not sensitive to the spatial frequency of the contrast-reversed grating, which is also the case for the data over a certain range of spatial frequencies. But at some point the lateral connectivity and other details of retinal circuitry do set a spatial scale beyond which the effect decreases until it is no longer seen.

5.6 Conclusion

In this paper, we analyzed the main differences between the sensory processing capabilities of networks built of ON and OFF cells (ON/OFF) with networks built of ON cells only (ON/ON). We have shown that both types of nets integrate spatiotemporal inputs differently. In the context of oscillatory responses reached via Andronov-Hopf bifurcations, symmetric ON/ON systems are more sensitive in the sense that they undergo Andronov-Hopf bifurcations with pulses of smaller amplitude and spatial widths; however, this transition is only allowed for positive inputs. In symmetric ON/OFF systems, the transition occurs on a narrower interval of input widths and amplitudes, but is observed for inputs of both positive and negative polarities. This situation changes with the degree of asymmetry in the spontaneous firing rates, controlled by the parameter V_o. We found that the asymmetry greatly influences the bifurcation properties of the system, and the propensity to respond to static step inputs with oscillations.

In the context of time-periodic inputs, we demonstrated that only ON/OFF systems exhibit lateral frequency doubling, while ON/ON systems instead show antiphasic lateral responses. We further found that ON/OFF systems possess a larger response amplitude compared to ON/ON systems, due to the temporal structure and timing of the feedback. Our analysis supports the observation of oscillations in the electrosensory system when a sufficient number of neurons share common input. Our model was also used to reproduce the response pattern found in the cat and guinea pig retina, where frequency doubling has been reported.

Even though the inclusion of OFF cells corresponds to a step towards more realistic models of early sensory systems, many physiological processes and components are believed to play an active part in information processing tasks of early sensory systems. Neural adaptation has been shown to influence the genesis of synchrony in recurrent networks [4, 39] as well as the formation of spatially organized activity patterns [132, 82, 133, 84]. We thus expect that the timing and strength of adaptation might augment the range of response possibilities of ON/OFF nets, and thus increase the physiological relevance of our model. The analysis of this problem is planned for later studies.

Inclusion of receptive field effects for both cell types is another obvious next step. This is also the case for the inclusion of other types of ON/OFF asymmetries seen e.g. in retina where both onset and offsets of the stimulus can lead to increases of firing rates [134]. The connectivity between primary receptors and the ON and OFF cells considered here is known to determine receptive field properties, and needs to be included in the analysis at some point. And finally, it will be interesting to determine whether the results found here in the context of asymmetric networks, where the ON and OFF cells can have different baseline or spontaneous activity, will respond to spatio-temporal stochastic signals in a way predicted by our analysis of deterministic signals here. This will reveal whether oscillations seen in data with spatially correlated stochastic stimuli are generically observed in ON/OFF cells, supporting our understanding of oscillations in the electrosensory system [32, 33, 34] and others with this type of forcing.

The circuitry investigated here assumes that both ON and OFF cells project to the same nucleus, which in turn feeds back symmetrically to all cells. The actual circuitry is not known in the electrosensory system, nor is it in most other systems. It may be that E cells project preferentially to E cells via the nucleus nP, and I cells to I cells. Future work will investigate whether it is possible to make predictions of the true connectivity by using a clever suite of

measurements. Of course, at the extreme where E's connect only to E's, and I's only to I's, one is faced with two separate recurrent systems, both of which will obey the rules described here for ON/ON systems. Future work will also explore possible ways of performing a combination of closed loop experiments in order to reveal the spontaneous firing rates, thus enabling an estimate of V_o without tampering with the feedback.

5.7 ON/OFF networks and stochastic driving

It has been established through many computational studies that circuits inspired by the electrosensory lateral line lobe(ELL) provide a suitable environment for the genesis of rhythmic states, given that sensory stimuli exhibit sufficient spatial correlation [33, 26, 135, 97]. In this context, we have been able to show how the spatial structure of the input interacts with delayed feedback to generate oscillations. Further, these result are supported by experimental findings, which clearly indicate that a global stimulus (i.e. all sites get stimulated) results in a strong Fourier component in the gamma range, while local ones (i.e. a fraction of the sites) do not [32, 26]. The aforementioned studies have considered only the presence of ON cells (known as E-cells), despite half of the cells being of the OFF type. They used LIF descriptions, and most importantly considered *realistic noisy stimuli*, in bright contrast to the static pulses considered throughout our work in Chapter 3, 4, 5 and 6.

One can indeed model the encoded signals from the primary afferents using white noise low pass filtered with a cut-off frequency of around 60Hz. As such, the neural field formulation has not yet been used to approach the specific problem of the presence of OFF cells with stochastic stimulation. We thus ask the following question: does a neural field model which combines ON and OFF cells undergo an Andronov-Hopf bifurcation with spatially correlated stochastic driving? Recent studies [100] have attempted to confirm this statement using a

model of the ELL built only of excitatory cells, which also incorporates spatial kernels. Thus, although the bifurcation analysis performed earlier does not hold per se for stochastic forcing, we expect that the system might undergo input induced Andronov-Hopf bifurcations as the input amplitude and/or width increases.

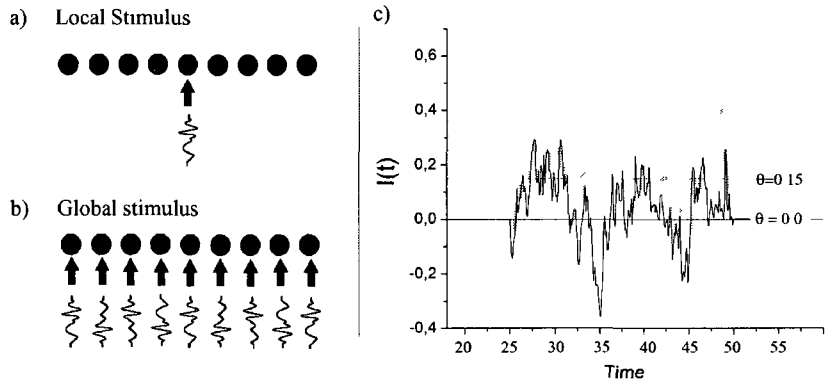

Figure 5.13: Stimulation profiles used to investigate the genesis of global oscillations. a) Schematic of local stimulation, performed by stimulating a single site of the network, using an additive noisy term, while in b) global stimulation, all network sites get stimulated by independent stochastic processes. The resulting activation of the recurrent connections is increased, compared to the local case. c) Sample of the white noise process stimulus used in Fig. 5.14. The process has a cut-off frequency of 60Hz, and is obtained via a Ornstein-Ohlenbeck process[1]. It is shown with two values of θ within the interval $25 < t < 50$. Parameters are $S = 0.6$ and $\tau_{ou} = 1.67$

Here we show that our ON/OFF model may be used to understand the properties of the system as the sources of noise increase in intensity. This part of the thesis will be used for a future article submission in which we aim to study the effect of noise intensity and spatial correlation on the transitions to oscillatory states. It is thus part of a work in progress. We have uncovered an interesting

[1]To obtain 0-60Hz gaussian white noise, the temporal component of the input $I(t)$ obeys an Ornstein-Ohlenbeck process, which we define by

$$\frac{I(t)}{dt} = -\frac{1}{\tau_{ou}}(I(t) - \theta) + S\xi(t)$$

where θ and τ_{ou} are respectively the mean and the time-scale of the process, and where $S = \sqrt{\frac{2\sigma^2}{\tau_{ou}}}$ corresponds to the amplitude of a gaussian white noise process, labelled $\xi(t)$, with a variance of σ. The resulting solution $I(t)$ is then multipled by a spatial step function in order to obtain the required spatial profile i e. global or local. See [136].

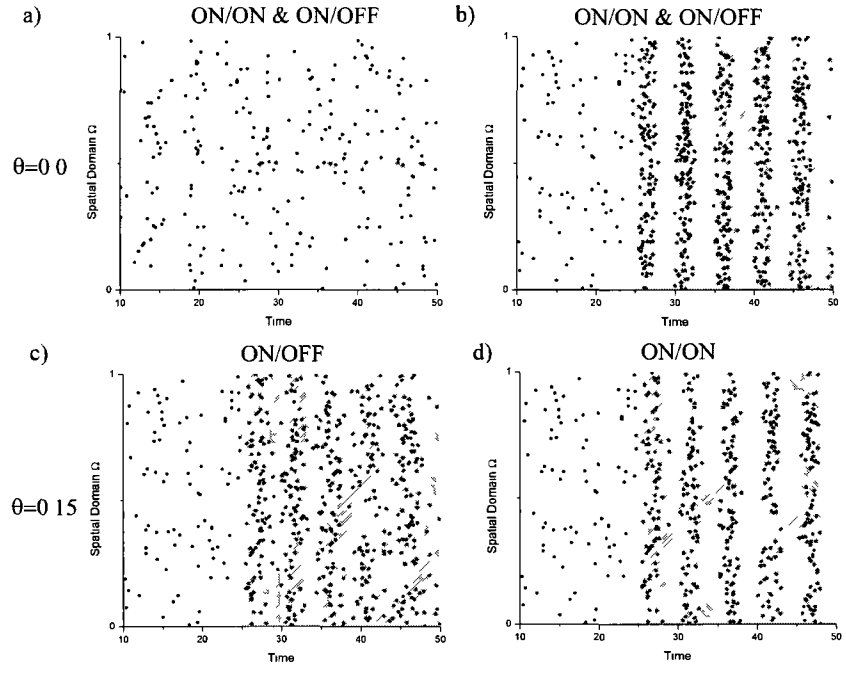

Figure 5 14 ON cells response to stochastic inputs with local and global profiles The input (shaded grey) is an additive low pass gaussian white noise process with a cut-off frequency of 60Hz When such a process has a zero mean i e $\theta = 0$ and $S = 1\,6$, ON/ON and ON/OFF network configurations display the exact same behavior Local stimuli do not trigger a rhythmic fluctuation of the firing rate (a) while global input profiles do (b) Once the mean is increased to non-zero values i e $\theta = 0\,15$, $S = 0\,6$, oscillatory responses become more prevalent in ON/ON networks (c) than in ON/OFF networks (d), as predicted by the bifurcation analysis performed earlier The input spatial profile evolves between global ($\Delta = 1\,0$) and local ($\Delta = 0\,05$) spatial width and the input is non-zero whenever $25 < t < 50$ Other parameters are $\Omega = 1$, $\tau = 1\,8$,$\tau_f = 0\,1$, $h = 1\,0$,$\mu = 0\,4$, $g = -0\,3$, $D = 1\,0$, $V_o = 0\,0$ and $\tau_{ou} = 1\,67$ for a network of $N = 1000$ Integrate and Fire cells as in Eq (6 12)

aspect of the response to stochastic forcing - one that hinges on the mean of the stochastic stimulus - which we report here This result will inform our full study into the effects of noise intensity and spatial correlations on oscillations

The stimulus corresponds to a Gaussian noise process with frequencies between 0 and 60Hz with an adjustable mean and a local or global spatial profile, as shown in Fig 5 13 Subject to this stimulation, we investigate the response of the system, whose cellular dynamics are governed by Eq 6 12 As shown in Fig 5 14, if the spatial extent of the stimulus is very small (i e "local stimu-

lus"), no rhythmic activity appears in either the ON/ON or ON/OFF network configurations, as expected. However, global oscillations appear once the input width is increased up to the size of the full network (i.e. "global stimulus"). The amplitude of the non-linear recurrent connection component increases up to the oscillation threshold and global rhythmic activity becomes stable. In analogy with the neural field description, this is because the local stimulus does not increase the value of the parameter R in Eq. (5.6) above R_c, while the global stimulus does.

An interesting consequence of the input spatio-temporal structure is an absence of distinction in the response threshold between ON/ON and ON/OFF networks when the mean of the process is chosen to be zero. As the input is built of such zero mean and spatially independent processes, one finds that, statistically, an even amount of ON and OFF cells across the network are excited and/or inhibited at a given moment, which implies that the feedback connections are not recruited preferentially in either the ON/ON or ON/OFF cases. Both ON/ON and ON/OFF systems display the same Andronov-Hopd threshold. This result further appears to be independent of the amplitude of the input.

However, we observe a response threshold discrepancy when the mean of the stochastic process is shifted from null to either positive or negative values, mimicking the pulse-shaped inputs situations considered in our previous analysis (although the envelope of the aforementioned pulse consists of noisy fluctuations). Indeed, stochastic inputs with non-zero means possess a statistical bias towards excitation or inhibition, which results in a coherent increase or decrease in firing rate contributions to the non-linear feedback components. ON/OFF systems are less likely to oscillate than ON/ON systems. This is due to the fact than all cells contribute coherently to the feedback signal in the ON/ON case, while only half of the neural population (either ON or OFF cells) does so in ON/OFF nets. Nevertheless, we may affirm that oscillations are easy to observe in a ON/OFF network if the stochastic stimulus has a zero mean.

Chapter 6

Neural adaptation facilitates oscillatory responses to static inputs in a recurrent network of ON and OFF cells

Lefebvre J., Longtin A., LeBlanc V.G. (2010) Submitted

Abstract

We investigate the role of adaptation in a neural field model, composed of ON and OFF cells, with delayed all-to-all recurrent connections. As external spatially profiled inputs drive the network, ON cells receive inputs directly, while OFF cells receive an inverted image of the original signals. Via global and delayed inhibitory connections, these signals can cause the system to enter states of sustained oscillatory activity. We perform a bifurcation analysis of our model to elucidate how neural adaptation influences the ability of the network to exhibit oscillatory activity. We show that slow adaptation encourages input-induced rhythmic states by decreasing the Andronov-Hopf bifurcation threshold. We further determine how the feedback and adaptation together shape the resonant properties of the ON and OFF cell network and how this affects the response to time-periodic input. By introducing an additional frequency in the system, adaptation alters the resonance frequency by shifting the peaks where the response is maximal. We support these results with numerical experiments of the neural field model. Although developed in the context of the circuitry of the electric sense, these results are applicable to any network of spontaneously firing cells with global inhibitory feedback to themselves, in which a fraction of these cells receive external input directly, while the remaining ones receive an inverted version of this input via feedforward di-synaptic inhibition. Thus the results are relevant beyond the many sensory systems where ON and OFF cells are usually identified, and provide the backbone for understanding dynamical network effects of lateral connections and various forms of ON/OFF responses.

6.1 Introduction

The behavior of neural systems is governed by a combination of circuitry and cellular attributes. Amongst these, spike frequency adaptation is found in almost all neurons, where it is thought to influence the processing of neural information mediated by action potentials. Adaptation corresponds to a stereotyped de-

crease in firing rate after prolonged stimulation, as the cell habituates to steady input currents. It is thought to play a particularly important role in sensory systems. There it can alter neuronal firing patterns in order to direct the system's response towards given stimulus attributes [137, 138, 139, 140, 39, 141] or to tune neural sensitivity to stimulus intensity [142]. Adaptation has further been shown to control repetitive firing [143] and influences both time and rate coding properties [144]. Various mechanisms underlying adaptation have been identified. Steady neuron firing can activate slow potassium currents [145], which may also be calcium-dependent [146], resulting in firing rate decay following a step input. Adaptation has also been linked in other cases to the inactivation of slow sodium currents [147]. Theoretical studies on Integrate-and-Fire models as well as conductance-based models have reproduced experimental recordings of adapting behavior (see [137, 148, 149] and references therein)

The goal of this paper is to investigate how adaptation shapes the frequency tuning of cells and stimulus-induced network oscillations in a realistic context of sensory feedback circuitry involving adaptive ON and OFF cells. We draw our main motivation for combining feedback, ON/OFF populations and adaptation from studies of the weakly electric fish (Apteronotus leptorhynchus). Adaptation has been studied there both at the level of the primary receptor known as the P-unit electroreceptor (which we do not focus on here), as well as at the level of the post-synaptic population of pyramidal cells. P-unit adaptation is very rapid (tens of milliseconds) and has been shown to influence the frequency-dependent encoding of electrosensory inputs [150, 33]. This adaptation further enables the separation of fast transient stimuli, related to communication signals, from slower oscillatory signals arising from the proximity of two fish [39]. This adaptation further participates in the appearance of input-induced states of synchrony [151], allowing transitions among P-units from states of synchrony to desynchrony and vice-versa due to rapid communication signals. Each P-unit axon then trifurcates, with each of the three processes reaching pyramidal cells in one of three topographic maps of the electrosensory lateral line lobe (ELL).

Cells especially in superficial layers of the ELL also exhibit adaptation which shapes their temporal filtering properties for oscillatory inputs that arise naturally during an encounter of two fish [152, 35, 29]. In fact adaptation becomes faster as one moves from central to lateral maps, which motivates the study here across adaptation time scales. The mechanism of this adaptation is not known but does seem to depend on calcium [153].

It is the adaptation exhibited by these latter pyramidal cells that is of interest in our paper because they are involved in recurrent circuitry with other nuclei - as opposed to receptors which are involved only in feedforward circuitry. In the visual system, the thalamo-cortical loop has similar properties and exhibits structures that also possess ON and OFF cells. We note that adaptation is in fact a form of negative feedback, and as such can interact with - and even mimic - other forms of feedback caused by network circuitry. Recent dynamical studies on large scale nets have shed light on the role of adaptation in the generation and stability of spatially localized patterns like breathers (localized time-periodic bumps of activity) and traveling waves [154, 84, 155]. Other studies demonstrated its impact on network oscillations [36, 37, 38] in the form of enhanced synchronization.

Of further interest is the fact that oscillatory states can appear in sensory pathways as a consequence of sensory inputs with sufficiently high spatial coherence and/or spatial binding [102, 97, 98]. In the weakly electric fish such oscillations are associated with temporally random stimuli of large spatial correlation (such as other animals) and relies on delayed feedback [32, 99, 33, 34]. Delayed feedback inhibition common to all cells often underlies oscillatory activity in the brain as it competes with excitatory feedback (see e.g. [156, 157, 97, 98, 158] and references therein). Also, frequency tuning effects have been observed in the electric fish that change with the spatial configuration of the stimulus, i.e. on its local versus global geometry [27, 32, 135]. These are due in part to cellular and circuit properties [26, 29]. It is known for example that a step increase in

stimulus contrast causes an increase followed by a decrease in ELL firing, i e by adaptive behavior rather than oscillatory behavior

These studies naturally lead to the question of how adaptation interacts with spatio-temporal stimuli that lead to oscillatory dynamics Does the presence of adaptation increase or decrease the propensity for an inhibitory recurrent network to oscillate in response to spatially correlated inputs? How does adaptation influence frequency tuning in the presence of recurrent inhibition? Cells in the ELL further display either simple ON or OFF behavior ON (OFF) cells encode positive (negative)-going fluctuations of input signals These signals occur as modulations of the amplitude (and sometimes frequency for communication calls) of the carrier oscillation emitted by the fish known as the electric organ discharge (EOD) ON cells (known as E cells) thus increase their firing rate when the amplitude of the EOD increases, and vice-versa for the OFF cells (known as I cells) [22, 159, 24] The incorporation of multiple neural populations is important to properly account for network activity and receptive field geometry and is still at the forefront of work in theoretical neuroscience [69, 87, 85, 88] In earlier work inspired by the electrosensory circuitry, we have shown how ON and OFF populations interact with delayed and non-delayed recurrent connections to generate oscillations triggered by static stimuli [111, 128] These studies, which used neural field formulations as well as stochastic Integrate-and-Fire neurons, did not consider the issue of cellular adaptation, in fact the dynamics of net works with both multiple populations and adaptation is a general open question

We note that the interplay of ON and OFF pathways also plays a fundamental role in vision from retina onwards [47, 140] as well as in audition [110, 129] and other senses The simple ON/OFF dichotomy described above, where each population responds preferentially to one polarity of the stimulus, is commonly present [116] Yet the circuitry and physiology, often involving many types of ON/OFF cells and complex network interactions, is far from clear and is slowly being elucidated [140, 124, 160, 129] Here we focus on this simple type of

ON/OFF behavior as opposed to other forms, such as that where both the onset and offset of a stimulus both cause firing rate increases [129] (in the simple dichotomy illustrated above, ON and OFF populations would have inverted responses with respect to one another for both onset and offset).

In contrast, ON/OFF circuitry (known as E/I circuitry) has been worked out for weakly electric fish, and can be summarized as follows: ON and OFF cells share common P-unit afferents, but the OFF pathway includes an interposed inhibitory interneuron, causing the OFF response to be inverted [22, 159]. Electroreception thus offers a relatively simpler sensory system, both anatomically and physiologically, in which to investigate the role of adaptive ON/OFF cells involved in recurrent circuitry. Such a study can then provide the dynamical backbone for more complex systems and forms of ON/OFF responses. It is important to note that earlier modeling studies of oscillations in ELL assumed only one population was at work (the ON population [32, 99, 33, 34]).

In this paper, we address the following questions: how does adaptation influence the oscillatory response threshold in networks of ON and OFF cells? Are global oscillations as common when adaptation is included? How does the combination of adaptation and feedback shape frequency tuning of cells embedded in the network? Our work here builds on our previous results about ON and OFF cells and delayed feedback without adaptation. We investigate how adaptation may underlie stimulus-induced oscillations in recurrent networks. To demonstrate this, we compare the Andronov-Hopf bifurcation scenario for the cases with and without adaptation. We thus expand the stability analysis around steady activity states in a recurrent model that now includes adaptation dynamics. We will highlight the effect of adaptation on the stability of input-induced limit cycles. We will also study how such a model responds to time-periodic input, and how adaptation shapes the resonance curve by introducing additional time-scales in the system.

In section 6.1, we describe the architecture of our ON/OFF network and we show how stable oscillations appear as a result of spatially localized stimulation. In Section 6.3, we perform a stability analysis of our model, incorporating adaptation, where we compare the instability point between the cases where adaptation is and is not present. There, our study has been made more analytically tractable by assuming identical adaptation dynamics for the ON and OFF cells. We further look at the impact of adaptation on the system's steady states, to determine how external input then interact with the feedback. Lastly, in Section 6.4, we investigate and compare the effects of adaptation and feedback on the amplitude of the cells response to time-varying inputs. We further motivate those results by comparing the resonance curves with those obtained with a noisy Integrate-and-Fire net.

6.2 Model

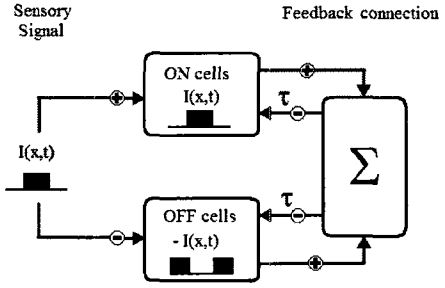

Figure 6.1: Network architecture of our model. It is inspired from the ELL of the weakly electric fish. The sensory layer, built of an equal number of ON and OFF cells, receives external sensory inputs with direct (ON) and inverted (OFF) polarity. The populations then project to higher centers, which accumulate the activity distributed across the network (sigma symbol). The recurrent connections allows the accumulated activity component to be sent back to all the cells in the sensory layer with some time lag τ.

Our model is based on electroreception, but is general enough to apply to other senses. We describe the evolution of the neural activity $u(x,t)$, corresponding to the mean somatic membrane potential of a sub-network of the whole network located at position x along a one-dimensional spatial domain Ω. This activity is further segregated into that of ON and OFF populations $u_{on.off}$. External sensory signals $I(x,t)$ propagate in a parallel fashion from the first receptors (not modeled explicitly) up to the "sensory" layer of pyramidal cells in the ELL, and excite and/or inhibit the local populations by altering their activity level. Further, recurrent connections allow the activity of the cells to propagate to higher brain centers (mainly area NP in the weakly electric fish [22]). For simplicity the activity there is summed across the network and then fed back to all the initial sites globally and with inhibitory polarity. This component of the circuit involves a significant processing and propagation time lag modeled with a fixed delay τ. The fields u_{on} and u_{off} obey the dynamics

$$\begin{aligned} (1 + a^{-1}\partial_t)u_{on}(x,t) &= -A(t-\tau) + I(x,t) \\ (1 + a^{-1}\partial_t)u_{off}(x,t) &= -A(t-\tau) - I(x,t), \end{aligned} \tag{6.1}$$

where a is the rate constant of the exponential synapses with response function $\eta(t) = ae^{-at}$, where $t > 0$, and A is the delayed inhibitory feedback connection, corresponding to the accumulation of activity of each unit across the network:

$$A(t-\tau) = \int_\Omega dy[\alpha_{on} f(u_{on}(y,t-\tau)) + \alpha_{off} f(u_{off}(y,t-\tau))].$$

Here, α_{on} and α_{off} are the relative proportions of ON and OFF cells in the network, which have been both set to 0.5. The function f is a sigmoidal firing rate function defined by $f(u) = (1 + exp(-\beta(u-h)))^{-1}$ for a gain of β and an activation threshold h. The feedback gain β is fixed to 25 troughout the analysis.

The ELL in the weakly electric fish exhibits a similar architecture to the one used in this model. Indeed, very few lateral connections exist within it, such that most of the processing is performed by the means of feedback connections

from higher muclei. Previous studies [111, 128] demonstrated that this model exhibits changes from stable activity equilibria to global oscillations as a result of increasing stimulus amplitude and/or spatial extent, due to the presence of an Andronov-Hopf bifurcation. Those neural field predictions were further supported by simulations of a network of noisy Integrate-and-Fire neurons with spatio-temporal forcing, as in [34, 32, 33] for the case where only ON cells were considered. Weaker effects of local non-delayed circuitry within the ELL itself have also been studied [128], and were shown to be of no qualitative consequence on the dynamics; such local effects are thus not modeled here.

Aside from their inhibitory response to positive inputs, OFF cells in-vivo can fire at a baseline mean rate even in absence of external stimulation, as may ON cells [50,45]. In the electric sense, both ON and OFF cells are spontaneously active because they receive tonic excitation from various sources. Thus, external input modulates the firing activity of both ON and OFF cells around this baseline activity. Experimental recordings in the electrosensory system indicate that the spontaneous firing rate may even be slightly higher for OFF cells than for ON cells. Our recent results, in the context where no adaptation is present, demonstrate that such a significant difference in spontaneous activity between these neural populations can qualitatively alter the input response of ON/OFF nets [45]. While the inclusion of this activity difference in our network with adaptation is easy to do (e.g. by adding a bias current to one neuron population) and would further enhance the connection of our results with the physiology of real ON/OFF systems, the analysis would become much more complicated as a function of this asymmetry. Thus, for simplicity, we assume throughout that both neural populations share the same baseline activity in the absence of input. This allows us to focus more clearly on the influence of adaptation on the resonance and oscillatory properties of such nets. Also, our results are generally applicable to any network of spontaneously firing cells with global inhibitory feedback to themselves, in which a fraction of these cells receive external input directly, while the remaining ones receive an inverted version of this input via

feedforward di-synaptic inhibition.

Without adaptation, observed global oscillations can emerge as network responses to spatially distributed signals. Figure 6.2 shows the response of ON and OFF populations to an input of the form $I(x,t) = I_o \neq 0$ if $x_1 < x < x_2$ and $t_1 < t < t_2$ (and $I = 0$ otherwise). The stimulus triggers a global oscillatory response by causing an Andronov-Hopf bifurcation, for which the details have already been worked out [111]. The linearization and subsequent eigenvalue analysis of system (6.1) for spatially homogeneous eigenmodes of the form $u_j(x,t) = \bar{u}_j(x) + \tilde{u}e^{\lambda t}$ for $\tilde{u}, \in \mathbb{R}$, $\lambda \in \mathbb{C}$, yields the characteristic equation

$$\lambda + 1 + Re^{\lambda\tau} = 0, \tag{6.2}$$

for $R = \frac{1}{2}[\int_\Omega dy f'(\bar{u}_{on}(y)) + \int_\Omega dy f'(\bar{u}_{off}(y))]$. The case with adaptation is more involved, as we show next.

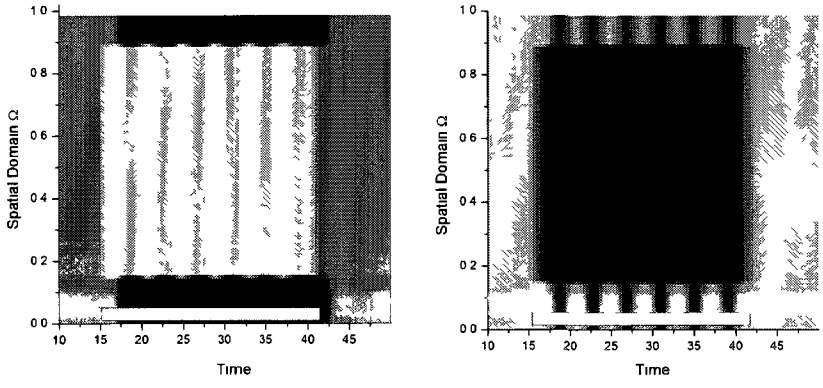

Figure 6.2. Oscillatory response of ON(left panel) and OFF(right panel) populations to a spatially localized pulse Parameters are $a = 1$, $\tau = 1\ 4$, $h = 0.1$ and $\Omega = [0,1]$. The input has an amplitude $I_o = 0.3$ and possess a spatial width $\Delta \equiv |x_2 - x_1| = 0.75$ where $x_1 = 0.15$ and $x_2 = 0.90$ and for $15 < t < 40$.

6.3 Neural adaptation

While the idealized network architecture of (6.1) allows the cellular populations to maintain a steady (or oscillating) level of activity, more realistic network descriptions typically include *adaptation*. As we will see, this local intrinsic component of cellular dynamics plays a crucial role in balancing the excitation-inhibition ratio across the system. It is therefore an important factor to consider in the genesis of global oscillations as well as possible resonance effects. Various biophysical mechanisms have been shown to cause adaptation, generating distinct effects on the spiking dynamics [149, 37, 144, 161]. Here we incorporate an intrinsic linear adaptation that is modeled as a second field, acting locally and subtractively on the activity field (6.1). Note that we are not modeling a specific outward current. Rather, this adaptation field can be seen as a subtractive current that approximates the impact of a number of realistic adaptation mechanisms on firing rate and resonance properties. This model adaptation field will thus reflect the effect of this linear component on the evolution of spatio-temporal activity. Our model now becomes:

$$\begin{aligned}(1+a^{-1}\partial_t)u_{on}(x,t) &= -A(t-\tau)+I(x,t)-\epsilon_{on}w_{on}(x,t) \qquad (6.3)\\ (1+a^{-1}\partial_t)u_{off}(x,t) &= -A(t-\tau)-I(x,t)-\epsilon_{off}w_{off}(x,t),\end{aligned}$$

where the adaptation fields $w_{on\ off}(x,t)$ obey

$$\begin{aligned}(1+b^{-1}\partial_t)w_{on}(x,t) &= u_{on}(x,t) \qquad (6.4)\\ (1+b^{-1}\partial_t)w_{off}(x,t) &= u_{off}(x,t).\end{aligned}$$

Here b is the rate of the adaptation (b^{-1} is the adaptation time constant) and $\epsilon_{on\ off} > 0$ corresponds to the gain or amplitude of the adaptation component, which acts as an inhibitory feedback. System (6.3) includes two additive inhibitory components which obey linear dynamics and operate on the time scale b^{-1}, which we assume is identical for ON and OFF cells. Further, the adaptation gain is assumed to be identical for both ON and OFF cells i.e. $\epsilon_{on} = \epsilon_{off} = \epsilon$.

The fields $w_{on.off}(x,t)$ are expected to locally inhibit the activity of both ON or OFF populations whenever the ON and OFF activities $u_{on.off}(x,t)$ increase. The instability threshold for which global oscillations can be triggered by static local stimuli will change according to the gain and relative time scale of this new inhibitory mechanism.

To determine the impact of adaptation, one needs to rework the stability analysis taking into account the increased dimensionality of the problem. This analysis relies on the symmetry between ON and OFF cells and is restricted to the choice of identical adaptation gains and time scales for both sub-populations. The steady states of the combined systems (6.3) and (6.4) are solutions of:

$$\begin{aligned} (1+\epsilon)\bar{u}_{on}(x) &= -A(\bar{u}_{on},\bar{u}_{off}) + I(x) \\ (1+\epsilon)\bar{u}_{off}(x) &= (1+\epsilon)\bar{u}_{on}(x) - 2I(x), \end{aligned} \tag{6.5}$$

where $\bar{w}_{on} = \bar{u}_{on}(x)$ and $\bar{w}_{off} = \bar{u}_{off}(x)$. Adaptation acts as a contracting components, reducing the amplitude of the steady states by a factor $(1+\epsilon_{on.off}) > 0$. Considering the spatially homogeneous eigenmodes $u_j(x,t) = \bar{u}_j(x) + \tilde{u}e^{\lambda t}$ and $w_j(x,t) = \bar{w}_j(x) + \tilde{w}e^{\lambda t}$, $\tilde{u}, \tilde{w} \in \mathbb{R}$, $\lambda \in \mathbb{C}$, one obtains from (6.3) and (6.4) the Jacobian with delayed components

$$\mathbb{J}(\lambda) = \begin{pmatrix} -a(1+R_{on}(\bar{u}_{on})e^{-\lambda\tau}) & -aR_{off}(\bar{u}_{off})e^{-\lambda\tau} & -a\epsilon & 0 \\ -aR_{on}(\bar{u}_{on})e^{-\lambda\tau} & -a(1+R_{off}(\bar{u}_{off})e^{-\lambda\tau}) & 0 & -a\epsilon \\ b & 0 & -b & 0 \\ 0 & b & 0 & -b \end{pmatrix}$$

$R_{on} = \frac{1}{2}[\int_\Omega dy f'(\bar{u}_{on}(y))]$ and $R_{off} = \frac{1}{2}[\int_\Omega dy f'(\bar{u}_{off}(y))]$. The characteristic equation follows as

$$0 = det(\mathbb{J}(\lambda) - \lambda \mathbb{I}_4), \tag{6.6}$$

with $\mathbb{I}_4$ being the 4×4 identity matrix. The resulting fourth-order polynomial in λ admits the following solutions

$$\lambda_{1.2} = -\frac{a+b}{2} \pm \frac{1}{2}\sqrt{b^2 - 2ab + a^2 - 4ab\epsilon}, \tag{6.7}$$

$$\lambda_{3.4} = -\frac{aRe^{-\imath w\tau} + a + b}{2}$$

$$\pm\frac{1}{2}\sqrt{(Rae^{-\lambda\tau})^2 + 2a^2Re^{-\lambda\tau} - 2abRe^{-\lambda\tau} + a^2 - 2ab + b^2 - 4ab\epsilon},$$

where the eigenvalues $\lambda_{3.4}$ are implicitly determined. The function R can be expressed as

$$R = R_{on}(\bar{u}_{on}) + R_{off}(\bar{u}_{off}) = \frac{1}{2}[\int_\Omega dy f'(\bar{u}_{on}(y)] + \frac{1}{2}[\int_\Omega dy f'(\bar{u}_{off}(y))]. \tag{6.8}$$

The eigenvalues $\lambda_{1.2}$ define the stability of Eq.(6.4) and thus do not depend on the delay τ. Given that $a, b, \epsilon > 0$, $\lambda_{1.2}$ remain bounded to the left of the imaginary axis and subsequently do not contribute to any oscillatory instability. They however introduce an additional frequency in the system, whenever $\lambda_{1.2} \in \mathbb{C}$ with non-zero imaginary parts. An input-induced oscillation requires the non-linear delayed feedback connections. We may therefore restrict the analysis to the eigenvalues $\lambda_{3.4}$, which depend on the delay τ as well as the parameter R. At the instability threshold, $\lambda_{3.4} = \{iw_k | \mathbb{R} \ni w_k > 0\}$, and we obtain the same criterion for an Andronov-Hopf bifurcation from both λ_3 and λ_4, namely

$$0 = (2iw + aRe^{-\imath w\tau} + a + b)^2 - a^2 - 2a^2Re^{-\imath w\tau} + 2ab - R^2a^2e^{-2\imath w\tau} \tag{6.9}$$

$$+2abRe^{-\imath w\tau} - b^2 + 4ab\epsilon.$$

Expanding and separating the real and imaginary components using $e^{-\imath w\tau} = cos(w\tau) - isin(w\tau)$, we obtain

$$\begin{aligned} 0 &= -w^2 + awRsin(w\tau) + ab(\epsilon + 1) + abRcos(w\tau) \qquad (6.10) \\ 0 &= awRcos(w\tau) + (a+b)w - abRsin(w\tau), \end{aligned}$$

Combining these equations, the instability threshold R_c becomes

$$R_c cos(w(R_c)\tau) = -\frac{b^2(\epsilon+1) + w(R_c)^2}{b^2 + w(R_c)^2}, \tag{6 11}$$

for which the frequencies can be shown to be

$$w(R_c, \epsilon, a, b) = \pm\frac{1}{2} * \sqrt{P_1(R_c, \epsilon, a, b) \pm 2\sqrt{P_2(R_c, \epsilon, a, b)}},$$

with the polynomials

$$P_1(R_c, \epsilon, a, b) = 2(R_c^2 - 1)a^2 - 2b^2 + 4ab\epsilon,$$

$$P_2(R_c, \epsilon, a, b) = b^4 - 4b^3a\epsilon - 2a^2b^2 + 2R_c^2a^2b^2 - 4a^3b\epsilon$$

$$+4a^3b\epsilon R_c^2 + a^4 - 2a^4R_c^2 + R_c^4a^4 - 8b^2a^2\epsilon$$

Equation (6 11) defines the instability threshold as a function of the adaptation gain ϵ and time scale b^{-1} The reader might notice that whenever ϵ, $b = 0$, one recovers the eigenvalue problem exposed in Eq (6 2), in which no adaptation was present

The problem of determining the overall effect of cellular adaptation on input-induced oscillations is twofold First, one must see how $\epsilon > 0$ and $b > 0$ change the value of the instability threshold R_c in Eq (6 11) with respect to the case without adaptation i e $\epsilon = 0$, $b = 0$ Secondly, one must see whether $\epsilon > 0$ reshapes the function R in Eq (6 8) by shifting the steady states Thus, we must consider the fact that adaptation might not only change the critical value R_c where an oscillatory response occurs, but also the trajectory in parameter space on which the system reaches stable cyclic solutions

Figure 6 3 exposes the effect of increasing gain and adaptation rate constant on the instability threshold R_c in Eq (6 11) For b small, $R(b, \epsilon) < R_c$ The Andronov-Hopf threshold becomes smaller as the gain increases $\epsilon > 0$, meaning

that oscillatory states require weaker inputs to be reached. As b increases, the opposite occurs, and the threshold increases away from the case $\epsilon = 0$. Cellular adaptation in the electrosensory system operates on time scales of roughly 100ms, slower than the intrinsic dynamics of the cells, which are on the order of 10-20ms [29]. As a result, b is more likely to be smaller than the cellular rate constant a, here fixed to $a = 1$. For this interval of b values, slow adaptation enhances the prevalence oscillatory responses by reducing the value of the bifurcation threshold.

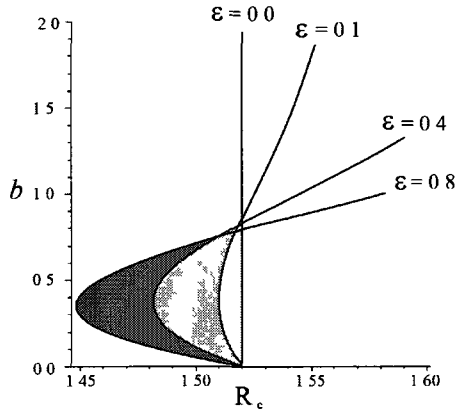

Figure 6.3: Oscillatory response threshold R_c as a function of the adaptation gain ϵ and time constant b^{-1}. Slow adaptation (b small) reduces the response threshold marginally, while on faster time scales, the threshold is increased, reducing the tendency of the system to enter oscillatory states of activity in response to static stimuli. The adaptation gain ϵ amplifies both effects. We note that for $b \approx 0.8$, the gain ϵ has almost no effect on the value of R_c. Parameters are $a = 1$, $\tau = 2.0$, $\alpha_{on\ off} = 0.5$ and $\Omega = [0, 1]$.

The effect of local stimulation on the function R for $\epsilon = 0$ has been investigated [111], but additional inhibitory components like adaptation influence the steady states as well. Indeed, from Eq. (6.5) and by considering the weak feedback regime i.e. $f(\bar{u}_{on\ off}) \approx 0$, adaptation reduces the response contrast by a factor $(1+\epsilon_{on\ off})^{-1}$. Figure 6.4 shows the response amplitude of stimulated cells as a function of the adaptation gain ϵ. The input contrast is defined by the activity

difference between stimulated and non-stimulated sites for networks with $\epsilon = 0$ and $\epsilon > 0$ in the steady state regime. This definition refers to the dynamics out of any oscillatory regimes and is used to specify the net impact of inputs on the activity of the sub-units. Once oscillations appear, we use the term "response" instead to qualify the magnitude of the oscillations (see section 6.4). As the adaptation gain increases, the response amplitude decreases. As a result, the amplitude of the inhibitory feedback for $\epsilon > 0$ is smaller than for $\epsilon = 0$; this allows the steady states to reach higher values. This can be verified numerically by solving Eq. (6.5) for both $\epsilon > 0$ and $\epsilon = 0$, or analytically by considering only the first Taylor expansion term of f.

Adaptation also reduces the magnitude of the feedback signal sent to the sensory layer in the same way that it limits the response contrast. Even though the same amount of feedback connections gets recruited, the amplitude of the return signal is reduced; the amount of inhibition in the system decreases. As such, increasing the adaptation gain does in part increase the activity of the ON and OFF populations. The behavior of the system with respect to stimulation is a trade-off between a weaker contrast and inhibition. As a consequence, this modification of the steady states significantly alters the way the system interacts with the non-linearities of Eq. (6.1) and thus changes the location in parameter space where a bifurcation occurs. To understand this effect, we need to investigate the consequences of $\epsilon > 0$ on the shape of the function $R = R(\epsilon)$ in Eq. (6.8).

The function R is an integral over the steady states across the network, via the derivative of the activation function f. It is maximal whenever $\bar{u}_{on.off} = h$, that is, the closer the equilibrium activities are to the threshold for firing (and thus for producing feedback activity), the higher R becomes. It may also be seen as the amount of non-linearity in the system. With adaptation, significant variations of the function R require large input amplitudes. In the context of a static pulse of width Δ and amplitude I_o, Fig. 6.5 illustrates points in (I_o, ϵ) parameter space for which an input-induced Andronov-Hopf bifurcation

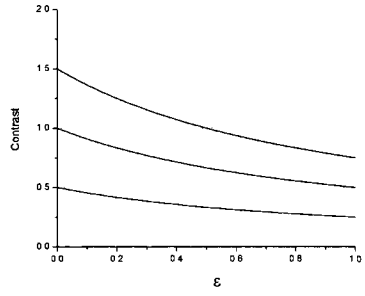

Figure 6.4: Input contrast for a static pulse of the form $I(x,t) = I_o$ if $x \in \Delta$ and $t_1 < t < t_2$ where Δ corresponds to the input spatial width, defined by $\Delta = |x_1 - x_2|$. The contrast is the difference in activity of units inside and outside the pulse. As the adaptation gain increases, the local response decreases. The activity levels have been chosen such that the feedback connections are weakly interacting with the ON and OFF population activities. The solid curves illustrate the contrast when adaptation is present and as a function of the gain ϵ for different input amplitudes, while the dashed lines show the response for $\epsilon = 0$.

occurs, i.e. for which $R(I_o, \epsilon) > R_c$. It illustrates how the function $R(I_o, \epsilon)$ behaves according to an input amplitude I_o and increasing adaptation gain ϵ. A diminished input amplitude implies that larger input amplitudes are required to bring the system in regions of parameter space where oscillations are stable (gray regions). But it also implies that once the system reaches those states, they are more robust and remain stable over a larger range of input amplitudes.

Cellular adaptation diminishes the variability of R. When h is low, more significant contributions are made by the lateral units to the non-linear connections; this is even more so as the adaptation gain increases. The steady states $\bar{u}_{on\ off}$ of lateral sites are higher for $\epsilon > 0$ due to less feedback inhibition, and are typically found closer to the activation threshold h. This results in higher values of the function $R(I_o, \epsilon)$: the system remains close to the Andronov-Hopf regime over a larger portion of parameter space because the adaptation disposes the lateral activities to maintain a higher degree of non-linearity. As shown in Fig. 6.5a, the minimal amplitude required for global oscillations is smaller for $\epsilon > 0$

than for $\epsilon = 0$. For high values of h, the effect of the adaptation gain on the lateral contributions is negligible, since the reduced contrast causes the function $R(I_o, \epsilon)$ to be much smaller when $\epsilon > 0$ than when $\epsilon = 0$. This is the case depicted in Fig. 6.5b. Nevertheless, the broadening of the amplitude intervals due to ϵ makes oscillations more prevalent in a system that incorporates adaptation. This supports previous results on recurrent nets with adaptation, where slow recurrent components were shown to facilitate the genesis of cyclic activity [36, 37, 162]. We note that whenever the input absolute amplitude increases, the system first enters the Andronov-Hopf regime where global oscillations are stable; but if the input amplitude becomes too high, the oscillations disappear via a reverse Andronov-Hopf bifurcation. This is so because the sub-unit activities are taken to values much higher than the threshold h, where the feedback A behaves linearly. The activity of ON and OFF cells is then inhibited sufficiently by the feedback to destroy the oscillations.

Our analytic work assumes that the adaptation rate and gains are equal between ON and OFF populations. However, it has been shown that in the electrosensory system these parameters vary between ON and OFF populations, and also across the various electrosensory spatial maps (Krahe et al. 2008, Mehaffey et al. 2008). In fact, this motivates varying the adaptation rates below in Fig.7. If the symmetry restriction is relaxed and two distinct adaptation rates b_{on} and b_{off} are introduced, the Andronov-Hopf regions of Fig. 5 become non-symmetric with respect to the vertical line $I_o = 0$, meaning that the system does not respond evenly to excitatory and inhibitory inputs anymore (not shown). In fact, the sub-population with the slowest adaptation dominates: whenever $b_{off} < b_{on}$, a wider range of inhibitory input amplitudes triggers oscillatory activity, i.e. the system becomes more sensitive to inhibitory inputs because OFF cell adaptation is slower. If $b_{on} < b_{off}$, the opposite occurs. This effect is amplified with the magnitude of $|b_{off} - b_{on}|$.

An interesting consequence of these effects is that the system may now respond

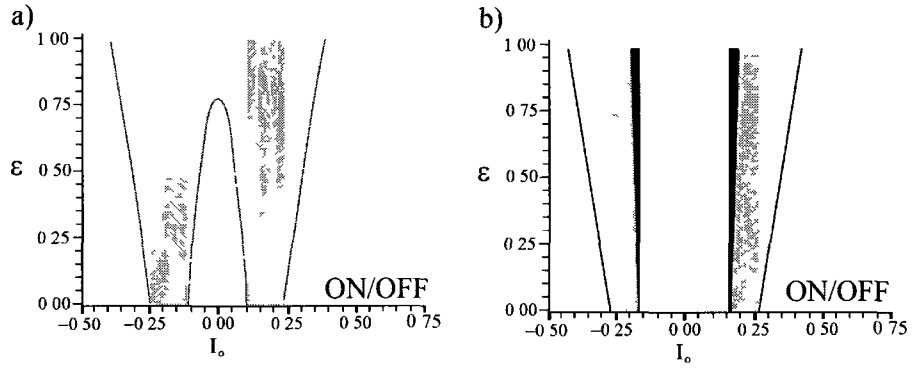

Figure 6.5: Points in (I_o, ϵ) parameter space for which a Andronov-Hopf bifurcation occurs. The input is a stationary pulse as in Fig. 6.4 for a fixed width. a) Due to the presence of ON and OFF cells, oscillatory responses are observed for both excitatory ($I_o > 0$) and inhibitory ($I_o < 0$) pulses, making the functional $R(I_o, \epsilon)$ symmetric with respect to I_o, irrespective of the spatial extent of the stimulus. Because h is small ($h = 0.07$), as ϵ increases, the minimal input amplitude causing a Andronov-Hopf bifurcation is smaller, enhancing the tendency of the system towards cyclic activity, and the interval of values broadens. The vertical dark gray bands correspond to the case without adaptation ($\epsilon = 0$). b) For larger feedback thresholds (i.e. $h = 0.1$), the mean value of the function $R(I_o, \epsilon)$ is smaller for $\epsilon > 0$. The minimal input amplitude causing a Andronov-Hopf bifurcation becomes larger as ϵ increases. Here, the feedback threshold is $h = 0.1$. Parameters are $a = 1$, $\tau = 2.0$, $\Omega = [0, 1]$. The pulse width is $\Delta = 0.5$. The rate constant b was set to 0.8, where the critical value R_c remains approximately constant as ϵ changes (see Fig. 6.3).

to pulses of smaller spatial extent, in a regime where h is smaller. As the mean value of R is larger for $\epsilon > 0$ in this case, input causing small fluctuations in the function R now becomes a candidate to cause a bifurcation, via either amplitude or width changes. This would not be the case if adaptation were not present, because the mean value of R would be much smaller. This effect is caused by a smaller amount of inhibition fed back to the sensory layer by the recurrent connections, as the units adapt as well to this steady return current. Fig. 6.6 shows how the regions in (I_o, ϵ) space changes as a function of input width. As the width Δ diminishes from 0.50 to 0 35, regions of stable oscillatory activity retract towards higher adaptation gains, meaning that adaptation is necessary for those smaller inputs to trigger stable oscillatory solutions. We note that this

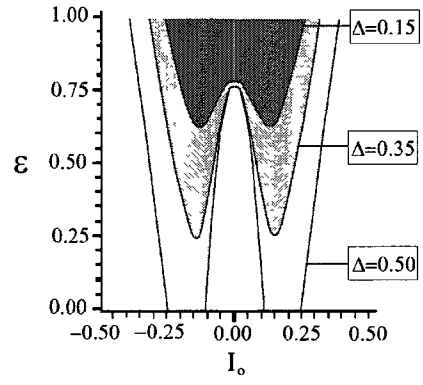

Figure 6.6: Points in (I_o, ϵ) parameter space for which $R(\epsilon) > R_c$ for a static pulse-shaped stimulus of amplitude I_o and various widths. Pulses of smaller widths only generate rhythmic responses when the adaptation gain is increased. Regions where the limit cycles are stable, plotted in shades of gray, are symmetric with respect to the line I_o. Parameters are $a = 1$, $\tau = 2.0$, $\Omega = [0, 1]$, $h = 0.07$ and $b = 0.8$.

behavior occurs because of the choice of a small feedback threshold h.

In [128], it was shown that if an additional non-delayed inhibitory feedback component is added to Eq. 6.1, the Andronov-Hopf threshold increases, thus reducing the tendency of the system to undergo oscillatory behavior with respect to spatially localized inputs. In many aspects, an adaptation current like the one considered here plays the same role as an extra instantaneous inhibitory feedback. As Fig. 6.5 shows, the minimal input amplitude required to generate global oscillations increases, which corroborates the results presented in [128] for this particular choice of large threshold values. This seems to contradict the results of Fig. 6.6, but this is not so. While the main effect of adaptation is to move equilibria in phase space, the non-delayed feedback components considered in [128] changed the bifurcation threshold considerably, which is not the case here. The oscillations triggered by small pulses as in Fig. 6.5 are the result of a special choice of h which brings the system close to the Andronov-Hopf regime.

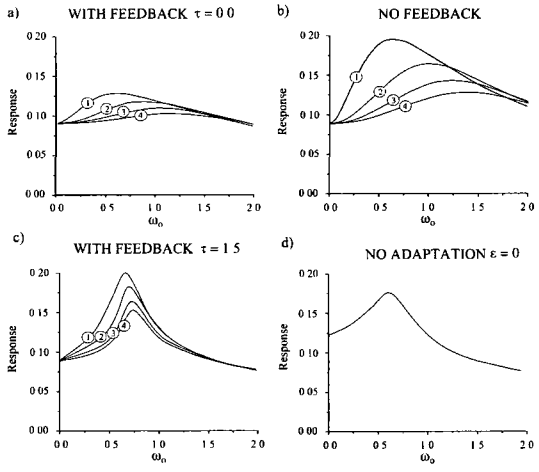

Figure 6.7: Response amplitude of ON cells to a spatially localized pulse sinusoidally modulated in time i.e $I(x) = I_o sin(w_o t)$ for $x \in \Delta$. The response is defined as the difference between the maximal amplitude of the activity reached by the solutions, and the activity level prior to any stimulus. For each trial, the adaptation time scale is increased, from slow to fast: **1**. b=0.2; **2**. b=0.5; **3**. b=0.8; **4**. b=1.1. a) With non-delayed feedback, the response is constant over the range of input frequencies. The system responds maximally to the adaptation intrinsic frequency, while the inhibitory feedback keeps the responses weak. One does not see the Hopf frequency because of the zero delay. b) Without feedback, the system demonstrates strong resonance near the adaptation frequencies. The response decreases in amplitude as the adaptation becomes faster. c) When delayed feedback is considered, dominant responses are seen near the Hopf frequency, where the change in adaptation time-scale does not seem to significantly shift the resonances, although the dynamics still become high pass. The delay chosen is $\tau = 1.5$. d) Without adaptation (i.e. $\epsilon = 0$), the resonance occurs at the Hopf frequency, and the response amplitude is generally larger (even for $w_o = 0.0$). Parameters are $a = 1$, $\Omega = [0, 1]$, $h = 0.1$, $I_o = 0.2$ and $\Delta = 0.4$. The adaptation gain was set in panel a)-c) to $\epsilon = 0.6$.

6.4 Time-varying inputs

The results presented in the foregoing analysis are based on changes of stability of steady states. However, one of the major role of cellular adaptation is to filter time-varying signals. Fast inputs are likely to significantly increase the cellular activity until the adaptive forces activate. This adaptive component typically acts on the system after the initial, transient response of the cells. As a result, apart from its effect on equilibria, adaptation influences the re-

sponses of the system with respect to fast varying signals As a final part of our overview of adaptation, we outline how the integration of time-dependent inputs varies according to the adaptation parameters ϵ and b Real sensory signals usually demonstrate a high degree of noise, which can include significant high frequencies However, studying time-periodic signals may highlight the frequency tuning properties of our model

The behavior of the solutions with respect to time-dependent inputs might help to understand the role of adaptation and its timing in transient dynamics In Fig 6 7, we plot the response amplitude of the ON cells to a time-periodic signal of frequency w_o for various adaptation time scales It is evident that as the adaptation rate constant b increases, the system filters out lower frequencies, thus acting more like a high-pass filter When no adaptation is present (Fig 6 7d), the system's maximal response occurs precisely at the Hopf frequency, as the input resonates with the intrinsic oscillations of the system If the feedback connections are removed (Fig 6 7b), the system becomes fully linear and input frequencies generating maximal responses are entirely determined by the amplitude of the solutions of Eq (6 3) which are function of a,b, w_o and ϵ In particular, as adaptation becomes faster (i e when b increases), the response peak is also shifted towards higher input frequencies A similar behavior occurs in the case with non-delayed feedback (i e setting $\tau = 0$), while the system responds maximally at the same frequencies as in Fig 6 7b, although the amplitudes of the oscillations are significantly smaller

When both delayed feedback and adaptation(Fig 6 7c) are considered, the system responds maximally at an input frequency near the Hopf frequency, which corresponds to a mixture of the cases seen in Fig 7b and d In this case, the maximal response frequency shift is much less significant, as the system appears to remain closer to the Hopf frequency as b increases Increasing the adaptation gain ϵ amplifies this effect (not shown)

The qualitative shape of the curves shown in Fig. 6.7 has also been obtained using a noisy Integrate-and-Fire model (LIF) that possesses both global feedback and adaptation, where the architecture is the same as in Eq. (6.3)-(6.4). The goal here is not to perform a thorough comparison of the neural field model dynamics to those of the LIF model - this will be left as part of a future study that will consider more biophysically realistic models of the electrosensory lateral line pyramidal cells, including adaptation, feedback and SK channels. Rather the goal is to show that an LIF description can reproduce the main qualitative features seen in our neural field model. The evolution of the membrane potential of the j-th LIF neuron, for $j = 1...N$ obeys

$$\begin{aligned}
\frac{dv_j^{on}(t)}{dt} &= -v_j^{on} + g\sum_{t_i}\eta(t_i - \tau) - \epsilon w_j^{on}(t) + \mu + \xi(t) + I(j,t) \qquad (6.12)\\
\frac{dv_j^{off}(t)}{dt} &= -v_j^{off} + g\sum_{t_i}\eta(t_i - \tau) - \epsilon w_j^{off}(t) + \mu + \xi(t) - I(j,t)\\
b^{-1}\frac{dw_j^{on}(t)}{dt} &= -w_j^{on}(t) + v_j^{on}(t)\\
b^{-1}\frac{dw_j^{off}(t)}{dt} &= -w_j^{off}(t) + v_j^{off}(t),
\end{aligned}$$

with Gaussian white noise $\xi(t)$ of intensity D, i.e. the autocorrelation is $\langle \xi(t)\xi(t')\rangle = 2D\delta(t-t')$. The feedback gain is denoted by g. The network contains N ON cells and N OFF cells, which receive inputs of the form $I(j,t)$. The individual spike times of neurons are denoted by t_i, and the bias current by μ. The synaptic response function η is an in Eq.6.1. The membrane time contsant was set to 1, while the refractory period is set to $\tau_m = 1$. Here as well, b^{-1} stands for the adaptation rate and ϵ is the adaptation gain.

Numerical results on resonance properties for the LIF with adaptation are shown in Fig. 6.8. The parameters of the LIF model with ON and OFF cells have been scaled to fit the neural field description, as in [111]. We see that the LIF model qualitatively reproduces the behavior of the resonance when the

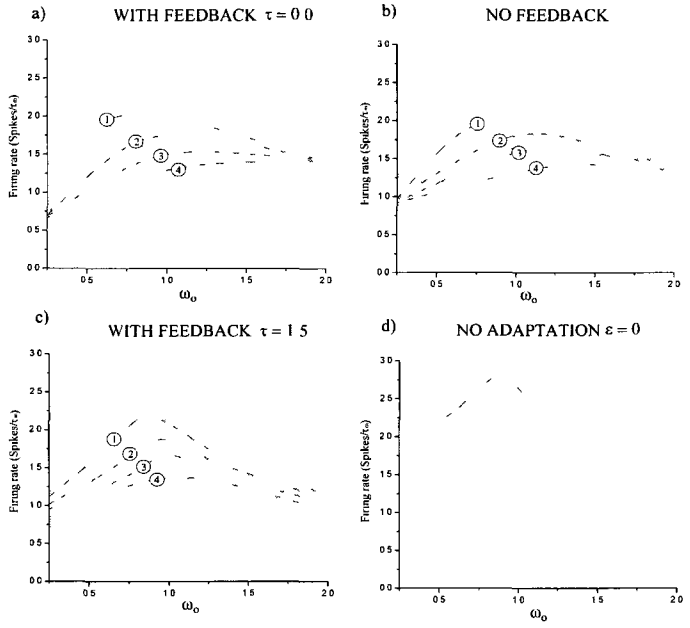

Figure 6.8: Mean firing rate fluctuations of stimulated ON cells in a noisy Integrate-and-Fire net as in Eq. (6.12). The input is a spatially localized pulse sinusoidally modulated in time i.e $I(x) = I_o sin(w_o t)$ for $x \in \Delta$. The plotted firing rates correspond to deviations from the non-stimulated state. As in Fig. 6.7, the adaptation time scale is increased in each panel: **1**. $b = 0.2$; **2**. $b = 0.5$; **3**. $b = 0.8$; **4**.$b = 1.1$. The circuit features are also changed in each panel: a) with non-delayed feedback i.e. $\tau = 0.0$; b) without feedback; c) with delayed feedback i.e. $\tau = 1.5$; and d) without adaptation (i.e. $\epsilon = 0$). In each case, the behavior observed with the neural field model is reproduced qualitatively. Parameters are $I_o = 1.0$, $\Omega = [0, 1]$, $h = 1.0$, $g = -0.2$, $\mu = 1.05$ and $\Delta = 0.4$. The noise has an amplitude $D = 1\ 0$ The adaptation gain was set in panel a)-c) to $\epsilon = 1.5$.

equivalent parameters are varied. This is particularly the case for the adaptation rate constant. Note that, in the LIF model, the increase in the feedback delay only changes the resonance slightly in comparison to the neural field model. This is likely due to the fact that the LIF includes a feedback kernel which convolves every spike emitted with a smooth function. This kernel already implements an "equivalent" delay, which already causes a resonance similar to the neural field with delay. Nevertheless, the response curves behave as in Fig. 6.7 to an increase of the adaptation time scale b, where the processes become more

high pass.

6.5 Discussion

In this article, we studied the effects of cellular adaptation on the genesis of oscillatory responses to spatially localized static or time-periodic pulses of varying amplitudes in a recurrent network of ON and OFF cells. Based on previous results, we performed the bifurcation analysis for an Andronov-Hopf bifurcation caused by an external stimulus in an adaptive system, and showed that both the time scale b^{-1} and gain ϵ of the adaptation term modified the instability threshold. The adaptation was shown to decrease the input contrast and the effect of negative feedback, resulting in an increase of steady state activities. It was further shown that for weak values of the adaptation rate and high values of the gain, adaptation enhances the genesis of oscillatory responses to stationary pulses.

Specifically, the results of Section 6.3 demonstrate that whenever the adaptation rate b is chosen to be small enough (resulting in slow adaptation dynamics), cyclic solutions are found to be more robust compared to a system that does not adapt at all. In this regime, adaptation causes the Andronov-Hopf threshold to be smaller. This was shown by performing a bifurcation analysis near the fixed points of our model for the case where the adaptation timing and gain are identical for both ON and OFF cells, and by investigating the effect of these on the bifurcation point. A complementary effect of adaptation may be elucidated by looking at how the activity equilibria behave in the presence of the terms w_{on} and w_{off}. Indeed, the adaptation gain affects the input contrast by decreasing the response amplitude of the stimulated units. A direct consequence of this is a wider interval of input amplitudes generating oscillations, making the system more sensitive to inputs of smaller widths. These results point toward a prevalence of oscillatory states generated by sensory stimuli. This result is also

consistent with the findings on neural oscillators which show that adaptation enhances the synchronization properties of networks [36, 37], where oscillatory solutions become stable in the presence of adaptation but aren't if feedback alone governs the dynamics [162, 155].

However, this conclusion holds only in a regime where the dynamics of $w_{on,off}$ are slow. In this case, the adaptation components may be seen as an additional source of slow inhibitory feedback (albeit instantaneous rather than delayed), reinforcing the presence of cyclic activity. If the adaptation becomes fast compared to the intrinsic dynamics of the units, the opposite occurs, and global oscillations become more difficult to obtain. This supports the results on a similar model without adaptation, where it was shown that additional non-delayed (and fast) inhibitory feedback components pushed back (i.e. raised) the Andronov-Hopf threshold [128].

Adaptation is also involved in the integration of temporal signals. It is thus important to see how this combines with the resonant properties of ON/OFF nets. In Section 6.4, resonance curves were plotted, in cases with and without feedback. The adaptation component introduces additional resonances in the system. This is apparent by looking at the resonance curves when no feedback is present, or when the feedback delay is chosen to be zero. The Hopf frequency, located at input frequencies where the response amplitude is maximal, depends on the choice of adaptation time scale. The presence of these new frequencies, brought up by two additional complex eigenvalues in Eq. (6.7), seems to corroborate previous results on frequency tuning regulation properties due to adaptation [149, 35]. Our results are also reproduced by numerical simulations on a network of noisy LIF cells with an equivalent circuitry.

In the perspective of extending the current model, the use of topographic feedback connections would further increase the connection of our work to the electrosensory system. Although an inhibitory spatially diffuse feedback connection

does exist between higher nuclei and the sensory layer, other spatially organized feedback connections branch to the pyramidal cells with glutamatergic as well as gabaergic connections. The topographic feedback in fact brings in a true spatial dimension to the all-to-all connected model. These feedback connections would greatly influence the stability of the activity distributions, especially regarding the presence of spatio-temporal stimuli. Topographic feedback, along with adaptation currents, has been shown to influence the stability of activity patterns and the propagation of oscillations [84, 155]. We thus expect that this will also be the case in our model. It would also be of interest to test whether the dynamics illustrated here differ if ON cells feedback more predominantly to ON cells, and the same for OFF cells. This could lead to predictions about this feedback connectivity.

Further, experimental studies on the weakly electric fish have shown that adaptation time scales vary across the different sensory maps into which the ELL is divided [29]. Likewise, the receptive field size of pyramidal cells increases going from central to lateral positions. In this context, it would be interesting to determine how frequency tuning properties of these maps relate to the adaptation time scales when ON and OFF cells are present, and how this tuning depends on receptive field size and topographic feedback. Finally, ON and OFF cells may have different firing rates in the absence of input ($I(x,t) = 0$). This activity difference, when sufficiently strong, can influence the dynamics of recurrent ON/OFF in the absence of adaptation [111]. The role that it may play in the frequency tuning of cells and oscillation susceptibility of the network with adaptation thus remains to be investigated.

Chapter 7

Conclusion

7.1 Comments on Chapter 3

The results of this article constitutes the initial point of the broader analysis presented in subsequent chapters. In Chapter 3, we perform a steady state analysis where we show how static pulses may cause global oscillations to become stable via a Andronov-Hopf bifurcation. The main purpose of this article is to demonstrate that the analysis of a single inhibitory feedback loop was general enough to apply to other cases where additional recurrent connections, delayed or not, might be involved. As exposed by the physiology of the ELL, both GABA-ergic and glutamatergic connections project back to the pyramidal cell layer via the StF (see Figure 5.5.1), all with similar delays. While the inhibitory component is spatially diffuse, the excitatory part of the feedback is local. Further, lateral connections within the pyramidal cells are also involved. Results presented in [32], which are the prime motivation of this thesis, did not consider additional feedback pathways nor ON and OFF responses. The study of multiple feedback loops is of foremost importance, as it has been shown that combined recurrent terms are involed in cases of multistability and even chaotic dynamics in presence of time-varying signals [107].

Our analysis clearly demonstrates that the inclusion of additional feedback loops

will not qualitatively change the response properties with respect to external stimuli as long as the total lumped polarity of the delayed components is preserved. Further, we have shown that non-delayed excitatory connections reduce the oscillatory response threshold as the gain of such components is increased. The implications of such results with regard to electroreception are two-fold: 1. from the point of view of physiology, it is secure to consider only a single inhibitory feedback component, as we know that the behaviour of the system holds even for many loops; and 2. the lack of local connections in our model does not affect the generality of our result with respect to oscillatory transitions. These results were necessary to validate our approach, which focuses of the direct ELL-Pd pathway.

In the case of the ELL, as well as in most sensory pathways, multiple feedback loops are involved in the integration of sensory inputs. Further, these loops are oftentimes topographic. The effects of multiple delays and spatial topography of feedback in the ELL-Pd system have been exposed in regard to oscillatory responses [100], although in the context of stochastic inputs and for a single neural population. Multiple delays are also crucial in the stability of steady states in motor control subject to visual feedback [163]. More insight on the role of multiple feedback loops in ON/OFF systems would first require the consideration of non-identical delays. Spatially profiled projections would regulate the distribution of activity on the network, and potentially give rise to spatially localized solutions like bumps and fronts.

The inclusion of spatially dependent kernels is however not trivial. In the perspective of stability, the current all-to-all anatomy of our model allows a time and space separation for which the eigenmodes are spatially homogeneous. In most cases, the stability analysis of spatially structured connectivity problems requires the use of so-called Evans functions [89, 90, 133], which are generalized eigenvalue problems. Given the fact that most of the sensory pathways in the ELL are parallel and exhibit very few lateral connections [22], the kernel we

used were kept constant. We however hypothesize, on the basis of numerical experiments we performed, that feedback spatial profiles would result in spatial organization of activity, but would otherwise preserve the bifurcation scenario exposed here at least qualitatively.

7.2 Comments on Chapter 4

Chapter 4 constitutes the core of this thesis. On the basis of the results of Chapter 3, a wide palette of effects are exposed and a complete bifurcation analysis of our model is performed. A special attention is given to the role of asymmetrical spontaneous firing rate with respect to the behaviour of feedback and its subsequent impact on dynamics. Global oscillations triggered by static inputs are shown to be more prevalent in a ON/ON net compared to a ON/OFF net, although the later may respond to both positive and negative inputs. Input-induced rhythmic activity is also observed in a noisy and leaky Integrate-And-Fire net (LIF) where the firing rates fluctuate according to the prediction obtained with the neural field formulation. Much insight about the response properties of our model is obtained away from the Andronov-Hopf regime, where the feedback behaves linearly. For instance, the lateral response contrast of ON/OFF nets to static pulses has been shown to follow a non-monotonic relation with respect to the pulse's amplitude. According to this property, the system can switch between excitatory and inhibitory responses, as the lateral activity increases and then decreases according to higher stimulus amplitude. Here again, the result was also obtained for a LIF network. Localized pulses with sinusoidally modulated amplitudes cause a central-lateral response discrepancy, where the lateral sites respond at twice the input frequency.

Several issues raised in the discussion of Chapter 4 initiated the topics found in subsequent chapters. One of the main underlying topics of this article is the distinction between ON/OFF and ON/ON network configurations, with respect to

the integration of sensory inputs. This concern was raised by one the referees involved in the editorial process, and resulted in the analysis presented in Chapter 5. There, we study in detail the question of how ON/ON and ON/OFF networks compare with respect to sensory input responses. To do this, we determine how the Andronov-Hopf threshold (beyond which input-induced oscillations become stable) varies according to the model's parameters in each case, as well as how these models integrate fluctuating inputs in the fixed point regime.

The result published in [32] is supported by our findings on input induced Andronov-Hopf bifurcations, and are in line with other computational studies [97, 98, 99]. However, our analysis restricts to spatially contiguous static inputs, while [32] focused on a stochastic driving to generate spectral power near the gamma range. As a natural extension to our work, the use of stochastic inputs would further warrant the physiological relevance of the stimulus spatial and temporal profiles. Further, some recent results demonstrate how additive noise might trigger spatio-temporal organization of activity in neural field models with delayed feedback [12, 100, 73]. One of the major concerns about this type of inputs is the opposed responses of ON and OFF populations. While noisy inputs with non-zero mean might result in a behaviour similar to the one we describe for static pulses by sustaining recurrent signals, electrosensory inputs are typically modelled using zero mean random processes (see for instance [135]). Some of these issues were addressed in section 5.7, where we showed that increasing noise across the network can bring on an oscillatory state. The analysis of the situation where the increased spatial correlation of the noise sources also produces an oscillatory state remains to be explored numerically, giving a more definitive assessment of the mechanism underlying the genesis of oscillations seen in [32] .

It is not known if the feedback pathway from the pyramidal cell layer possesses a cellular-type profile. Are ON cells projecting back preferentially to ON cells via the Pd and/or EGp? What about OFF cells? A species-specific

feedback pathway would greatly influence the tendency of the system to enter states of oscillatory activity, by altering the balance between excitatory and inhibitory responses. Much insight about this particular setup could be obtained by analyzing the following system

$$(1 + a^{-1}\partial_t)u_{on}(x,t) = -\epsilon \int_\Omega f(u_{on}(y,t-\tau))dy$$

$$-(1-\epsilon)\int_\Omega f(u_{off}(y,t-\tau))dy + I(x,t)$$

$$(1 + a^{-1}\partial_t)u_{off}(x,t) = -(1-\epsilon)\int_\Omega f(u_{on}(y,t-\tau))dy$$

$$-\epsilon \int_\Omega f(u_{off}(y,t-\tau))dy + V_o - I(x,t)$$

where $\epsilon \in [0,1]$ is a crossing parameter determining the amount of ON (resp. OFF) cells projecting back to themselves via the delayed feedback loop. For $\epsilon = 1$, ON and OFF pathways are fully uncoupled, while we retrieve our initial model for $\epsilon = 0$. This analysis was left for future work.

The non-monotonic shape of the lateral response curve is responsible for transient excitatory responses of ON and OFF units at the onset and offset of static pulses. This behaviour is expected from ON and OFF cells, as they typically exhibit transient responses characterized by bursts of spikes at stimulus onset and offset. This behavior is usually a consequence of sensitivity to the voltage derivative, which is not incorporated in our model. We however argue that feedback generates a similar behaviour in ON/OFF systems, and thus that it might play a role in recorded data, when the cells evolve in recurrent network.

Time-periodic stimuli were studied far away from the Andronov-Hopf regime by choosing a small feedback delay. This is so because bifurcations might occur whenever the input amplitude increases. It becomes difficult then to separate Andronov-Hopf oscillations from the local drive and feedback echoes generated by the stimulus. We have nevetheless addressed this problem in Chapter 5,

where the sinusoidal stimuli has a small frequency. This problem, which arises naturally in the context of fluctuating systems, illustrates the challenge that the analysis of non-autonomous delay equations represents. It further supports the approach we have developped in Appendix A to analyze similar problems.

Another important result suggested by our analysis is the strong correlation between neural field and Integrate-And-Fire descriptions. While many studies have shed light on the close relationship between LIF and rate models [54, 57, 56, 58, 59, 60], the explicit mapping between neural field and spiking dynamics is not fully known. Our goal in comparing neural field to LIF is to show that both these popular network formulations produce the same qualitative behaviour with respect to our findings, and that the dynamics we found was a consequence of the network circuitry, and not of its formulation.

7.3 Comments on Chapter 5

This chapter addresses an important question: how is the dynamics of recurrent nets impacted by the presence of OFF cells? Chapter 3 and 4 have exposed a variety of dynamical effects caused by sensory stimuli. The focus of these chapters was to highlight network mechanisms by which sensory signals would influence the stability or structure of activity states, in presence of ON **and** OFF cells. The main purpose of Chapter 5 was to contextualize the results presented in the first two chapters, and try to elucidate the functional advantages gained by sensory systems exhibiting di-synaptic circuitry. The analysis performed shows that ON/OFF networks have unique input response properties. In the particular context of network oscillations, past results on the ELL [32, 33, 26] and on delayed feedback nets [98, 34, 135] relate to networks built solely of ON (or equivalently E-type) cells. In contrast, our model demonstrates that these findings occur even when both ON and OFF populations are involved. Furthermore, our populations do not possess the same baseline activity, an addition

that greatly influences the dynamics.

Openings offered by the results of this chapter are similar to the ones of Chapter 4 and 3, namely more realistic feedback projections from the EGp and the consideration of receptive fields effects. We however believe that the radically different response behavior between ON/ON and ON/OFF nets to stochastic signals (as opposed to deterministic and static ones) presented in Section 5.7 is a promising path. These results show that, in the context of Andronov-Hopf bifurcations induced by stochastic signals, ON/ON and ON/OFF nets are equivalent. Synchronous firing states are not prevalent in either network configurations, due to the statistical properties of the stimulus, which is a noisy process of zero mean. In [32, 33, 135, 34], only the spatial contiguity or correlation was involved in the stability of rhythmic states, not its amplitude. In contrast, our result show that differentiation in oscillatory behavior only occurs when the input has a non-zero mean, where the predictions made by the neural field model are supported by numerical simulations on an equivalent LIF network. These results on OFF cells point towards the consideration of non-zero mean inputs as valid sensory signals, and further illustrates that the encoding of electrosensory afferent signals performed by feedback and ON and OFF cells depends on both the spatial organization and mean amplitude (or mean in noisy contexts). As such, one could hypothesize that the input spatial organization could elicit synchrony, while the mean of the signal would both modulate the frequency of the oscillations and emphasize the ON versus OFF differentiation.

7.4 Comments on Chapter 6

With respect to positive stimuli, the dynamics discussed in the previous chapters consider feedback and inhibitory responses of OFF cells as the only sources of inhibition in the system. However, real neural systems exhibit a certain level of habituation to stimulation that has been shown to depend on the input spatial

distribution. This important feature of neural systems is thus likely to influence the response properties of sensory networks. In the prospect of reproducing the experimental recordings found in the literature (for instance [32, 27, 26, 33]), the inclusion of adaptation in our model is of prime physiological relevance. Chapter 6 presents the effects of intrinsic cellular adaptation on the oscillatory dynamics exposed in Chapters 3, 4 and 5. To do so, we included two additional state variables to our model in order represent the effect of adaptation on both ON and OFF cells. Additionally, parameters specifying the gain and time scale of this new inhibitory component were introduced. The goal of Chapter 6 is to determine how an adaptation alters the rhythmic responses identified and studied in previous chapters. To answer this question, we performed a complete bifurcation analysis of our system and we parameterized the Andronov-Hopf threshold in terms of the adaptation gain and rate.

Our model predicts that slow and strong adaptation makes oscillatory responses easier to achieve in ON/OFF nets by increasing the system sensitivity to inputs of small spatial extent. Further, in the case of sinusoidally modulated pulses of varying periods, adaptation also influences the resonance properties of the network by introducing new frequencies in the system.

An important question raised by the results of Chapter 6 is: are ON/ON and ON/OFF nets impacted equivalently by adaptation? Based on Chapter 3 results, one could hypothesize that adaptation may in fact emphasize the distinctiveness between ON/ON and ON/OFF systems with respect to oscillatory behavior. Slow adaptation currents are preferentially recruited by either static or slow stimuli that evolve on a similar time scale. This is made apparent by the shapes of the response curves shown in Fig. 6.7. In the context of our study, the static pulses used maximize the expression of adaptation, where its effect on the instability threshold may be understood directly from the steady states. However, past studies [34, 26, 33] have used stochastic inputs to reproduce the signal sent by the receptors to the pyramidal cells, not deterministic ones. These

signals typically fluctuate on much faster time scales than the sinusoidally modulated pulses we have considered in Section 6.4. A relatively slower adaptation current might thus not have the time to build up - the effect on the dynamics would then be less significant. This consideration will play a crucial role if one wants to incorporate adaptation to the dynamics explored in Section 5.7 where stochastic inputs drive both ON/ON and ON/OFF nets.

Appendix A

Non-autonomous center manifold reduction in a model of delayed feedback

The center manifold theorem has proven to be tool of choice in the analysis of non-linear dynamical systems. In particular, it has been applied in the past decades to various delayed models [105, 164, 165, 166, 167], where it provides an accurate description of system dynamics in the vicinity of non-hyperbolic fixed points. This theorem guarantees that one can find a simplified reduced form of the full dynamics of the system in the vicinity of a bifurcation point. This so-called normal form provides a description of the different kinds of solutions available to the system as the parameter moves in parameter space around the bifurcation, i.e. it enables an "unfolding" of the dynamics around this point. The procedure to compute this normal form is technically very involved for delay-differential equations.

Non-linear delay-differential equations (DDEs) have also been used in a variety of contexts where the state variables are driven by an additive time-dependent force. The question whether the center manifold theorem may be extended to

these non-autonomous delayed problems is currently unanswered. They are indications that center manifolds do exist in infinite dimensional non-autonomous dynamical systems [168]. Furthermore, stochastic center manifold theory has been established in non-delayed systems [169], and a similar approach has been used in the numerical analysis of non-linear ODEs, subject to time-dependent forcing, providing an accurate description of dynamics[170]. Nevertheless, it is still unclear how to apply and compute center manifolds in the specific case of non-autonomous delayed systems. A solution to this problem would greatly enhance the possibilities of theoretical analysis of delayed systems, of particular relevance in mathematical neuroscience. The aim of this Appendix is not to detail the approach and subsequent calculations performed in the development of our method. We will overview the main idea underlying non-autonomous center manifolds reduction that we present in this preprint: [171].

Many studies use center manifolds to analyse delayed system [165, 164, 172, 173, 174], while the fundamental steps and working details are rarely addressed nor discussed. Further, some use computerized algorithms to generate their result. In contrast, more specialized works do address the technical details [175, 176], although not in the context of non-autonomous equations. Given the current state of the literature, we wrote a practical review of the center manifold reduction procedure for non-linear DDEs. This was done in the spirit of making the approach more accessible to an audience with a physics and applied mathematics background.

The main goal is to adapt the center manifold theorem to unstable non-autonomous systems, in order to allow the computation of the mapping that exists between stable and unstable modes. The center manifold theorem was not validated in the context of time-dependent DDEs. The major dilemma lies in the apparent non-existence of a fixed point and eigenbases of the linear problem. Motivated by the results on stochastic systems [169], as well as on numerical results concerning driven ODEs [170], we apply the center manifold theorem to our model,

considering the additive input as a non-linearity acting on a fast time scale. We justify this step by a recent work [168], where the center manifold theorem for weak solutions of non-autonomous abstract ODEs on infinite-dimensional spaces is proven, given that certain spectral gap conditions are satisfied. Non-autonomous forcing results in a time-dependent corrective term, added to the center manifold equation of the autonomous problem.

Our result has been tested numerically to approximate the dynamics near a transcritical bifurcation. We compare the time series of the original driven DDE to the dynamics of the order parameter equation (related to the aforementioned normal form), which dictates the behavior of the flow on the unstable subspace, and find good agreement. We were able to compare the benefits of higher order expansions as well as time-dependent corrections with respect to the precision of the center manifold reduction. This result will eventually be used to investigate the behavior of neural fields models with delays and time-dependent input.

Bibliography

[1] A. Hutt and F. Atay. Analysis of nonlocal neural fields for both general and gamma-distributed connectivities. *Physica D*, 203:30–54, 2005.

[2] A. Roxin et al. The role of delays in shaping spatio-temporal dynamics of neuronal activity in large networks. *Phys. Rev. Lett.*, **94**, 238103 (2005).

[3] Kukjin Kang, Michael Shelley, and Haim Sompolinsky. Mexican hats and pinwheels in visual cortex. *Proc. Natl. Acad. Sci. USA*, 100:2848–2853, 2003.

[4] B. Ermentrout et al. The effects of spike frequency adaptation and negative feedback on the synchronization of neural oscillators. *Neural Comput.*, 13:1285–1310, 2001.

[5] H. Sompolinsky et al. Global processing of visual stimuli in a neural network of coupled oscillators. *Proc. Natl. Acad. Sci. USA*, 87:7200–7204, 1990.

[6] M. Van den Heuvel et al. Delayed visual feedback reveals distinct time scales in balance control. *Neurosci. Lett.*, 452:37–41, 2009.

[7] L. G. Ungerleider, S.M. Courtney, and J. V. Haxby. A neural system for human visual working memory. *Proc. Natl. Acad. Sci. USA*, 95:883–890, 1998.

[8] Aijun Zhou et al. *ISNN 2009: Advances in Neural Networks*, chapter Memory State Feedback Stabilization for Time-Varying Delayed Neural Networks Systems. Springer Berlin / Heidelberg, 2009.

[9] L. Schwabe et al. The role of feedback in shaping the extra-classical receptive field of cortical neurons: A recurrent network model. *J. Neurosci.*, 26:9117–9129, 2006.

[10] J. Bechhoefer. Feedback for physicists: A tutorial essay on control. *Rev. Mod. Phys.*, 77, 2005.

[11] C.R. Laing and A. Longtin. Noise-induced stabilization of bumps in systems with long-range spatial coupling. *Physica D*, 160:149–172, 2001.

[12] A. Hutt, A. Longtin, and L. Schimansky-Geier. Additive global noise delays turing bifurcations. *Phys. Rev. Lett.*, 98(230601), 2007.

[13] A. Hutt, A. Longtin, and L. Schimansky-Geier. Additive noise-induced turing transitions in spatial systems with applications to neural fields and wsift-hohenberg equations. *Physica D*, 237:755–773, 2008.

[14] J. de la Rocha et al. Correlation between neural spike trains increases with firing rate. *Nature*, 448:802–806, 2007.

[15] A. Longtin. Stochastic resonance in neuron models. . *J. Stat. Phys.*, 70:309–327, 1993.

[16] A. Longtin. *Scholarpedia: Neuronal Noise.* online access.

[17] A.V.Holden. *Models of the stochastic activity of neuronsfv*, volume 12 of *Lecture notes in Biomathematics* Springer, Berlin, 1976.

[18] H.C. Tuckwell. *Introduction to theoretic neurobiology.* Cambridge University Press, Cambridge, 1988.

[19] N. Fourcaud-Trocmé, D. Hansel, C. van Vreeswijk, and N. Brunel. How spike generation mechanisms determine the neuronal response to fluctuating inputs. *J. Neurosci* , 17:11628–11640, 2003.

[20] W. Heiligenberg. *Neural Nets in Electric Fish.* MIT Press, 1991.

[21] J. Bastian and W. Heiligenberg. Phase-sensitive midbrain neurons in eigenmannia: neural correlates of the jamming avoidance response. *Science*, 209:828–831, 1980.

[22] N.J. Berman and L. Maler. Neural architecture of the electrosensory lateral line lobe: adaptations for coincidence detection, a sensory searchlight and frequency-dependent adaptive filtering. *J. exp. Biol.*, **202**, 1243 (1999).

[23] L. Maler. Receptive field organization across multiple electrosensory maps. ii. computational analysis of the effects of receptive field size on prey localization. *J. Comp. Neurol.*, 516:394–422, 2009.

[24] L. Maler et al. An atlas of the brain of the electric fish apteronotus leptorhynchus. *J. Chem. Neuroanat.*, 4:1–38, 1991.

[25] J.E. Lewis and L. Maler. Neuronal population codes and the perception of object distance in electric fish. *J Neurosci.*, 21:2842–2850, 2001.

[26] M. Chacron et al. Feedback and feedforward control of frequency tuning to naturalistic stimuli. *J. Neurosci.*, 25:5521–5532, 2005.

[27] J. Bastian et al. Receptive field organization determines pyramidal cell stimulus-encoding capability and spatial stimulus selectivity. *J. Neurosci.*, 22:4577–4590, 2002.

[28] J. Lewis et al. Control of neuronal firing by dynamic parallel fiber feedback: implications for electrosensory reafference suppression. *J. Exp. Biol.*, 210:4427–4437, 2007.

[29] R. Krahe et al. Temporal processing across multiple topographic maps in the electrosensory system. *J Neurophysiol*, 100:852–867, 2008.

[30] G. Marín, J. Mpodozisand E Sentis, T. Ossandón, and J.C.Letelier. scillatory bursts in the optic tectum of birds represent re-entrant signals from the nucleus isthmi pars parvocellularis. *J. Neurosci.*, (25):7081–7089, 2005.

[31] S.F. Brandt and R. Wessel. Winner-take-all selection in a neural system with delayed feedback. *J. Neurosci.*, 97:221–228, 2007.

[32] B. Doiron et al. Inhibitory feedback required for network oscillatory response to communication but not prey stimuli. *Nature*, **421**, 539 (2003).

[33] B. Doiron et al. Oscillatory activity in electrosensory neurons increases with the spatial correlation of the stochastic input stimulus. *Phys. Rev. Lett.*, **93**, 4 (2004).

[34] B. Lindner et al. Theory of oscillatory firing induced by spatially correlated noise and delayed inhibitory feedback. *Phys. Rev. E*, **72**, 061919 2005.

[35] W. H. Mehaffey et al. Intrinsic frequency tuning in ell pyramidal cells varies across electrosensory maps. *J. Neurophysiol.*, 99:2641–2655, 2008.

[36] S. Crook et al. Spike-frequency adaptation affects the synchronization properties of cortical oscillators. *Neural. Comput.*, 10:837–854, 1998.

[37] B. Ermentrout et al. The effects of spike frequency adaptation and negative feedback on the synchronization of neural oscillators. *Neural Comput.*, 13:1285–1310, 2001.

[38] C. ven Vreeswijk and D. Hansel. Patterns of synchrony in neural networks with spike adaptation. *Neural Comput.*, 13:959–992, 2001.

[39] J. Benda et al. Spike-frequency adaptation separates transient communication signals from background oscillations. *J. Neurosci.*, 25:2312–2321, 2005.

[40] A. Hutt. Sleep and anesthesia. *Frontiers Neurosci.*, 3(3):408–409, 2009.

[41] A. Compte et al. Synaptic mechanisms and network dynamics underlying spatial working memory in a cortical network model. *Cerebral Cortex*, 10:910–923, 2000.

[42] C.R. Laing et al. Multiple bumps in a neuronal model of working memory. *SIAM J. Appl. Math.*, 63:62-97, 2002.

[43] P.C. Bressloff et al. What geometric visual hallucinations tell us about the visual cortex. *Neural Comput.*, 14:473–491, 2002.

[44] D. Pinto and B. Ermentrout. Spatially structured activity in synaptically coupled neuronal networks: I-ii. *I-II, SIAM J. Appl Math.*, **62**, 206;243 (2001).

[45] P. Dayan and L.F. Abbott. *Theoretical Neuroscience: Computational and Mathematical Modeling of Neural Systems.* MIT Press, 2001.

[46] E.M. Izhikevich. *Dynamical Systems in Neuroscience: The Geometry of Excitability and Bursting.* MIT Press, 2007.

[47] E.R. Kandel and J.H. Schwarz. *Principles of Neural Science.* Elsevier, New York, (1983).

[48] C. Koch. *Biophysics of Computation: Information Processing in SIngle Neurons.* Oxford University Press, 1999.

[49] J. Feng, editor. *Computational Neuroscience: a Comprehensive Approach.* Chapman & Hall/CRC, 2004.

[50] T. Sejnowski et al. Computational neuroscience. *Science*, 241:1299–1309, 1988.

[51] N. Brunel and M.C.W. van Rossum. Lapicque s 1907 paper: from frogs to integrate-and-fire. *Biol. Cybern.*, 97:337–339, 2007.

[52] A. Hodgkin and A. Huxley. A quantitative description of membrane current and its application to conduction and excitation in nerve. *J. Physiol.*, 117:500–544, 1952.

[53] N. T. Carnevale and M. L. Hines. *The NEURON book.* Cambridge University Press, 2006.

[54] P. C. Bressloff and S. Coombes. Dynamics of strongly coupled spiking neurons. *Neural Comput.*, 12:91–129, 2000.

[55] W. Gerstner and W. K. Kistler. *Spiking Neuron Models.* Cambridge University Press, Cambridge, UK, 2002.

[56] N. Masuda and K. Aihara. Bridging rate coding and temporal spike coding by effect of noise. *Phys. Rev. Lett.*, 88(24):248101, May 2002.

[57] D. Cremers and A.V.M. HerzS. Traveling waves of excitation in neural field models: Equivalence of rate descriptions and integrate-and-fire dynamics. *Neural Comput.*, 14:1651–1667, 2002.

[58] O. Shriki et al. Rate models for conductance-based cortical neuronal networks. *Neural Comput.*, 15:1809–1841, 2003.

[59] Y. Aviel and W. Gerstner. From spiking neurons to rate models: A cascade model as an approximation to spiking neuron models with refractoriness. *Phys. Rev. E*, 73:051908, 2006.

[60] Gustavo Deco, Viktor K. Jirsa, Peter A. Robinson, Michael Breakspear, and Karl Friston. The dynamic brain: From spiking neurons to neural masses and cortical fields. *PLoS Comput Biol*, 4:e1000092, 2008.

[61] W.S. McCulloch and W. Pitts. A logical calculus of the ideas immanent in nervous activity. *Bull. Math. Biophys*, 5.115–133, 1943.

[62] F. Rosenblatt. The perceptron: A probabilistic model for information storage and organization in the brain. *Psychological Review*, 65:386–408, 1958.

[63] D.O. Hebb. *The organization of behavior.* Wiley, New York, 1949.

[64] J.-J Hopfield. Neural networks and physical systems with emergent collective computational abilities. *Proc. Natl. Acad. Sci. USA*, 79:2554–2558, 1982.

[65] J. Cowan. Discussion: Mcculluch-pitts and related neural nets from 1943 to1989. *Bull. Math. Biol.*, 52:73–97, 1990.

[66] G. Leuba and L. J. Garey. Comparison of neuronal and glial numerical density in primary and secondary visual cortex of man. *Experimental Brain Research*, 77:31–38, 1989.

[67] W. J. Freeman. *Mass Action in the Nervous System.* Academic Press., 1975.

[68] V. K. Jirsa. Neural field dynamics with local and global connectivity and time delay. *Philos. Trans. Roy. Soc. London Ser. A*, 367:1131–1143, 2009.

[69] H.R. Wilson and J.D. Cowan. Excitatory and inhibitory interactions in localized populations of model neurons. *Biophys. J.*, **12**:1–24, (1972).

[70] H.R. Wilson and J.D. Cowan. A mathematical theory of the functional dynamics of cortical and thalamic nervous tissue. *Kybernetic*, **13**:55–80, (1973).

[71] S. Amari. Dynamics of pattern formation in lateral-inhibition type neural fields. *Biol. Cybern.*, 1977.

[72] P.C. Bressloff and S. Coombes. Physics of the extended neuron. *Int. J. Mod. Phys. B*, 11:2343–2392, 1997.

[73] A. Hutt. Additive noise may change the stability of non-linear systems. *Europhys. Lett.*, 84:1–4, 2008.

[74] S. Coombes. Waves and bumps in neural field theories. *Biol. Cybern.*, 93:91–108, 2005.

[75] S. Coombes. *Scholarpedia: Neural fields.* online access.

[76] B. Ermentrout. Neural networks as spatio-temporal pattern-forming systems. *Rep. Prog. Phys.*, 61:353–430, 1998.

[77] A. Hutt et al. Pattern formation in intracortical neuronal fields *Network: Comput. Neural Syst* , 14:351–368, 2003.

[78] V. K. Jirsa. Connectivity and dynamics of neural information processing. *Neuroinformatics*, pages 183–204, 2004.

[79] S. E. Folias and P. C. Bressloff. Breathing pulses in an excitatory neural network. *SIAM J. Appl. Dyn.. Sys.*, 3, 2004.

[80] S.E. Folias and P. Bressloff. Stimulus-locked waves and breathers in an excitatory neural network. *SIAM J. Appl. Math.*, **65**, 2067 (2005).

[81] S. Coombes et al. Waves and bumps in neuronal networks with axo-dendritic synaptic interactions. *Physica D*, 178:219–241, 2003.

[82] S. Coombes et al. Waves and bumps in neuronal networks with axo-dendritic synaptic interactions. *Physica D*, 78:219–241, 2003.

[83] C. Laing et al. Coarse-grained dynamics of an activity bump in a neural field model. *Nonlinearity*, 20:2127–2146, 2007.

[84] S.E. Folias and P. Bressloff. Breathers in two-dimensional neural media. *Phys. Rev. Lett.*, 95:208107, 2005.

[85] C. Laing and S. Coombes. The importance of different timings of excitatory and inhibitory pathways in neural field models. *Network*, **17**, 151 (2006).

[86] P. Bressloff et al. Oscillatory waves in inhomogeneous neural media. *Phys. Rev. Lett.*, **91**, 178101 (2003)

[87] D. Golomb et G.B. Ermentrout. Bistability in pulse propagation in networks of excitatory and inhibitory populations. *Phys. Rev. Lett.*, **86**, 4179 (2001).

[88] P. Blomquist et al. Localized activity patterns in two-population neuronal networks. *Physica D*, **206**, 180 (2005).

[89] S. Coombes and M.R. Owen. Evans functions for integral neural field equations with heaviside firing rate function. *SIAM J. Appl. Dyn. Sys.*, 34:574–600, 2004.

[90] B. Sandstede. Evans functions and nonlinear stability of travelling waves in neuronal network models. *Internat. J. Bifur. Chaos Appl. Sci. Engrg*, 17:2693–2704, 2007.

[91] E. Kolb, E. Fernandez, and R. Nelson. *http://webvision.med.utah.edu/*. University of Utah, online access. also available the Library of Medicines Bookshelf at the National Institutes of Health http://web.ncbi.nlm.nih.gov/books/bv.fcgi?rid=webvision.

[92] E. Harvey-Girard. *www.apteronote.com*. online access.

[93] M. S. Landy and J. A. Movshon. *Computational Models of Visual Processing*. MIT Press, 1991.

[94] G. Mileva et al. In vitro studies of closed-loop feedback and electrosensory processing in apteronotus leptorhynchus. *J Physiol Paris*, 102:173–180, 2008.

[95] A.K. Engel et al. Temporal coding in the visual cortex: new vistas on integration in the nervous system. *Trends Neurosci.*, 15:218–226, 1992.

[96] D.L. Wang. Selection based on oscillatory correlation. *Neur. Net.*, **12**, 579 (1999).

[97] C. Borgers and N. Kopell. Synchronization in networks of excitatory and inhibitory neurons with sparse, random connectivity. *Neural Comput.*, 15:509–538, 2003.

[98] C. Borgers et al. Gamma oscillations mediate stimulus competition and attentional selection in a cortical network model. *Proc Nat. Acad. Sci. (USA)*, **105**, 18023 (2008).

[99] D. Marinazzo et al. Input-driven oscillations in networks with excitatory and inhibitory neurons with dynamic synapses. *Neural Comput.*, 19:1739–1765, 2007.

[100] A. Hutt et al. Driving neural oscillations with correlated spatial inputs and topographic feedback. *Phys. Rev. E*, 78:021911, 2008.

[101] J. Guckenheimer and P. Holmes. *This bifurcation involves the loss of stability of a fixed point and the appearance of two new stable fixed points symmetrically on each side of it.* Spinger-Verlag, 1983.

[102] C.M. Gray and W. Singer. Stimulus-specific neuronal oscillations in orientation columns of cat visual cortex. *Proc. Natl. Acad. Sci. USA*, 86:1698–1702, 1989.

[103] D. Lumer et al. Neural dynamics in a model of the thalamocortical system. i. layers, loops and the emergence of fast synchronous rhythms. *Cerebral Cortex*, **7**, 207 (1997).

[104] A.V. Galazyuk and A.S. Feng. Oscillation may play a role in time domain central auditory processing. *J. Neurosci.*, 21:147:1–5, 2001.

[105] S.A. Campbell et al. Limit cycles, tori and complex dynamics in a second-order differential equation with delayed negative feedback. *J. Dyn. Diff. Eq.*, **7**, 213 (1995).

[106] M. Dhamala et al. Enhancement of neural synchrony by time delay. *Phys. Rev. Lett.*, **92**, 074104 (2004).

[107] C.R. Laing and A. Longtin. Dynamics of deterministic and stochastic paired excitatory– inhibitory delayed feedback. *Neural Comput.*, 15:2779 –2822, 2003.

[108] R. Hahnloser et al. Feedback interactions between neuronal pointers and maps for attentional processing. *Nature Neuroscience*, 2:746 – 752, 1999.

[109] H L. Fields et al. Dorsal horn projection targets of on and off cells in the rostral ventromedial medulla. *J. Neurophysiol.*, **74**, 1742 - 59 (1995).

[110] D.A. Robin and F.L. Royer. Auditory temporal processing: Two-tone flutter fusion and a model of temporal integration. *J. Acoust. Soc. Am.*, **82**, 1207 (1987).

[111] J. Lefebvre, André Longtin, and V.G. LeBlanc. Dynamics of driven recurrent networks of on and off cells. *Phys. Rev. E*, 80:041912, 2009.

[112] U. Meyer et al. Distributed delays stabilize neural feedback systems. *Biol Cybern.*, **99**, 79-87 2008.

[113] V.M. Eguiluz et al. Scale-free brain functional networks. *Phys. Rev. Lett.*, **94**, 018102 (2005).

[114] M.N. Artyomov et al. Purely stochastic binary decisions in cell signaling models without underlying deterministic bistabilities. *Proc. Nat. Acad. Sci. (USA)*, **104**, 18958 2007.

[115] B. Vladimirski et al. Episodic activity in a heterogeneous network, from spiking neurons to mean field. *J. Comput. Neurosci.*, **25**, 39 (2008).

[116] F. Gabbiani. Coding of time-varying signals in spike trains of linear and half-wave rectifying neurons. *Net. Comput. Neural Syst.*, **7**, 61 (1996).

[117] J.U. Ramcharitar et al. Global electrosensory oscillations enhance directional responses of midbrain neurons in eigenmannia. *J. Neurophysiol.*, **96**, 2319-26 2008.

[118] *L. Maler, personal communication.*

[119] N. Brunel and V. Hakim. Fast global oscillations in networks of integrate-and-fire neurons with low firing rates. *Neural Comp.*, **11**, 1621-1671 1999.

[120] N. Brunel and X.-J. Wang. What determines the frequency of fast network oscillations with irregular neural discharges? *J. Neurophysiol.*, **90**, 415-430 2003.

[121] S.M. Crook et al. The role of axonal delay in the synchronization of networks of coupled cortical oscillators. *J-Comput-Neurosci.*, 4:161–172, 1997.

[122] G.B. Ermentrout and N. Kopell. Fine structure of neural spiking and synchronization in the presence of conduction delays. *Proc. Natl. Acad.Sci. USA.*, 95:1259–1264, 1998.

[123] J. Foss et al. Multistability and delayed recurrent loops. *Phys. Rev Lett.*, 76:708–711, 1996.

[124] T. Gollisch and M. Meister. Modeling convergent on and off pathways in the early visual system. *Biol. Cybern.*, 99:263–278, 2008.

[125] F.R. Amthor et al. Morphologies of rabbit retinal ganglion cells with concentric receptive fields a-b. *J. Comp. Neurol.*, 280:72–121, 1989.

[126] M.H. Hennig et al. The influence of different retinal subcircuits on the nonlinearity of ganglion cell behavior. *J. Neurosci.*, 22:8726–8738, 2002.

[127] J.B. Demb et al. Functional circuitry of the retinal ganglion cell's nonlinear receptive field. *The Journal of Neuroscience*, 19:9756–9767, 1999.

[128] J. Lefebvre, A. Longtin, and V. G. Leblanc. Oscillatory response in a sensory network of ON and OFF cells with instantaneous and delayed recurrent connections. *Philos. Trans. Roy. Soc. London Ser. A*, 368:455–467, 2010.

[129] B. Scholl et al. Nonoverlapping sets of synapses drive on responses and off responses in auditory cortex. *Neuron*, 65:412–421, 2010.

[130] T. Erneux. *Applied Delay Differential Equations.* Surveys and Tutorials in the Applied Mathematical Sciences. Springer, 2009.

[131] N. Masuda et al. Coding of temporally varying signals in networks of spiking neurons with global delayed feedback. *Neural Comput.*, 10:2139–75, 2005.

[132] Z.P. Kilpatrick and P. Bressloff. Effects of synaptic depression and adaptation on spatiotemporal dynamics of an excitatory neuronal network. *Physica D*, 2009. in press.

[133] S. Coombes and M.R. Owen. Bumps, breathers, and waves in a neural network with spike frequency adaptation. *Phys. Rev. Lett.*, 94:148102, 2005.

[134] J. Gao et al. An oscillatory circuit underlying the detection of disruptions in temporally-periodic patterns. *Network*, 20:106–135, 2009.

[135] M. Chacron et al. Delayed excitatory and inhibitory feedback shape neural information transmission. *Phys. Rev. E*, **72**, 051917 2005.

[136] B. Lindner and A. Longtin. Comment on: "characterization of subthreshold voltage fluctuations in neuronal membranes" by m. rudolph and a. destexhe. *Neural Comput.*, 18:1896–1931, 2006.

[137] J. Benda et al. Spike-frequency adaptation: Phenomenological model and experimental tests. *Neurocomputing*, 38-40:105–110., 2001.

[138] K.J. Kim and F. Rieke. Temporal contrast adaptation in the input and output signals of salamander retinal ganglion cells. *J. Neurosci.*, 21:287–299, 2001.

[139] X.J. Wang, Y. Liu, M.V. Sanchez-Vives, and D.A. McCormick. Adaptation and temporal decorrelation by single neurons in the primary visual cortex. *J. Neurophysiol.*, 89:3279–3293, 2003.

[140] T. Gollisch and A.V.M. Herz. Input-driven components of spike-frequency adaptationcan be unmasked in vivo. *J. Neurosci.*, 24:7435–7444, 2004.

[141] F. Gabbiani and H.G. Krapp. Spike-frequency adaptation and intrinsic properties of an identified, looming-sensitive neuron. *J. Neurophysiol.*, 96:2951–2962, 2006.

[142] E. Sobel and D.W. Tank. In vivo ca2+ dynamics in a cricket auditory neuron: an example of chemical computation. *Science*, 263:823–826, 1994.

[143] Prescott S.A. et al. Nonlinear interaction between shunting and adaptation controls a switch between integration and coincidence detection in pyramidal neurons. *J. Neurosci.*, 26:9084–9097, 2006.

[144] S. A. Prescott and T.J. Sejnowski. Spike-rate coding and spike-time coding are affected oppositely by different adaptation mechanisms. *J. Neurosci.*, 28:13649–13661, 2008.

[145] J.F. Storm. Potassium currents in hippocampal pyramidal cells. *Prog Brain Res*, 83:161–187, 1990.

[146] P. Sah and P. Davies. Calcium-activated potassium currents in mammalian neurons. *Clin Exp Pharmacol Physiol*, 27:657–663, 2000.

[147] K.J. Kim and F. Rieke. Slow na+ inactivation and variance adaptation in salamander retinal ganglion cells. *J. Neurosci.*, 23:1506–1516, 2003.

[148] Y.H. Liu and X.J. Wang. Spike-frequency adaptation of a generalized leaky integrate-and-fire model neuron. *J. Comput. Neurosci.*, 10:25–45, 2001.

[149] J. Benda and A. Herz. A universal model for spike-frequency adaptation. *Neural Comput.*, 15:2523–2564, 2003.

[150] Z. Xu, J.R. Payne, and M.E. Nelson. Logarythmic time course of sensory adaptation in electrosensory afferent nerve fibers in a weakly electric fish. *J. Neurophysiol* , 76:2020–2032, 1996.

[151] J. Benda, A. Longtin, and L. Maler. A synchronization-desynchronization code for natural communication signals. *Neuron*, 52:347–358, 2006.

[152] W.B. Mathieson and L. Maler. Morphological and electrophysiological properties of a novel in vitro preparation: the electrosensory lateral line lobe brain slice. *J Comp Physiol A.*, 163:489–506, 1988.

[153] *Dr. Len Maler, personal communication.*

[154] R. Curtu and B. Ermentrout. Pattern formation in a network of excitatory and inhibitory cells with adaptation. *SIAM J. Appl. Dyn. Sys.*, 3:191–231, 2004.

[155] Z. P. Kilpatrick and P. C. Bressloff. Effects of synaptic depression and adaptation on spatiotemporal dynamics of an excitatory neuronal network. *Physica D*, 239:547–560, 2010.

[156] Q. Pauluis, S.N. Baker, and E. Olivier. Emergent oscillations in a realistic network: The role of inhibition and the effect of the spatiotemporal distribution of the input. *J. Computat. Neurosci.*, 6:27–48, 1999.

[157] Q. Pauluis. Statistical signs of common inhibitory feedback with delay. *Neural Comput.*, 12:2513–2518, 2000.

[158] S.F. Brandt and R. Wessel. Winner-take-all selection in a neural system with delayed feedback. *Biol. Cybern.*, 97:221–228, 2007.

[159] N.J. Berman and L. Maler. *J Neurophysiol*, 80:3214–3232, 1998.

[160] Z. Liang and M.A. Freed. The on pathway rectifies the off pathway of the mammalian retina. *J. Neurosci.*, 30:5533–5543, 2010.

[161] J. Benda, L. Maler, and A. Longtin. Linear versus nonlinear signal transmission in integrate-and-fire models with adaptation currents or dynamic thresholds. *J. Neurophysiol.*, 2010. In Press.

[162] C. Ly and G.B. Ermentrout. Analysis of recurrent networks of pulse-coupled noisy neural oscillators. *SIAM J. Applied Dynamical Systems*, 9:113–137, 2010.

[163] J. Boulet, R. Balasubramaniam, A. Daffertshofer, and A. Longtin. Stochastic two delay-differential model of delayed visual feedback effects on postural dynamics. *Phil. Trans. Royal Soc. A*, 2009. in press

[164] S.-A. Campbell and J. Belair. Analytical and symbolically-assisted investigations of hopf bifurcations in delay-differential equations. *Canad. Appl. Math. Quart.*, 3:137–154, 1995.

[165] B. Redmond, V.G. LeBlanc, and A . Longtin. Bifurcation analysis of a class of first-order nonlinear delay-differential equations with reflectional symmetry. *Physica D*, 166:131–146, 2002.

[166] T. Faria and L. T. Magalhaes. Normal forms for retarded functional differential equations with parameters and applications to hopf bifurcation. *J. Differential Equations*, 122:281, 1995.

[167] M. Schanz and A. Pelster. Synergetic system analysis for the delay-induced hopf bifurcation in the wright equation. *SIAM J. Appl. Dyn. Sys.*, 2(3):277–296, 2003.

[168] C. Chicone and Y. Latushkin. Center manifolds for infinite dimensional nonautonomous differential equations. *J.Differential Equations*, 141:356–399, 1997.

[169] P. Boxler. A stochastic version of center manifold theory. *Probab. Theory Relat. Fields*, 83:509, 1989.

[170] S.M. Cox and A.J. Roberts. Center manifolds of forced dynamical systems. *J. Austral. Math. Soc. Ser. B*, 32:401–436, 1991.

[171] J. Lefebvre, A. Hutt, A. Longtin, and V.G. LeBlanc. Non-autonomous center manifold reduction in a model of delayed feedback. 2009.

[172] J.C. Li and C.H. Hansen. Forced phase-locked response of a nonlinear system with time delay after hopf bifurcation. *Chaos, Solitons and Fractals*, 25:461–473, 2005.

[173] X.-P. Yan and W.-T. Li. Hopf bifurcation and global periodic solutions in a delayed predator-prey system. *Appl. Math. Comput.*, 177:427–445, 2006.

[174] G. Orosz. Hopf bifurcation calculations in delayed systems. *Periodica Polytechnica Ser. mech. Eng.*, 48(2):198–200, 2004.

[175] S.-A. Campbell. *Delay Differential Equations: Recent Advances and New Directions*, chapter Calculating Center Manifolds for Delay Differential Equations Using Maple. Spinger-Verlag, New York, 2008.

[176] W. Wischert, A Wunderlin, and A. Pelster. Delay-induced instabilities in nonlinear feedback systems. *Phys. Rev. E*, 49(1), 1994.

[177] B. Mensour and A. Longtin. Synchronization of delay-differential equations with applications to private communication. *Phys. Rev. A*, 244:59–70, 1998.

[178] S. Wiggins. *Introduction to Applied Nonlinear Dynamical Systems and Chaos.* Springer-Verlag, 1990.

[179] D.K. Arrowsmith and C.M. Place. *An introduction to Dynamical Systems.* Cambridge University Press, 1990.

[180] S.H. Strogatz. *Nonlinear dynamics and chaos.* Addison Wesley, 1994.

[181] A. Amann, E. Schoell, and W. Just. Some basic remarks on eigenmode expansions of time-delay dynamics. *Physica A*, 373:191–202, 2007.

[182] F.M. Asl and A.G. Ulsoy. Analysis of a system of linear delay differential equations. *Journal of Dynamic Systems, Measurement, and Control*, 125, 2003.

[183] R. Bellmann and K.L. Cooke. *Differential-Difference Equations.* Academic Press, New York, 1963.

[184] T. D. Frank and P. J. Beek. Stationary solutions of linear stochastic delay differential equations: Applications to biological systems. *Phys. Rev. E*, 64:021917, 2001.

[185] S. Guillouzic, I. L'Heureux, and A. Longtin. Small delay approximation of stochastic delay differential equation. *Phys. Rev. E*, 59(4):3970, 1999.

[186] J.K. Hale and S.M.V. Lunel. *Introduction to functional differential equations.* Springer, Berlin, 1993.

[187] N. Yeganefar, P. Pepe, and M. Dambrine. Input-to-state stability of time-delay systems : A link with exponential stability. *IEEE Trans. Automat. Control*, 53:1526–1531, 2008.

[188] J. Xu and K.W. Chung. Effects of time delayed position feedback on a van der pol-duffing oscillator. *Physica D*, 180:17–39, 2003.

[189] J. Carr. *Applications of Center Manifold Theory.* Applied Mathematical Sciences 35. Springer verlag, New York, 1981.

[190] O. Arino, M.L. Hbid, and E. Ait Dads. *Delay Differential Equations and Applications.* NATO science series. Springer Verlag, 1999.

[191] J. Guckenheimer and P. Holmes. *Nonlinear Oscillations, Dynamical Systems and Bifurcation of Vector Fields.* Applied Mathematical Sciences 42. Spinger Verlag, 1983.

[192] R. Quesmi, M. Ait Babram, and M.L. Hbid. A maple program for computing a terms of a center manifold, and element of bifurcations for a class of retarded functional differential equations with hopf singularity. *Appl. Math. Comput.*, 175:932–968, 2006.

[193] R. Quesmi, M. Ait Babram, and M.L. Hbid. Center manifolds and normal forms for a class of retarded functional differential equations with parameter associated with fold-hopf singularity. *Appl. Math. Comput.*, 181:220–246, 2006.

[194] H. Haken. *Synergetics - An Introduction.* Springer, third and enlarged edition edition, 1983.

[195] N. MacDonald. *Biological Delay Systems: Linear Stability Theory.* ambridge Studies in Mathematical Biology Vol.8. Cambridge University Press, Cambridge, UK, 1989.

[196] L. Glass, A. Beuter, and D. Larocque. Time delays, oscillations, and chaos in physiological control systems. *Math. Biosci.*, 90:111, 1988.

[197] C.W. Eurich and J.G. Milton. Noise-induced transitions in human postural sway. *Phys. Rev. E*, 54:6681–6684, 1996.

[198] M.C. Mackey and L. Glass. Oscillation and chaos in physiological control systems. *Science*, 197:287–289, 1977.

[199] A. Longtin and J.G. Milton. Modelling autonomous oscillations in the human pupil light reflex using nonlinear delay-differential equations. *Bull. Math. Biol.*, 51:605–624, 1989.

[200] J. Bélair, S.A. Campbell, and P. van den Driessche. Frustration, stability and delay-induced oscillations in a neural network model. *SIAM J. Appl. Math.*, 56:245–255, 1996.

[201] A. Hutt and F.M. Atay. Neural fields with distributed transmission speeds and long-range feedback delays. *SIAM J. Appl. Dyn. Syst.*, 5(4):670–698, 2006.

[202] R. Eckhorn. Feature linking via synchronization among distributed assemblies:simulations of results from cat visual cortex. *Neural Comput.*, 2:293–307, 1990.

[203] R. Eckhorn et al. Coherent oscillations: a mechanism of feature linking in the visual cortex? *Biol. Cybern.*, 60:121–130, 1989.

[204] C. Sutherland. Spatio-temporal feedback in stochastic neural networks. Master's thesis, University of Ottawa, 2006.

[205] N. Masuda and K. Aihara. Global and local synchrony of coupled neurons in small-world networks. *Biol. Cybern.*, 90:302–309, 2004.

[206] H. Markham. The blue brain project. *Nat. Rev. Neurosci.*, 7:153–160, 2006.

[207] J. Deppisch. Alternating oscillatory and stochastic states in a network of spiking neurons. *Network*, 4:243–257, 1993.

[208] M.E. Nelson et al. Characterization of p-type electrosensory afferent responses to amplitude modulations in a wave-type electric fish. *J. Comp. Physiol.*, 181:532–544, 1997.

[209] Z. Liang and M.A. Freed. The on pathway rectifies the off pathway of the mammalian retina. *J. Neurosci.*, 30:5533–5543, 2010.

[210] Y.H. Liu and X.J. Wang. Spike-frequency adaptation of a generalized leaky integrate-and-fire model neuron. *J. Comput. Neurosci.*, 10:25–45, 2001.